An AFM study of cell surface mechanics and its correlation with cell physiology and cytoskeleton

A dissertation submitted to
THE GRADUATE SCHOOL OF ENGINEERING SCIENCE
OSAKA UNIVERSITY
in partial fulfillment of the requirements for the degree of
DOCTOR OF PHILOSOPHY IN ENGINEERING

By

SEYED MOHAMMAD ALI HAGHPARAST

SEPTEMBER 2012

In childhood we strove to go to school

Our turn to teach, joyous as a rule

The end of story is sad and cruel

From dust we came, and gone with winds cool.

Omar Khayyam

Acknowledgements

It would not have been possible to complete this PhD thesis without encouragement and support of many kind people over the course of the years that I have been involved in this demanding work, to only some of whom it is possible to give particular mention here.

My sincere appreciation goes first and foremost to my PhD supervisor Professor Jun Miyake, for his support and careful guidance during my stay at the Bio-System engineering laboratory. His consistent advice an instruction has been invaluable on both my academic and personal life, for which I am very grateful.

My gratitude also goes to Assistant Professor Takanori Kihara. I'm indebted to him for valuable discussions and technical assistance throughout this study and for all the things he has taught me.

I would like to thank Professor Tsutomu Araki, Professor Shigeo Wada, and Professor Hisao Ohtake for serving on my committee and for their helpful comments and constructive criticism for improving the final form of this written document.

I'm again thankful to Professor Hisao Ohtake, Department of Biotechnology, Graduate School of Engineering, Osaka University and also Professor Takeshi Omasa, Institute of Technology and Science, The University of Tokushima for giving me the valuable opportunity to pursue my academic career at the graduate level.

I want to express my thanks to Professor emeritus Koichi Hatada and all other respected members of Toyonaka Rotary Club for their kindness and caring manner, and for supporting my daily life financially.

I would like to thank the friendship and cooperation of previous and current members of Bio-system engineering group, especially Yuji Shimizu.

I wish to acknowledge the academic, technical and financial support of Osaka University and its staff particularly Graduate School of Engineering Science that provided the necessary support for this research.

For everything they have done throughout my life, I owe more than mere words and thanks to my parents and brothers especially my late brother, Reza, who left his footprints in the dust and in my soul.

Above all, I must thank my loving wife, Eileen, and my adorable daughter, Arshida, for standing beside me all the way with patience and understanding. They gave me the hope and courage to overcome difficulties and the motivation to move my career forward. For them, all my endeavors seem worthwhile and attainable.

Abstract

Distinct mechanical properties of each cell are now regarded as novel biomarkers. These properties which denote cell state, function and fate are regulated by cytoskeleton. The main components of the cytoskeleton are actin filaments (F-actin). They are bundled and crosslinked by actin-binding proteins into higher-order types of actin networks and structures such as ‘stress fibers, filopodia, lamellipodia, cortical actin, basal actin and perinuclear actin cap which together are referred to as actin cytoskeleton. These biopolymer microstructures dynamically contribute to cellular mechanics and processes under different physiological conditions.

In fact cells sense and respond to forces in the environment through organizing diverse actin microstructures according to their functional demands. Such polymorphism in F-actin organization requires spatial and temporal variations in actin cytoskeleton architecture and results in heterogeneity of mechanical properties across cell surface. Therefore the key cytoskeletal determinants for cell mechanics and morphology probably vary across different cells, and it is essential to determine the dominant actin cytoskeleton assemblies which provide mechanical properties and specific morphology in each cell type and state.

Several techniques have been successfully employed to study cell mechanical properties, including micropipette aspiration, magnetic twisting cytometry, optical traps, and atomic force microscopy (AFM). In particular, AFM can be used to analyze live cells and to investigate their mechanical properties in physiological conditions in a relatively

non-destructive manner. A common experimental strategy in studying the cell mechanics with cytoskeleton involvement is to combine AFM with confocal laser scanning microscopy (CLSM) and actin cytoskeleton modifying drugs which rendering a comprehensive mechano-structural overview of the cells.

The work contained in this thesis focuses on detailed mechanical and cytoskeletal characterization of normal and cancer cell types under both adherent and suspended states and alterations of actin cytoskeleton and elastic modulus during cell cycle. It also provides better insights into the possible links between actin cytoskeleton structures, mechanical features and physiological states of the cells. The presented findings are expected to have prime implications for biomedicine, biotechnology and biomechanics.

Table of Contents

Acknowledgements 3

Abstract 5

Table of contents 7

Chapter 1 12

Introduction

1.1 Cell as a physical object 12

1.2 Cytoskeleton architecture and components 15

1.3 Previous reports on biomechanical approaches 16

1.4 Atomic force microscope 20

1.4.1 Specifications 20

1.4.2 Principles 21

1.4.3 Modes of operation 23

1.4.4 Force measurement 26

1.4.5 Force curve acquisition 27

1.4.6 Elasticity measurement 29

Chapter 2 31

Elastic properties of mesenchymal stem cells (MSCs)

2.1 Introduction 31

2.2 Experimental procedure 33

2.2.1 Materials 33

2.2.2 Preparation and culture of MSCs 34

2.2.3 AFM measurements 34

2.2.4 Cell proliferation assay 37

2.2.5 Evaluation of perinuclear actin cap 37

2.3 Results 39

2.3.1 Relationship between stiffness and thickness of MSCs 39

2.3.2 Regulation of stiffness and thickness of MSCs by actin cytoskeleton 43

2.3.3 Actin cap correlation with cell thickness and stiffness of MSCs 47

2.3.4 Effect of actin cytoskeleton on proliferation activity of MSCs 49

2.3.5 Role of actin cytoskeleton in replicative lifespan of MSCs 51

2.4 Discussion 54

2.5 Summary 57

Chapter 3 58

Elastic features of adherent and suspended cells

3.1 Introduction 58

3.2 Experimental procedure 62

3.2.1 Materials 62

3.2.2 Preparation of BAM-coated dishes 62

3.2.3 Preparation and culture of MSCs 63

3.2.4 Cell cultures and drug treatment 63

3.2.5 Evaluation of actin cytoskeleton 64

3.2.6 AFM measurements 65

3.2.7 Statistic analysis 66

3.3 Results 66

3.3.1 Actin cytoskeleton organization of adherent and suspended cancer and normal cells 66

3.3.2 Biomechanical properties of adherent and suspended cancer and normal cells 73

3.3.3 Mechanical responsiveness of cancer and normal cells 78

3.4 Discussion 83

3.5 Summary 88

Chapter 4 89

Elastic character of round mitotic and trypsinized cells

4.1 Introduction 89

4.2 Experimental procedure 93

4.2.1 Materials 93

4.2.2 Preparation of BAM-coated dishes 93

4.2.3 Cell cultures 94

4.2.4 AFM measurements 95

4.2.5 F-actin imaging 97

4.3 Results 97

4.3.1 Cortical actin imaging of Hela.S-Fucci and NMuMG-Fucci Cells 97

4.3.2 Young's modulus of mitotic and trypsinized round cells 101

4.4 Discussion 105

4.5 Summary 109

Conclusion and perspective 110

Bibliography 115

Publication list 132

Chapter 1
Introduction

1.1 Cell as physical object

Genuine understanding of life entails a comprehensive study of building block of living matter i.e. the cell. As suggested by Paul A. Weiss in 1960 [1], cell should be regarded as an integrated whole or a hierarchically ordered system of highly interdependent constituent elements which contribute to a wide range of functions and features to which life depends on. This complex living system can be defined more explicitly by learning about its multidimensional properties and interaction of its subsystems. To this end, novel insights and tools should be employed as an aid to break the limits of cell biology and boost the cell system intuition.

The interdisciplinary field of cell mechanics has attracted a lot of attention and experienced rapid growth over the last years. Recent developments have included studies of cytoskeleton dynamics and cell–extracellular matrix (ECM) interactions as related to the shape, function, deformability, and mechanical properties of whole cells; the viscoelasticity and connectivity of subcellular structures such as microtubules, actin filaments, and intermediate filaments; the biophysical aspects of cell adhesion and cell locomotion at both cellular and molecular levels; injury of cells owing to mechanical forces; and the effects of mechanical perturbations on cellular processes. The role of mechanical forces in biology is certainly not a new idea but is currently gaining wider acceptance [2].

Numerous cell components exhibit distinct mechanical characteristics and many cellular processes involve mechanical phenomena. During many physiological functions, cells change their mechanical properties by responding to forces in their microenvironment. Morphology of the cell serves its specialized function within tissue and is maintained through structural stiffness. In response to internal and external stimuli cells alter their mechanical parameters and morphology via gene expression and protein synthesis. On the basis of stated facts, proposed model here (Fig.1.1) assumes cell as a physical object in which three interlinked domains namely morphology, physiology and mechanics are in close relation with central dogma (genes). Mechanical properties are known to be determined by the actin cytoskeleton which has received special attention as well.

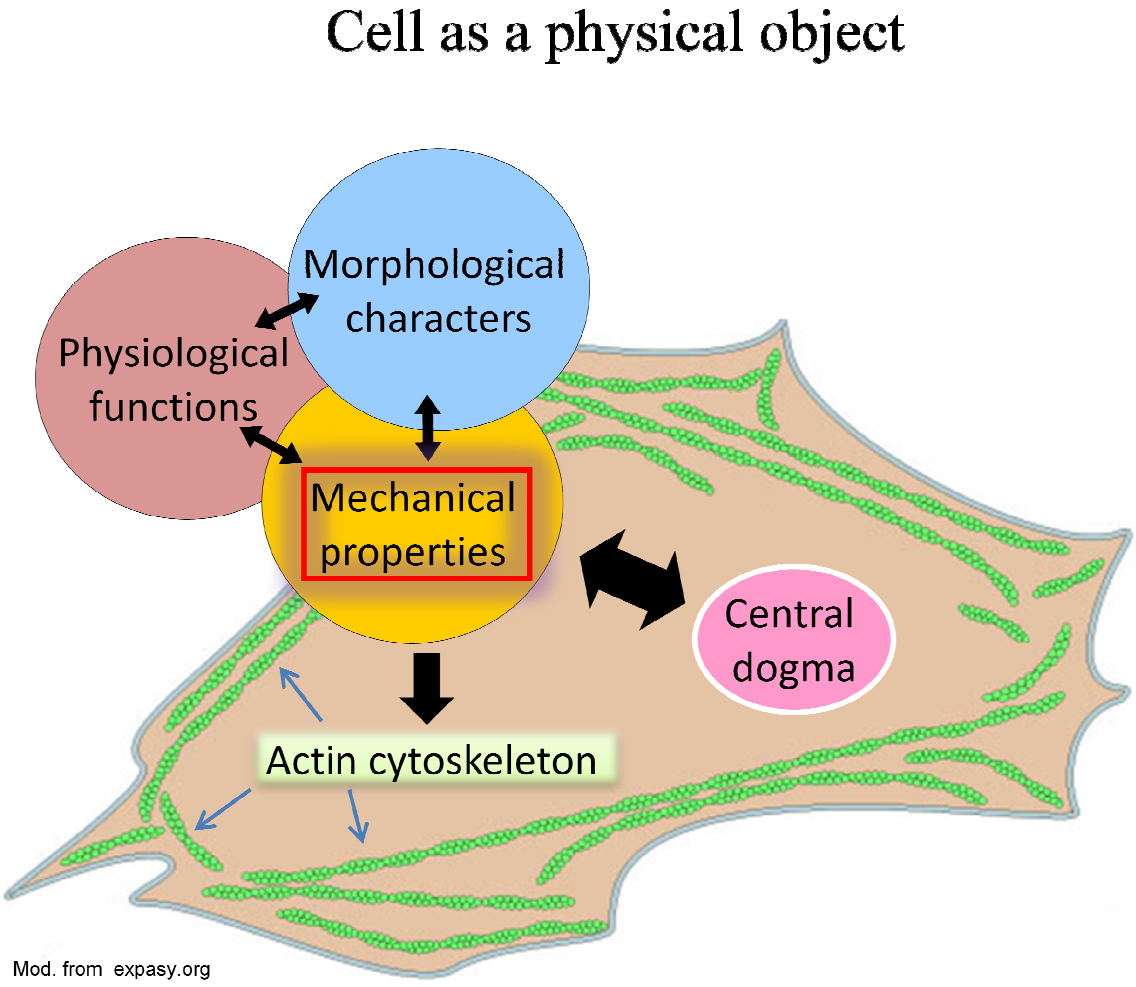

Fig.1.1 Conceptual view of this research

1.2 Cytoskeleton architecture and components

Cytoskeleton is an intricate and extensive biopolymer construction which is made of structural proteins and their associated binding proteins. The term “cytoskeleton” was first proposed in 1903 by Nikolai K. Koltsov as a network of tubules which determine the shape of the cell. There are three major types of cytoskeletal filaments in eukaryotic cells which are classified based on the diameter of filament: Microfilaments (6nm), intermediate filaments (10nm) and microtubules (25nm). Microfilaments which are also referred to as actin filaments are the potential regulatory structures of cell mechanics. Actin is one of the most ubiquitous and conserved proteins with a molecular weight of around 42 kDa which was discovered in 1943 by Bruno F.Straub [3]. Three main actin isoforms have been identified in animal cells: alpha, beta and gamma. Contrary to α actin which is found only in muscle cells, β and γ actin coexist in all cell types. Actin exists basically as the monomeric or globular (G-actin) form which can be polymerized and generate filamentous actin (F-actin). Actin filaments are in a constant state of flux by either adding new monomers at the ‘barbed’ or ‘plus’ end or depolymerizing at the ‘pointed’ or ‘minus’ end. These filaments can diassemble and reassemble into different structures based on the cell state. The presence of high concentrations of crosslinkers that bind to actin filaments promotes the assembly of highly organized, stiff structures, including isotropic networks, bundled networks and branched networks [4]. In bundles, actin filaments are packed in parallel, while in networks these filaments are crosslinked with different angles and density.

These actin biopolymer bundles and networks which are referred to as actin cytoskeleton are responsible for mechanical stability and structural integrity of cells. Actin

cytoskeleton is highly dynamic and contributes into many vital cellular processes through constant reorganization of F-actin assemblies. Actin cytoskeleton is involved directly in various pathogenic states such as bacterial and viral infections. Therefore studying the actin cytoskeleton is crucial for understanding the mechanical behavior of cells, mechanical regulatory structures of cells and mechanical interaction between cells and their environment. It further provides valuable clues for better identification of the diseases and searching for new effective therapeutic drugs.

1.3 Previous reports on biomechanical approaches

The field of cell biomechanics studies how cells move, deform, and interact, as well as how they sense, generate, and respond to mechanical stimuli [5]. A variety of experimental methods including cell poking, scanning acoustic microscopy, optical trap, magnetic twisting cytometry, shear flow, micropipette aspiration, cytoindenter, substrate stretching, microplates, hydrostatic pressure, microfabricated arrays, micromachines and atomic force microscopy have been used to investigate the local or overall mechanical properties of the cells by applying mechanical loads and examining the cell response to induced deformation. Also by using computational approaches, mechanical models could be made to describe the physical interactions between adjacent cells or the cell its microenvironment.

In cell poking a fine glass stylus is used to indent the exposed surface of a cell adherent to a rigid substratum. The force of the cellular resistance to indentation is registered as a function of the depth of indentation [6]. Scanning acoustic microscope uses

high frequency waves to generate high resolution images. By analyzing single acoustic images, sound attenuation and sound velocity, the latter corresponding to stiffness (elasticity) of the cortical cytoplasm can be determined [7]. Optical traps are based on the controlled displacement of dielectric objects that are either attached o the cell membrane or placed inside the cell so that when dielectric object moves toward the laser focal point under a force and thus can be used to impose force through translocation of focal point or to measure externally applied force by the resolution mode of the tapped object [8]. Magnetic twisting cytometry relies on the use of ferromagnetic beads to measure pointwise displacement in which cells partially engulf beads ranging in diameter from 250 nm to 5 μm which impose cell displacement [9]. In shear flow method, precise amounts of shear force in the form of laminar and turbulent flows can be applied to surface-attached cells and many cellular responses can be measured as a function of shear which is especially appropriate for the cells which should resist a shear flow in their natural habitat [10]. Micropipette aspiration technique involves sucking up the cell into a glass tube via stepwise application of aspiration pressure which is maintained over a specified duration, and the attendant extension of the cell into the pipette is monitored via optical microscope [11]. In cytoindentation technique, displacement-controlled indentation tests are conducted on the cell surface by a cell-indentation apparatus equipped with a thin cantilever-like indenter and the corresponding surface reaction force of the cell is measured [12]. The procedure for microplate substrate stretching involves culturing the cells on a thin-sheet polymer substrate, such as silicone, which is coated with extra cellular matrix (ECM) molecules for cell adhesion. The substrate is then mechanically deformed by pulling while maintaining the cell's viability in vitro and

in this manner the effects of mechanical loading on the cell can be examined [13]. In microplates method rectangular glass bars are used. After appropriate chemical treatment, microplates can support cell adhesion and/or spreading. Rigid microplates are used to hold cells, whereas more flexible ones serve as stress sensors. Microplate-based manipulations include: compression, traction, aspiration and adhesion rapture [14]. To understand behavior the cells that are subjected to high pressures under normal and abnormal conditions, hydrostatic loading technique can be used in which a piston pressurizes the fluid above the monolayer of cells. When cells are grown in a three dimensional matrix, pressure can be applied directly to the cell assemblage [15]. The microfabricated array detector has arrays of closely spaced vertical microneedles (posts) of silicone elastomer to encourage cells to attach and spread across multiple posts. As the cells probe the surface the posts behave like simple springs such that their deflection is directly proportional to the force applied by the attached cell [16]. Micromachines such as microelectromechanical systems are very small devices which use a cluster of microneedles to detect the cell-matrix mechanical interactions [17] or use multiple active and passive cantilever beams to apply localized deformation and to measure focal forces generated by the cell [18].

Atomic force microscopy (AFM) which was developed by Binnig, Quate and Gerber from scanning tunneling microscopy in 1986 uses a tiny tip at the free end of a flexible cantilever which scans over the surface of a sample and sense the force interaction between atoms of the tip and atoms of the sample. The mechanical probing of the sample surface by AFM tip allows imaging, measuring and indentation of the sample which provides valuable information for nanoscale characterization of the examined matter. Progress in nanobiotechnology strongly relies on the development of scanning probe techniques, particularly AFM [19]. Since there is no need for fixation or staining, AFM can image and

manipulate the live cells under physiological condition with high resolution and minimal damage. Using the AFM probe as a lab-on-a- tip enables us to probe simultaneously the structure and specific biological, chemical and physical parameters of cell's machinery [20]. AFM has emerged as a powerful toolbox in a variety of research fields and is expected to find more applications especially in biology, medicine and nanobiotechnology (Fig.1.2).

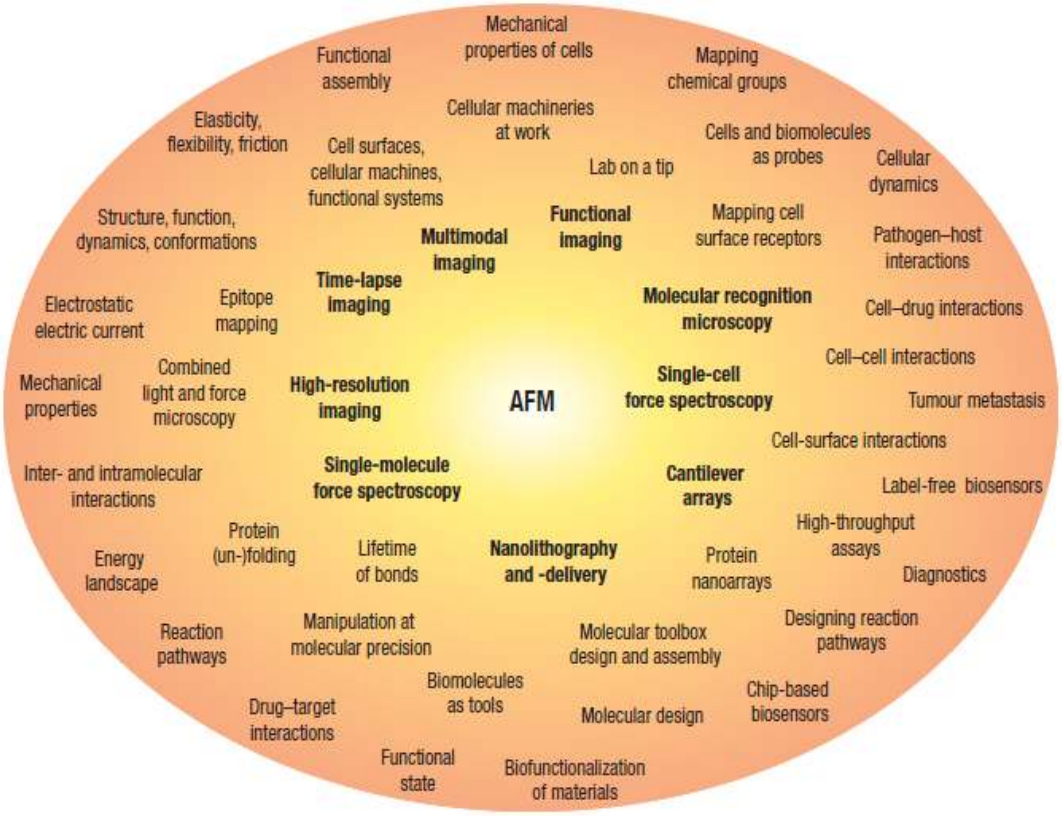

Fig.1.2 AFM can characterize and manipulate biological systems on the nanometer scale [from ref 20].

1.4 Atomic force microscope

1.4.1 Specifications

AFM system (Nanowizard I; JPK Instruments AG, Berlin, Germany) consists of several main parts (Fig.1.3). The most important parts are AFM head and controller. The AFM head is installed on an inverted optical microscope which is equipped with a special stage. The entire set of AFM and optical microscope can be placed on an active vibration isolation table to reduce the unwanted vibrations. The AFM head is connected to both controller and computer.

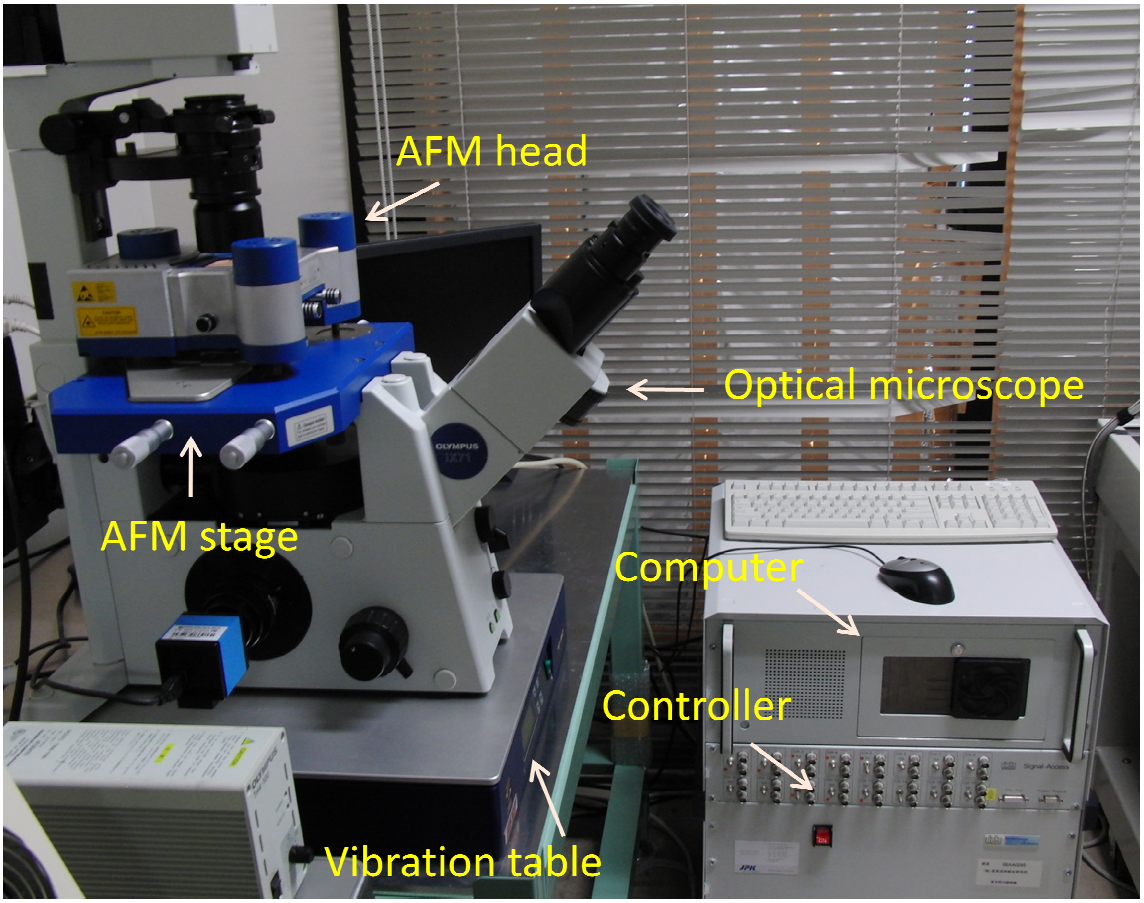

Fig.1.3 Main parts of AFM system

1.4.2 Principles

Atomic force microscope which is also referred to as scanning force microscope was primarily invented for imaging purposes. It has evolved into a multifunctional toolbox which is particularly suited for biological studies due to its ability in probing the live cells in their native microenvironment. Atomic force microscope uses a cantilever made of silicon or silicon nitride which has a very low spring constant and a sharp tip is attached to its free end. The atomic force microscope works on the basis of the physical interaction between a fine tip and the sample surface. The tip is placed on the sample in a controlled way using piezoelectric actuator. Cantilever behaves like a spring and deflects when the tip is brought into contact with sample. The bending of cantilever is monitored by detecting the translocation of a laser beam bouncing from the back of the cantilever by a four-quadrant photodetector (Fig.1.4). A feedback system controls the piezo movement and stops it when the set deflection/force (defined by the user) is reached. In case of an interaction between the tip and the surface of the sample, cantilever will be pulled down toward the surface until the force necessary for breaking the mutual interaction between the tip and the surface is reached.

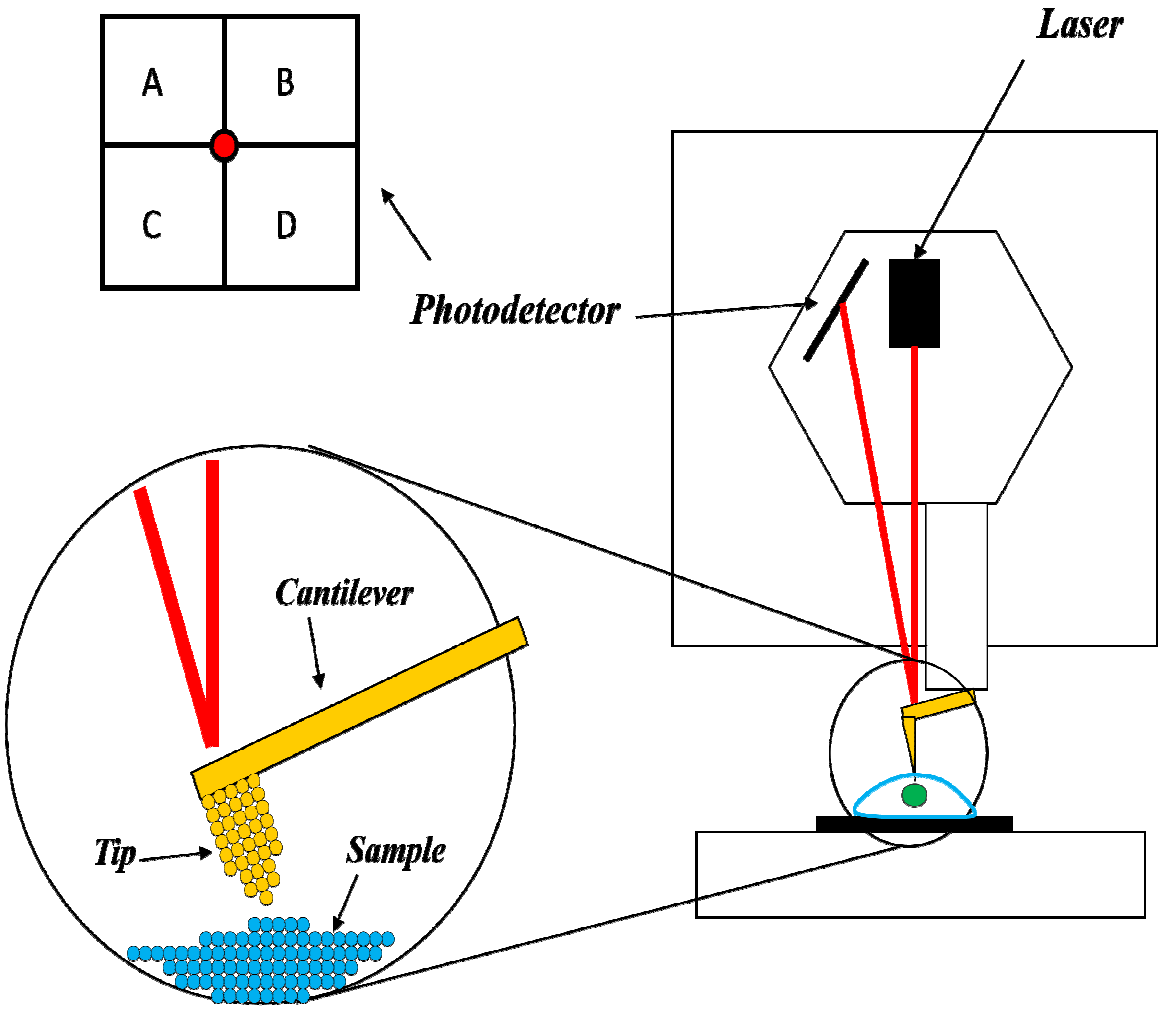

Fig.1.4 Principle of the AFM

1.4.3 Modes of operation

Atomic force microscope can operate in different modes based on the type of tip-sample interaction and style of tip movement. Contact mode (also known as repulsive mode), intermittent contact mode (also termed as tapping mode) and non-contact mode are the major scan modes. The non-contact mode is largely nondestructive but yields low resolution the surface topography. In contrast, contact-mode force microscopy has the potential of high spatial resolution though it may damage the surface. Intermittent contact mode combines the merits of the two modes by oscillating the tip-sample contact and exerting much lower energy from the oscillating probe to the sample surface. Therefore the intermittent-contact mode is more effective than non-contact AFM for imaging soft samples like living cells [21]. The contact mode was used throughout this research for biomechanical investigations because it allows the adjustment of tip loading force and controlled manipulation of the target cells.

The forces which act between the tip and the specimen are either repulsive or attractive. Van der Waals force, mechanical force of the cantilever and capillary force of fluid between the cantilever and the sample surface are the three involved forces between the tip and the sample [22]. In practice, the dominant interactions at short probe-sample distances in the atomic force microscope are due to Van der Waals forces. To illustrate the operating modes, the plot of tip-sample force as a function of tip-sample separation can be created (Fig.1.5). The forces that fall below or stay above the axis are attractive (negative) and repulsive (positive) respectively. During contact mode, the probe predominately

experiences repulsive forces which lead to the tip deflection. As the tip moves further away from the surface attractive forces are dominant (non-contact mode). In the intermittent mode which is a combination of the other two operation modes, tip-sample force interaction oscillates repeatedly between the attractive and repulsive forces.

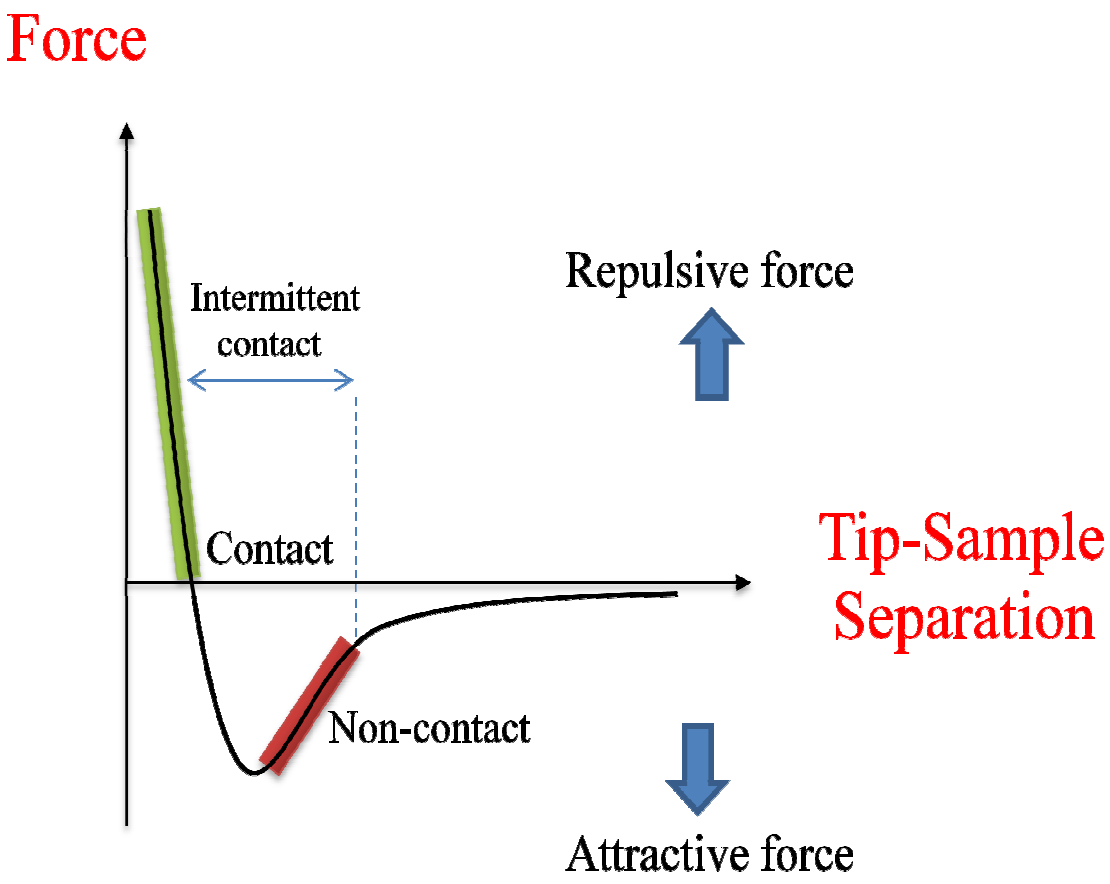

Fig.1.5 Diagram of tip-sample force vs. separation distance

1.4.4 Force measurement

The force which causes the cantilever deflection can be determined based on the Hook's Law: $\Delta Z = F/\mathrm{K_c}$ where ΔZ is the deflection, F is the acting force and $\mathrm{K_c}$ is the spring (Fig.1.6)

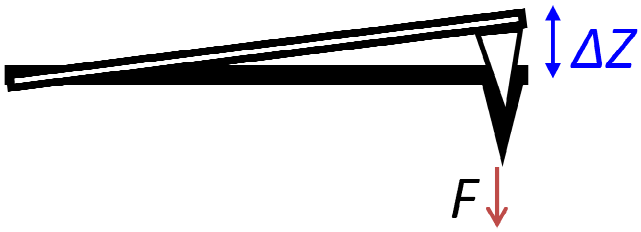

Fig.1.6 Cantilever deflects as the tip is pushed towards the sample

Apart from using attractive and repulsive forces for imaging the sample with nanometer resolution, atomic force microscope can also measure these forces with pico-Newton precision. In the contact force spectroscopy of cells, the cantilever approaches the cell surface, pushes into it and then retracts again. The velocity of the cantilever and indentation depth can be controlled. During this process the height information z-piezo and the deflection of the cantilever are recorded from which a force-distance curve is produced. Three typical probe-sample interactions which exist in each cycle are no contact, attraction and repulse (Fig.1.7).

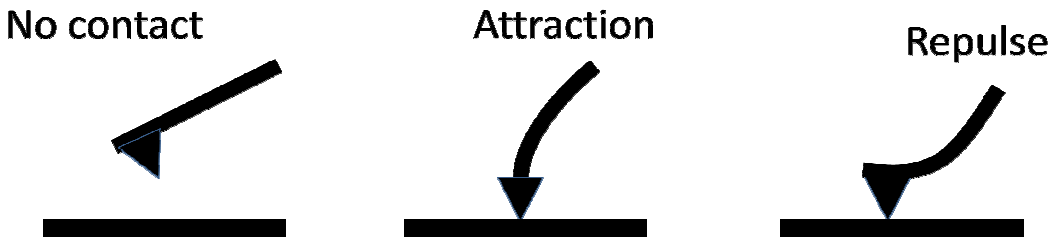

Fig.1.7 Typical probe-sample interactions

1.4.5 Force curve acquisition

On a hard surface this gives an ideal force-distance graph (Fig.1.8). To interpret this, the graph has to be read from right to left, due to the higher cantilever position at the beginning of the measurement [23]. First the cantilever is moved down without touching the sample, i.e. no deflection but a decreasing distance is recorded (A). Very close to the surface the cantilever can suddenly be attracted by the sample due to attractive forces (e.g. electrostatic interaction), i.e. the cantilever flicks down the remaining distance and gives a small downward deflection (B). When the cantilever is moved further down, the cantilever is bent upwards in direct proportion to the z-piezo height (C). As soon as a defined setpoint of deflection is reached the cantilever is withdrawn (D). While moving upwards again, the deflection of the cantilever decreases. Passing the contact point, the tip usually stays attached to the surface by adhesion, which causes the cantilever to bend in the opposite direction (E). At some point it suddenly loses contact and flicks back into its initial position (F). Further retraction causes no change of vertical deflection (G).

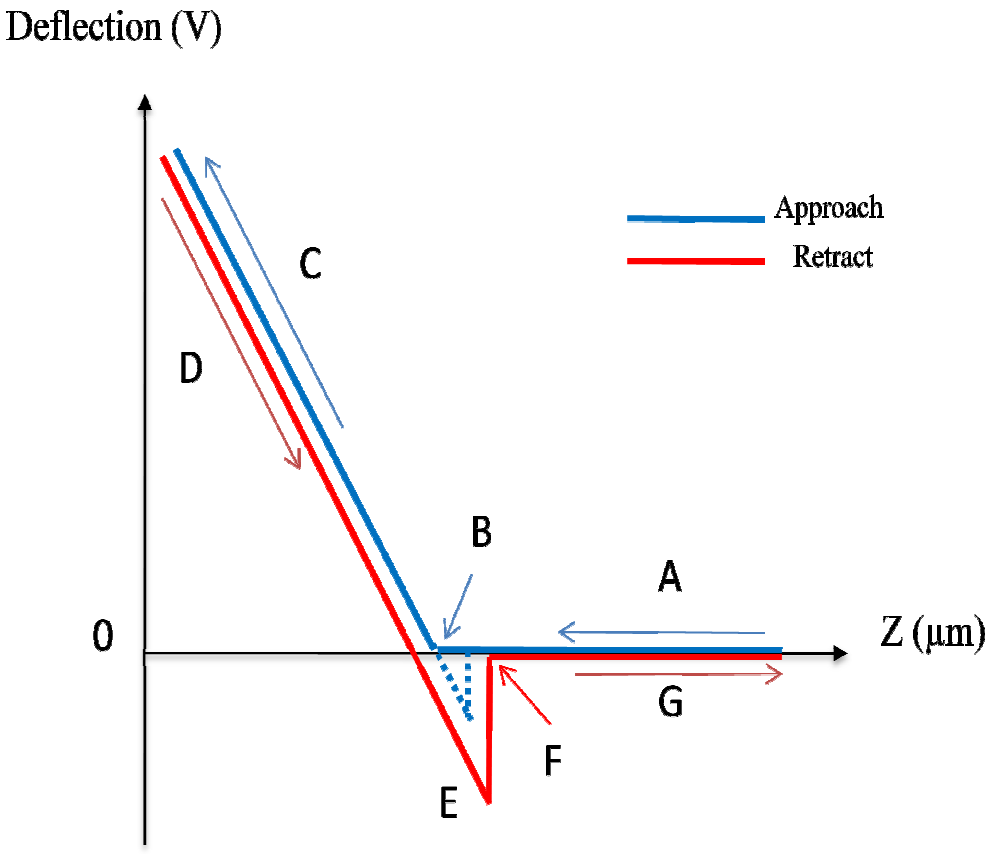

Fig.1.8 Diagram of an ideal force-distance curve

1.4.6 Elasticity measurement

Force curve analyses can be used to determine chemical and mechanical properties of the material of the interest. The tip can be used to indent the specimen and, from the resulting surface deformation, one can determine the mechanical properties of the sample [24]. Second, the shape of the force curve during retraction of the tip from a surface can be used to elucidate attractive forces of nonspecific nature, as well as highly specific binding between biological molecules [25, 26]. Moreover stretching and unfolding experiments on single molecules can be conducted [27]. In particular, the elastic modulus E (also called Young's modulus) of a wide range of biological samples from tissues and cells to protein layers [28].

Young's modulus is an elastic property of a material, and is defined as the stress of a material divided by the strain [29]. This is normalized measure of the compressibility so that stiff materials have high Young's modulus values. If a material is compressed homogenously (Fig.1.9), the calculation of the Young's modulus can be done as follows:

$$E = {tensile\ stress}/{tensile\ strain}$$

$$Tensile\ stress = {tensile\ force}/{cross - setional\ area} = {F}/{A}$$

$$Tensile\ strain = {extention}/{original\ length} = {\Delta L}/{L}$$

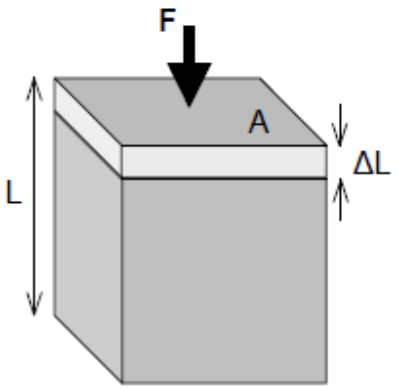

Fig.1.9 Illustration of physical quantities for defining the Young's modulus (from ref. 29)

In practice, for calculation of elastic modulus from the AFM measurements of biological samples other parameters such as indenters' shape and thickness of the sample should be considered. The Hertz model [30] is the standard model used for extracting elasticity from force-distance curves. Based on this model the sample is an isotropic solid with linear elasticity, indenter is not deformable, and that there are no other interactions between the two. Moreover, to apply Hertz model to the elastic measurement of the cells the indentation depth and the viscosity response of cytoplasm should be considered [31, 32] because biological materials are heterogeneous and mostly viscoelastic. Due to these mentioned limitations, it is advisable to consider the extracted elasticity of the cells as the "apparent Young's modulus" or "apparent modulus of elasticity ($E_{apparent}$)", throughout this manuscript. However, for the purpose of simplicity and practicality, the customary form of "Young's modulus" has been used here instead.

Chapter 2

Elastic properties of mesenchymal stem cells (MSCs)

2.1 Introduction

Mesenchymal stem cells (MSCs) are a heterogeneous population of stem/progenitor cells with the pluripotent capacity to differentiate into mesodermal and non-mesodermal cell lineages (Fig.2.1).

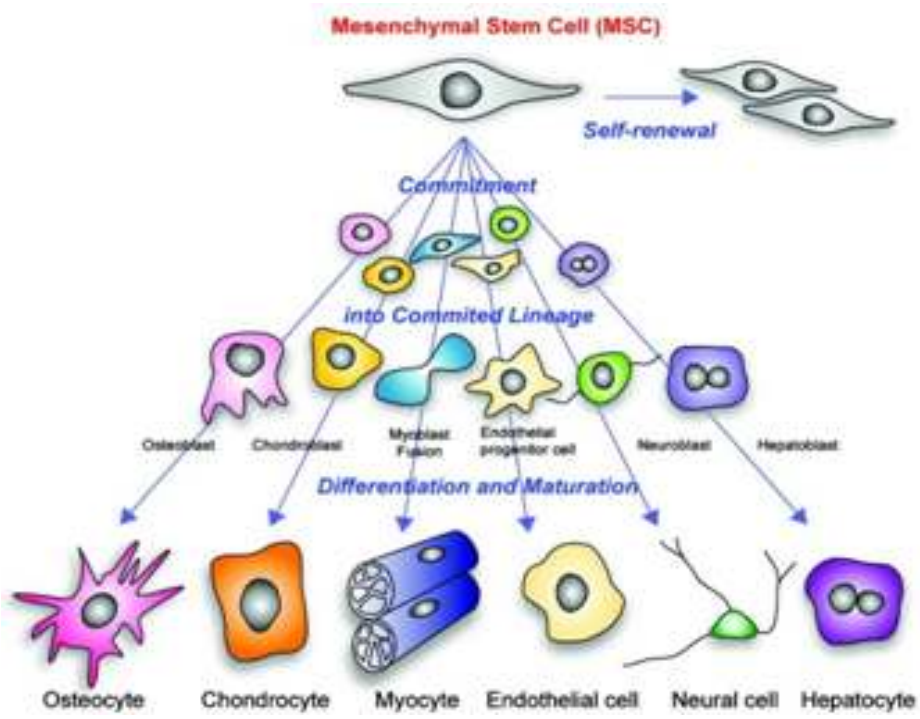

Fig.2.1 Self-renewal and pluripotency of MSC (mod. from Kotobuki N, Artif. Organs, 2004).

They have generated a great deal of interest owing to their potential use in regenerative medicine and tissue engineering [33, 34]. In order to maximize the potential of MSCs for

biomedical applications, a more comprehensive characterization of MSCs is required. To achieve this goal, the development of a direct, relatively non-destructive method for measuring physical properties, which reflect the fate and physiological state of MSCs, is necessary. Population thickness (height) of adhered human MSCs may be related to various cell functions, such as proliferation activity and cell cycle [35, 36]. However, a more comprehensive view of the physical properties of MSCs is required. Mechanical properties such as cytoskeleton organization and elasticity, membrane tension, cell shape, and adhesion strength may play important roles in stem-cell fate and differentiation [37, 38].

A change in mechanical properties, and in particular, in the stiffness (elasticity) of tissue cells, has been recognized as an indication of cancer [39]. Several techniques have been successfully employed to study cell mechanical properties, including micropipette aspiration, magnetic twisting cytometry, optical traps, and atomic force microscopy [40, 8]. In particular, AFM can be used to analyze live cells and to investigate their mechanical properties in physiological conditions in a relatively nondestructive manner [41-44].

Surface mechanical properties of a cell are dominantly defined by the actin cytoskeleton [45−48]. Stress fibers are specific determinants of cell mechanics [49], and cortical actin promotes cortical rigidity [50, 51]. Dominant types of actin cytoskeleton differ by cell types as well as position. Therefore, the key determinants for cell mechanics probably vary across different cell types, and it is necessary to determine the character of cell mechanics in each cell type. Previously, it was reported that the elastic modulus of human MSCs decreased dramatically by actin de-polymerization, whereas the cell thickness increased [79]. The elasticity and the thickness of an actin de-polymerized MSC

and a bare nucleus were almost the same. Thus, regulatory factors of nuclear thickness and cell elasticity are possibly the same, and these may be related to the actin cytoskeleton. Recently, Khatau et al. reported that a perinuclear actin cap, which is an actin filament structure that forms a cap or dome above the apical surface of the nucleus, tightly regulates the nuclear shape of adherent fibroblasts [53]. In this part of study, I examined the regulatory effect of the perinuclear actin cap on thickness and stiffness of adherent rat MSCs by using several actin cytoskeleton-modifying drugs.

2.2 Experimental procedure

2.2.1 Materials

The AFM probe (ATEC-CONT; spring constant: 0.02−0.75 N/m) was purchased from Nanosensors (Neuchatel, Switzerland). Cell culture media was purchased from Nacalai Tesque (Kyoto, Japan), and fetal bovine serum (FBS) was purchased from JRH Biosciences (Lenexa, KS). Antibiotics were purchased from Sigma−Aldrich (St.Louis, MO) Fisher 344 male rats were purchased from Japan SLC (Shizuoka, Japan). ATP bioluminescence assay kit was purchased from Toyo Ink (Tokyo, Japan). Other reagents were purchased from Sigma−Aldrich, Wako Pure Chemical Industries Ltd. (Osaka, Japan), or Invitrogen (Carlsbad, CA).

2.2.2 Preparation and culture of MSCs

Rat MSCs were isolated and primarily cultured as described previously [54]. In brief, bone marrow cells were obtained from the femoral shafts of 7-week-old male Fisher 344 rats. The cells were obtained from at least 2 rats and mixed. The culture medium was Eagle's minimal essential medium (with Earle's Salt and L-glutamine) containing 15% FBS and antibiotics (100 U/mL penicillin G, 100 μg/mL streptomycin sulfate, and 0.25 μg/mL amphotericin B). The medium was renewed twice a week, and cells at passages 2−6 were used in this study. Y-27632 (10 μM), blebbistatin (5 μM), cell permeable C3 transferase (20 ng/mL), calyculin A (0.15 nM), and wiskostatin (1 μM) were used to analyze inhibition or acceleration of the actin cytoskeleton. Cells were cultured in the medium containing these reagents for 2 days and then examined by AFM.

2.2.3 AFM measurements

Rat MSCs cultured on 35-mm culture dishes in the medium were examined by AFM at room temperature. The probe was indented into the cells up to 50 nN at 10 μm/s. The Young's modulus of the cell was calculated according to the Hertz model. Although the Hertz model is accommodated in an elastic body, various kinds of cellular stiffness have been evaluated by this model as Young's modules [55]. The force−distance curve at the region up to 400 nm of cell surface indentation was fitted to the model (Fig.2.2).

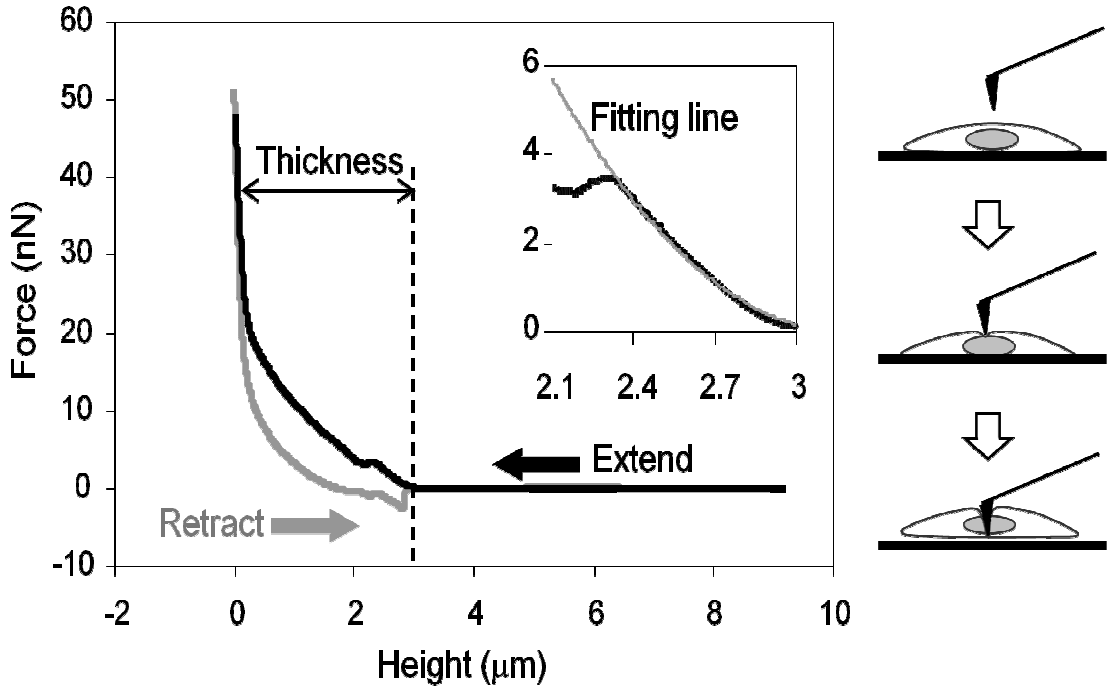

Fig.2.2 Typical force−distance curves obtained from the indentation of and pulling up from the surface of rat MSCs are shown at the left, and the schema for cell manipulation by AFM is shown at the right. Cell thickness is represented as the distance between the contact point of cell surface and substrate. Stiffness is calculated from the force curve at the region of indentation (up to 400 nm) by fitting it to the Hertz model (inset).

Although the ATEC-CONT is a tetrahedral probe, the edge of the probe is conical. Thus, the following equation was used in the model of indentation:

$$F = \frac{E}{1-\nu^2}\frac{2\tan\alpha}{\pi}\delta^2$$

where F = force, δ = depth of indentation, α = semi-opening angle of the cone (5°), ν = Poisson's ratio (0.5), and E = Young's modulus. Cell thickness was derived from the length, from the cell contact point to the substrate (Fig.2.2). All experiments were performed in more than 10 cells, and each cell was examined at 9 different points within a size-defined grid (Fig.2.3a) on the nuclear region of the membrane. In this study, I assumed that the distribution of Young's moduli and the thickness of cells were in accordance with the log-normal distribution, and a median value of 9 points was adopted for the Young's modulus of each cell (Fig2.3b).

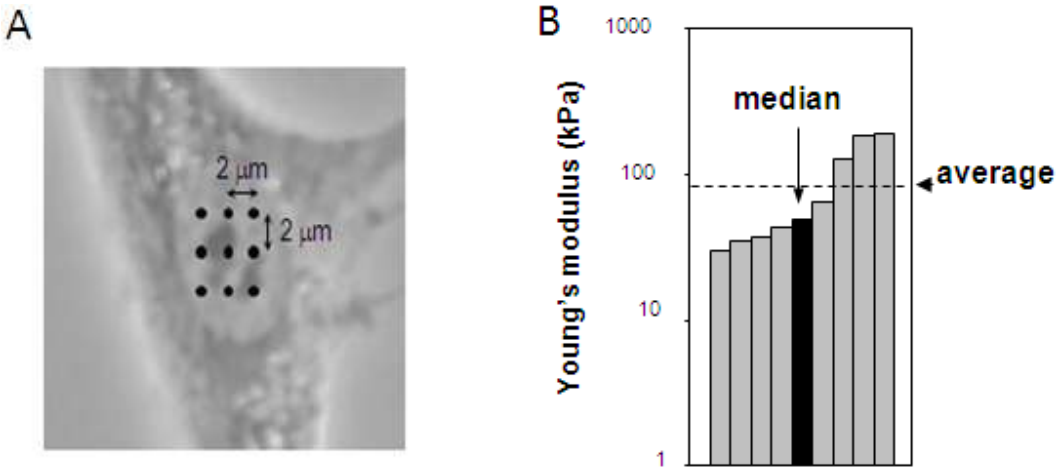

Fig.2.3 Representation of AFM-manipulated points and adoption of proper value. (A) A grid of 9 points was examined on the top of cell nucleus. (B) Median value was adopted for elasticity of each cell.

2.2.4 Cell proliferation assay

Approximate cell number was determined using an ATP bioluminescence assay kit according to the manufacturer's instructions. Rat MSCs were plated at a density of 1×10^3 cells/well into white 96-well culture plates and cultured in the culture medium containing the cytoskeleton-modifying reagent for 6 days. The ATP bioluminescence reagent was added to the wells, and the cultured cells were shaken for 1 min and then incubated for another 10 min at 25°C. Luminescence was measured with Synergy HT (BioTek, Winooski, VT).

2.2.5 Evaluation of perinuclear actin cap

The perinuclear actin cap was evaluated by staining the actin filaments of rat MSCs. Cells cultured for 2 days with the cytoskeleton- modifying reagent were fixed with 4% paraformaldehyde, permeabilized with 0.5% Triton X-100, and then stained with FITC-labeled phalloidin for actin filaments and propidium iodide for nucleus. Specimens were observed by confocal laser scanning microscope (FV-1000; Olympus, Japan) in 0.5 lm serial sections. The presence of the perinuclear actin cap was determined from the status of actin filaments over the nucleus in more than 23 cells for each condition (Fig.2.4).

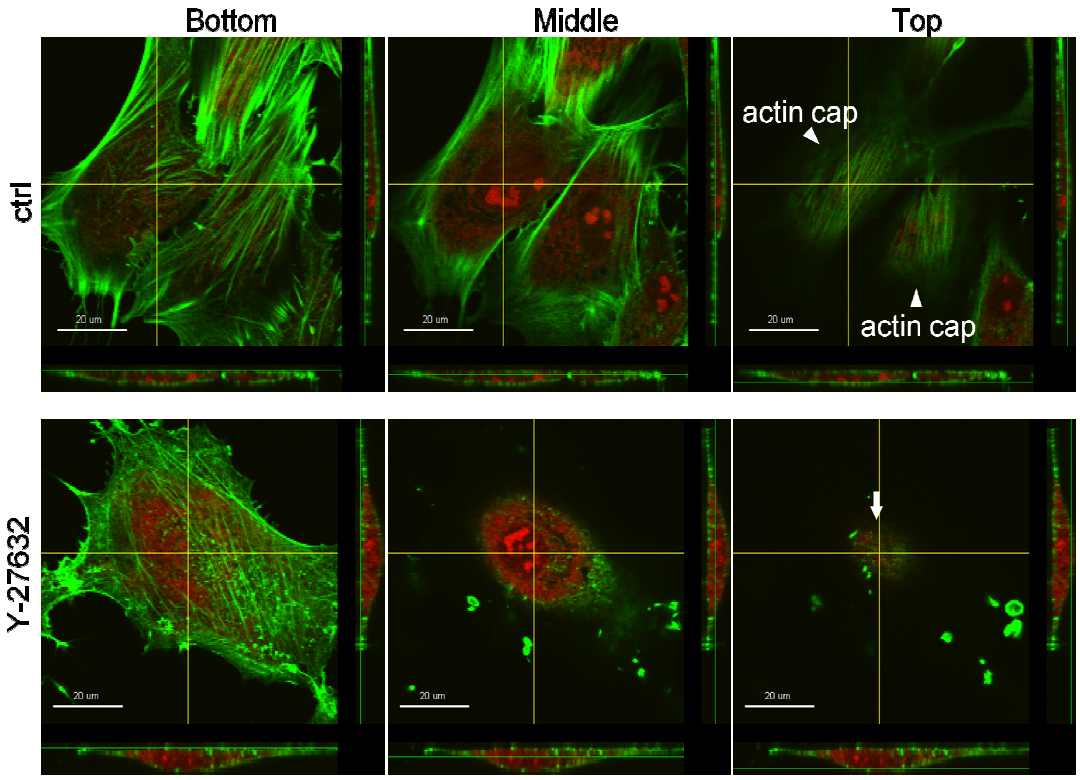

Fig.2.4 Perinuclear actin cap of rat MSCs. The actin filaments of cells were stained with FITC-labelled phalloidin and then three-dimensional images of the actin filaments were observed by CLSM. Green color shows FITC-labelled phalloidin and red color shows PI. Typical images of normal MSCs (ctrl) and Y-27632 treated cells are shown. Yellow lines show the locations of Z-axis image planes. Arrowheads represent actin cap. Arrow represents no/disruption of actin cap. Bar is 20 μm.

2.3 Results

2.3.1 Relationship between stiffness and thickness of MSCs

First, I examined the relation between every AFM-measured Young's modulus and the thickness of each rat MSC (Fig.2.5). Compared with the thickness, the measured Young's modulus varied widely for each cell manipulation by AFM. This was due to the fact that cellular mechanical properties are local and can change dramatically based on the location being probed [56]. Since it was difficult to determine the cell stiffness from these scattered Young's moduli, I examined the distribution of Young's moduli of rat MSCs in single cells and found that the distribution of Young's moduli corresponded to a log-normal pattern of distribution (Fig.2.6). Therefore, I selected the median value of the widely spread Young's moduli of each cell in this study, because the median provides a better estimate of the target value than the mean in a log-normal distribution (Fig.2.3b). Thickness versus Young's modulus of each adherent rat MSC was then plotted. Analyses of 100 cells revealed that Young's modulus of various adherent rat MSCs varied largely, and that it had a weak inverse correlation with cell thickness in each cell (Fig.2.7). The correlation coefficient R between these 2 factors was 0.35 ($P = 0.0004$). In short, flat, adherent MSCs tended to be rigid, whereas tall MSCs showed a relatively elastic property.

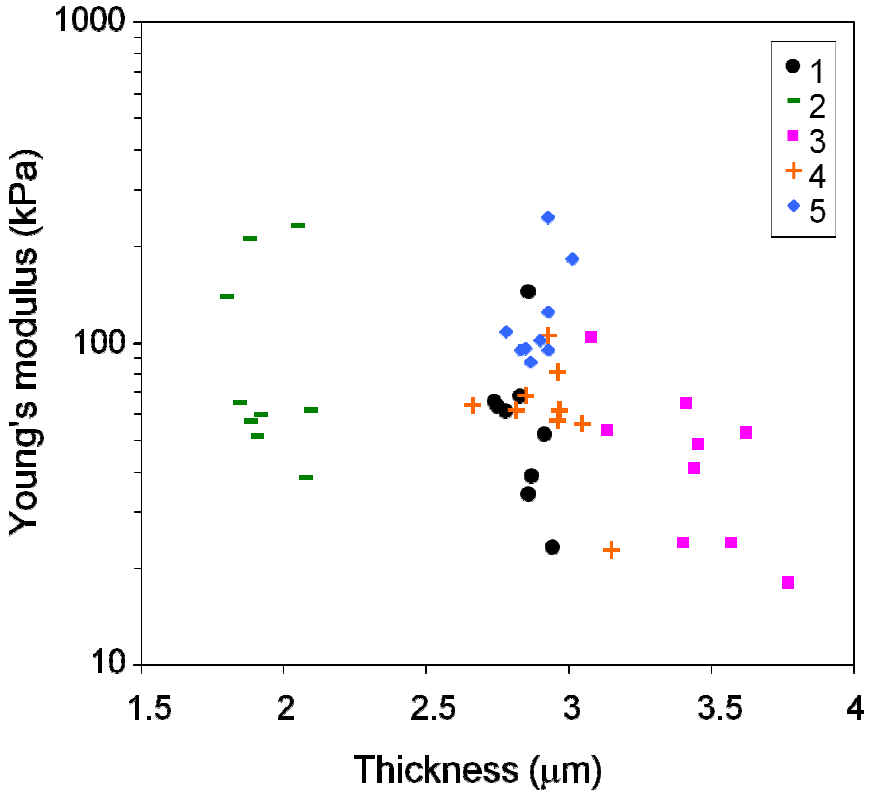

Fig.2.5 Young's modulus and cell thickness of each manipulation for the same cells. Each point indicates a single AFM manipulation and 9 points of the same code belong to a single cell (total 5 cells indication). The dispersion of Young's modulus is larger than that of thickness in each manipulation.

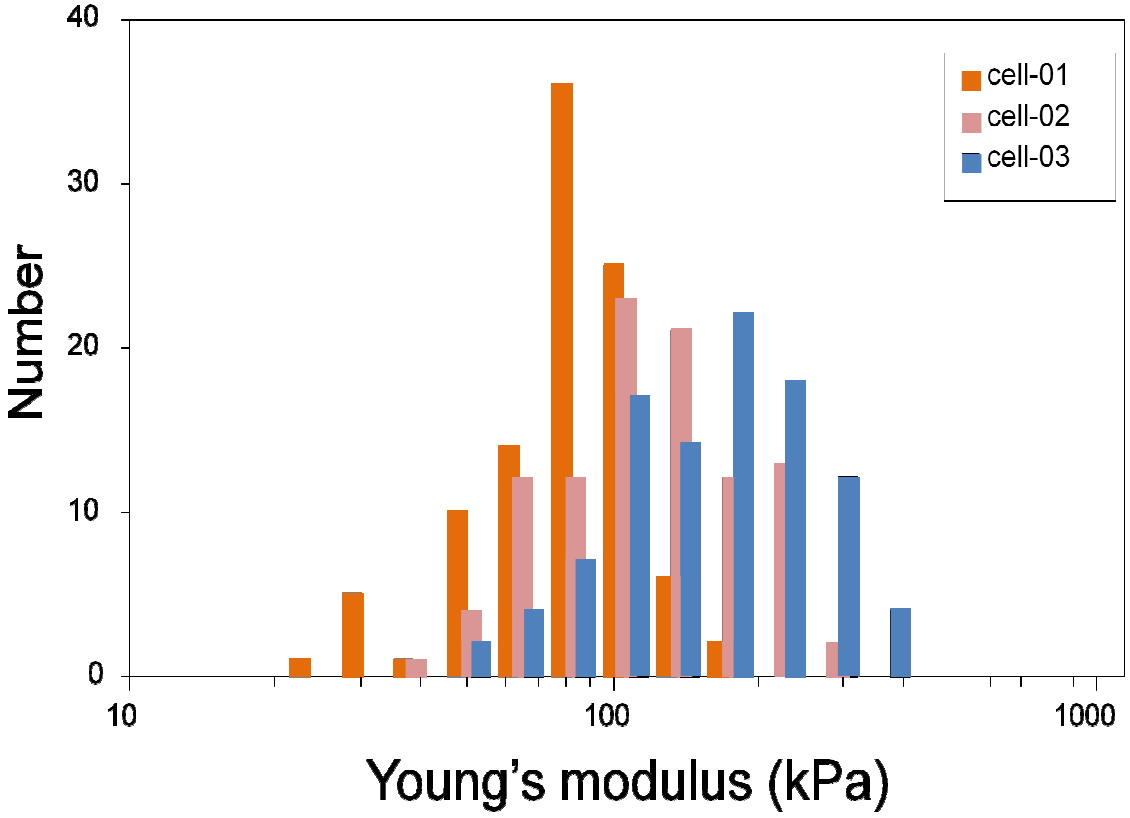

Fig.2.6 Distribution of Young's modulus of same MSCs. The Young's modulus of each cell (total 3 cells) is measured at 100 times repeatedly. The distribution pattern of Young's modulus of rat MSCs shows log-normal pattern.

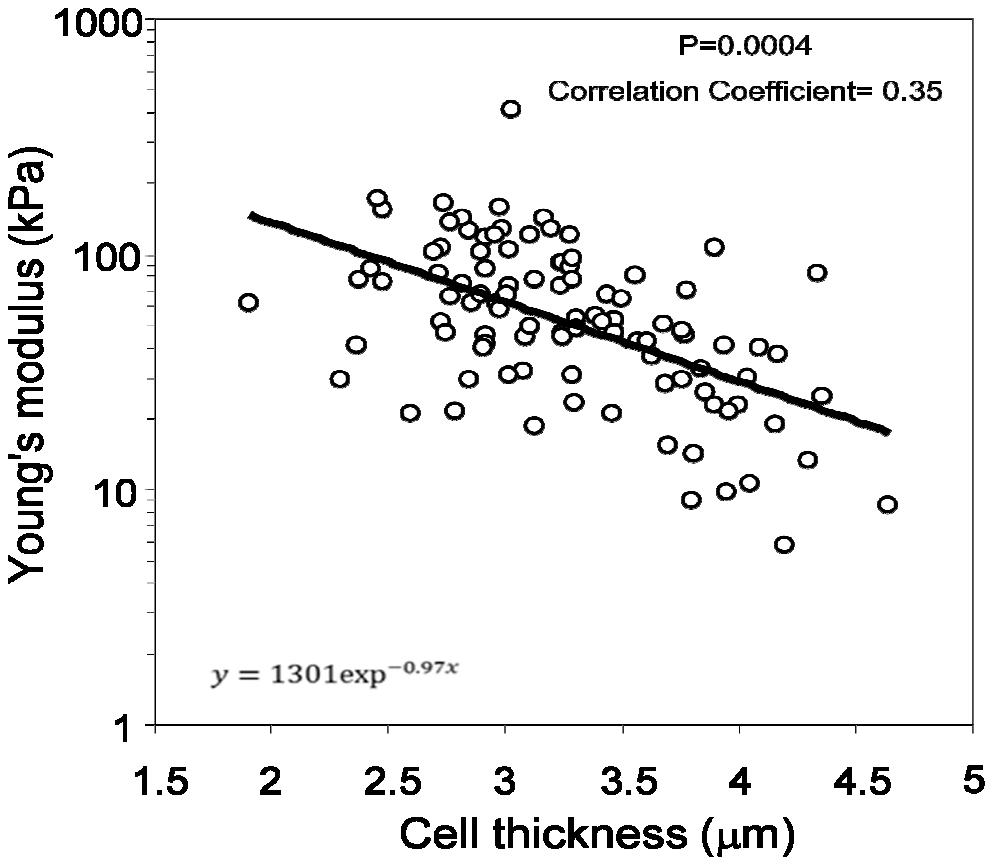

Fig.2.7 Relationship between cell elasticity and thickness in rat MSCs. Each data point is for one cell (total 100 cells). The line shows approximated curve for the points (R = 0.35, P = 0.00043).

2.3.2 Regulation of stiffness and thickness of MSCs by actin cytoskeleton

An intact actin cytoskeleton contributes a major part of cell stiffness, yet there are several forms of actin cytoskeleton in a cell, e.g., stress fibers, lamellipodia, filopodia, and cortical actin. Here, I examined the effect of actin stress fibers and lamellipodia on stiffness and thickness of adherent rat MSCs, using several pharmacological agents that affect the actin cytoskeleton (Fig.2.8). I used gentle concentrations of all agents to avoid inducing obvious morphological changes (Fig.2.9). Ras homolog (Rho) inhibitor C3 transferase, Rho-kinase (ROCK) inhibitor Y-27632, and myosin II ATPase inhibitor blebbistatin prevent and attenuate stress fiber formation [57−59]. The Young's moduli of the cells treated with these agents decreased relatively while their thickness increased (Fig.2.10). On the other hand, the properties of the cells treated with myosin light chain phosphatase inhibitor calyculin A [60], which activates actomyosin formation and enhances actin polymerization in stress fibers, lamellipodia formation, and cortical actin, were hardly altered (Fig.2.10). Moreover, cells treated with the N-WASP inhibitor wiskostatin, which inhibits lamellipodia formation [61], showed no changes in either the Young's modulus or thickness (Fig.2.10). Thus, the cell stiffness and thickness of adherent rat MSCs were strongly affected by attenuation of actin stress fibers, but were barely influenced by activation of actomyosin formation or inhibition of lamellipodia formation.

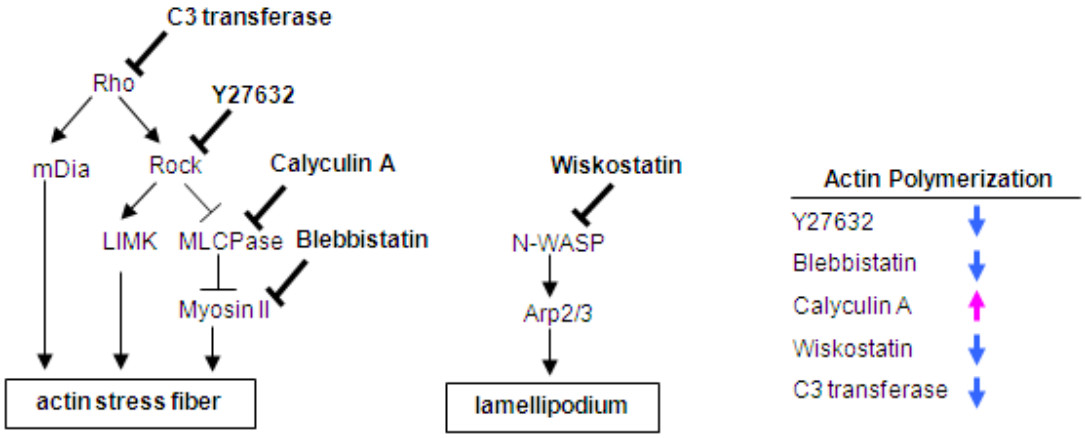

Fig.2.8 Schematics of the chemical agents effects on actin cytoskeleton. C3 transferase, Y-27632, and blebbistatin inhibit actin polymerization and stress fiber formation. Oppositely, calyculin A inhibits myosin light chain phosphatase and results in actin polymerization including stress fiber and cortical actin formation. Wiskostatin inhibits lamellipodium formation.

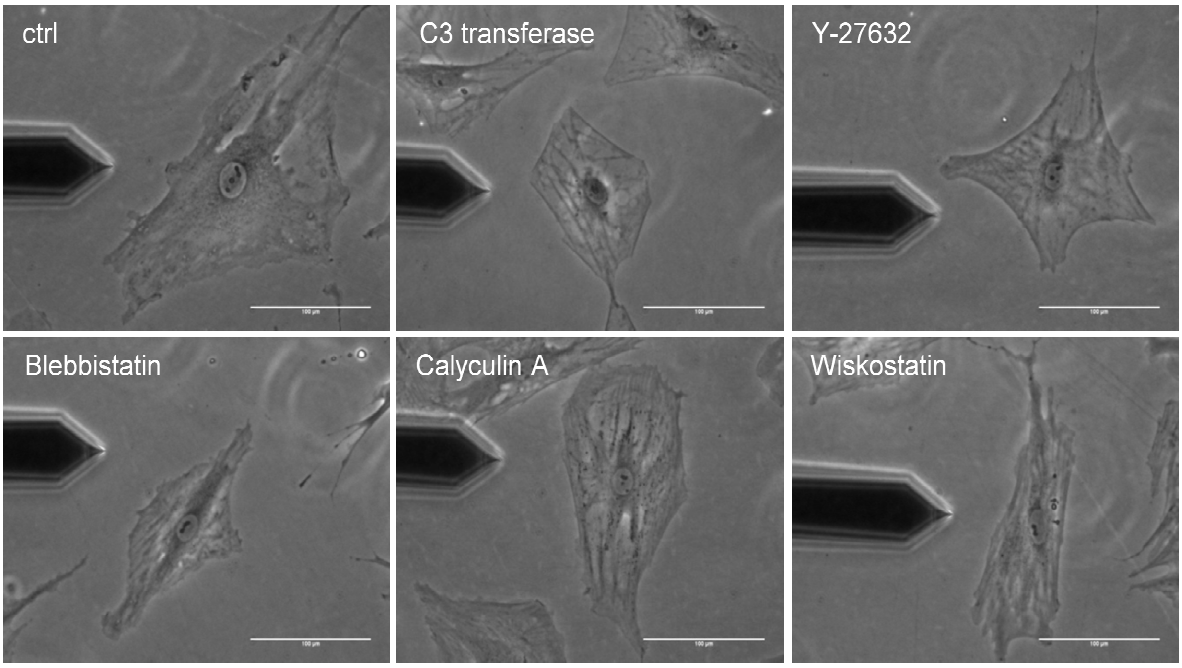

Fig.2.9 Phase contrast images of agents treated rat MSCs. The AFM probe is observed at left side in each image. Bar is 100 μm.

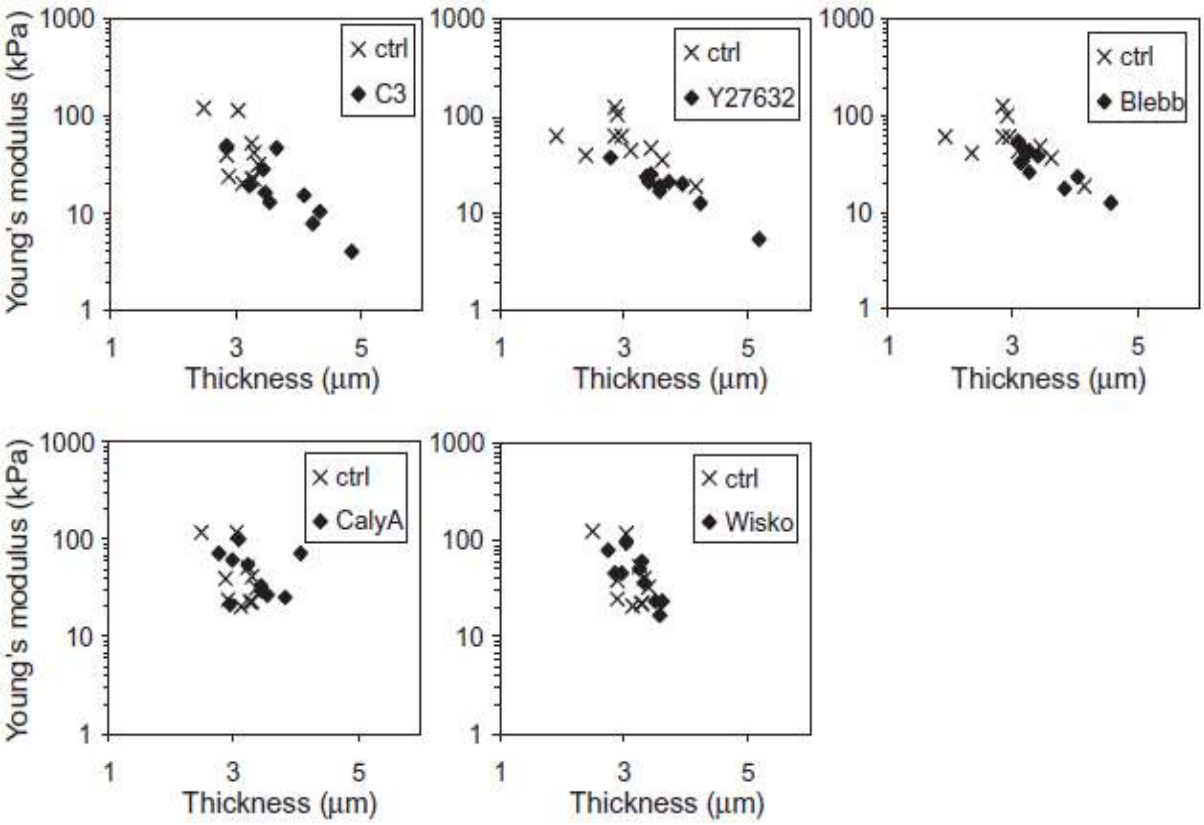

Fig.2.10 Influence of the agents on Young's modulus and thickness of rat MSCs. Each point indicates a data from each cell (a total of 10 cells for each condition). C3 transferase (C3), Y-27632 (Y27632), and blebbistatin (Blebb) decreased surface rigidity of rat MSCs and increased cell thickness. On the other hand, calyculin A (CalyA) and wiskostatin (Wisko) had little impact on these physical properties of MSCs.

2.3.3 Actin cap correlation with cell thickness and stiffness of MSCs

Actin filament structures that form a cap or dome located above the apical surface of the nucleus, referred to as the perinuclear actin cap, regulate the nuclear shapes of adherent fibroblasts [23]. The perinuclear actin cap is specifically disorganized or eliminated by the inhibition of actomyosin contractility. To identify a possible role of the perinuclear actin cap in regulation of stiffness and thickness of rat MSC, I examined the changes in the actin cap organization in rat MSC under the presence of each actin cytoskeleton- modifying agent by observing with confocal laser scanning microscope. The majority of rat MSCs had a well-developed perinuclear actin cap under normal culture conditions (Fig.2.4), rendering a flat shape to rat MSCs. Analysis of collected images demonstrated that treatment with actin stress fiber-formation inhibitors, namely, C3 transferase, blebbistatin, and particularly Y-27362, led to an increase in the number of cells with no actin cap as compared to the control cells (Fig.2.11). In contrast, more MSCs possessed an organized actin cap after treatment with calyculin A and wiskostatin (Fig.2.11). Attenuation of actin stress fibers results in reduction of perinuclear actin cap organization, which corresponds to the data of the cell thickness and stiffness of rat MSCs (Figs.2.10 & 2.11). However, augmentation of actin cap organization had little impact on the cell thickness and stiffness of rat MSCs (Figs.2.10 & 2.11).

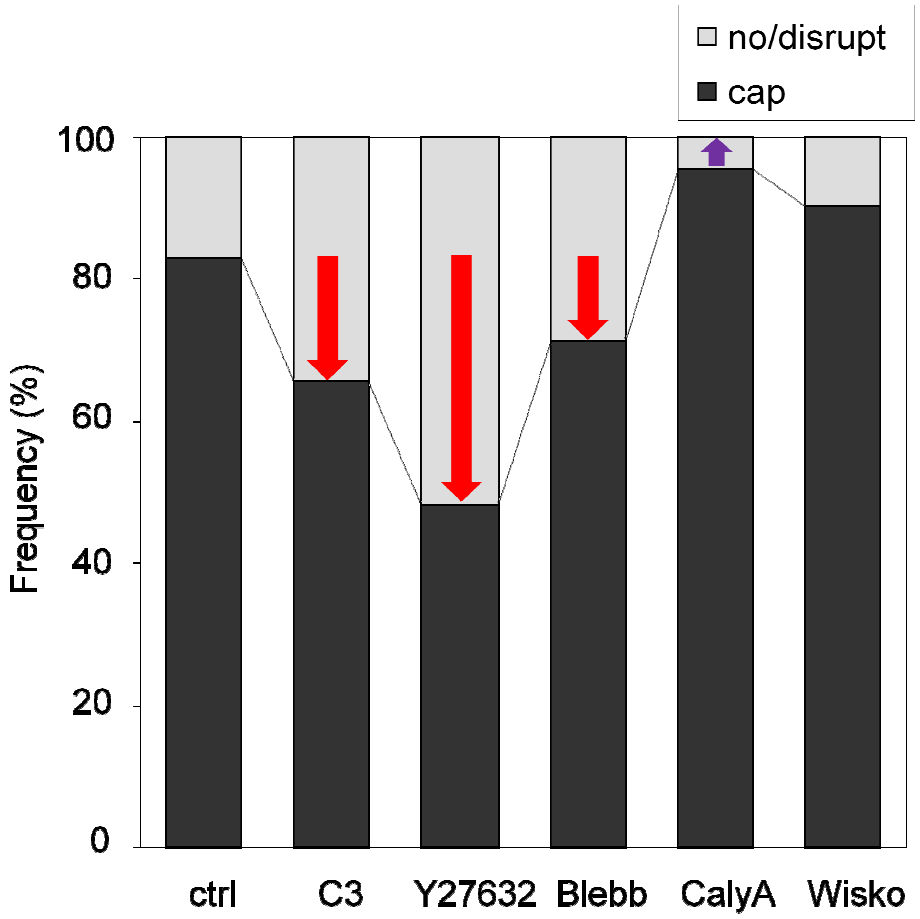

Fig.2.11 Organization of perinuclear actin cap of rat MSCs in treatment of the agents. Frequencies of organization and no/disruption of perinuclear actin cap are shown. The presence of the perinuclear actin cap of each condition was determined from more than 23 cells. C3 transferase (C3), Y-27632 (Y27632), and blebbistatin (Blebb) decreased actin cap organization, on the other hand, calyculin A (CalyA) slightly increased actin cap organization.

2.3.4 Effect of actin cytoskeleton on proliferation activity of MSCs

Population thickness of adhered human MSCs may be related to proliferation activity at the donor level [3]. I thus examined the possible affect of actin cytoskeleton on proliferation activity of rat MSC population to determine whether cell stiffness relates with proliferation. Adding the agents to the cell culture media revealed that Y-27632, C3 transferase, and blebbistatin, which attenuate the actin stress fibers and the perinuclear actin cap, slightly increased the growth activity of rat MSCs (Fig.2.12). On the other hand, upregulation of perinuclear actin cap formation, as caused by treating the MSCs with wiskostatin or calyculin A, had little effect on cell proliferation (Fig.2.12). These data consist with the results of cell thickness and stiffness. I therefore propose that actin cap organization regulates the proliferation activity and cell thickness and stiffness of rat MSC.

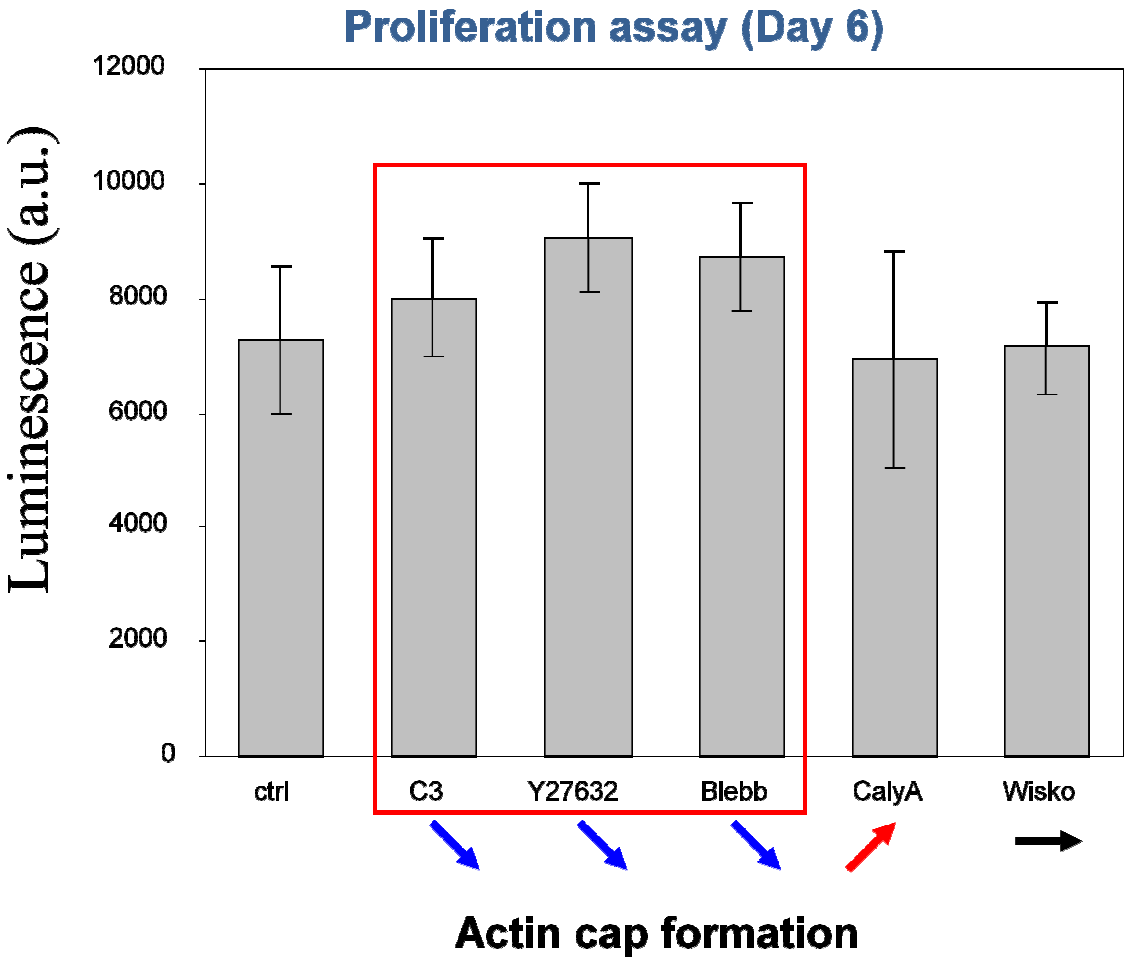

Fig.2.12 Proliferation activity of rat MSCs culturing with the agents. The cell number for 6 days culturing was evaluated by measuring the intracellular ATP concentration with chemiluminescence system. C3 transferase (C3), Y-27632 (Y27632), and blebbistatin (Blebb) slightly increased the cell numbers, on the other hand, calyculin A (CalyA) and wiskostatin (Wisko) do not influence on the proliferation.

2.3.5 Role of actin cytoskeleton in replicative lifespan of MSCs

In vitro cell expansion is an essential process. Since MSCs harvested from patients are limited in quantities. However, they have a finite life span in vitro and stop growing due to cellular senescence. In other words, they grow larger, flatten shape, express senescence-associated marker (β-galactosidase) and lose their proliferative activity after several passages [62]. To examine the effect of actin cytoskeleton on long-term culture of MCSs, the cells were treated with 2 and 10 μM concentrations of ROCK inhibitor Y-27632 and the population doubling was recorded over the culture days. The results show that downregulation of F-actin polymerization has the potential to boost the growth kinetics of cultured MSCs (Fig. 2.12). To confirm the role of actin cytoskeleton in aging of MSCs, cellular senescence assay was performed by staining for β-galactosidase. Compare to control cells, treatment with Y-27632 notably reduced the percentage of MSCs which express the senescence related enzyme (Fig.2.13).

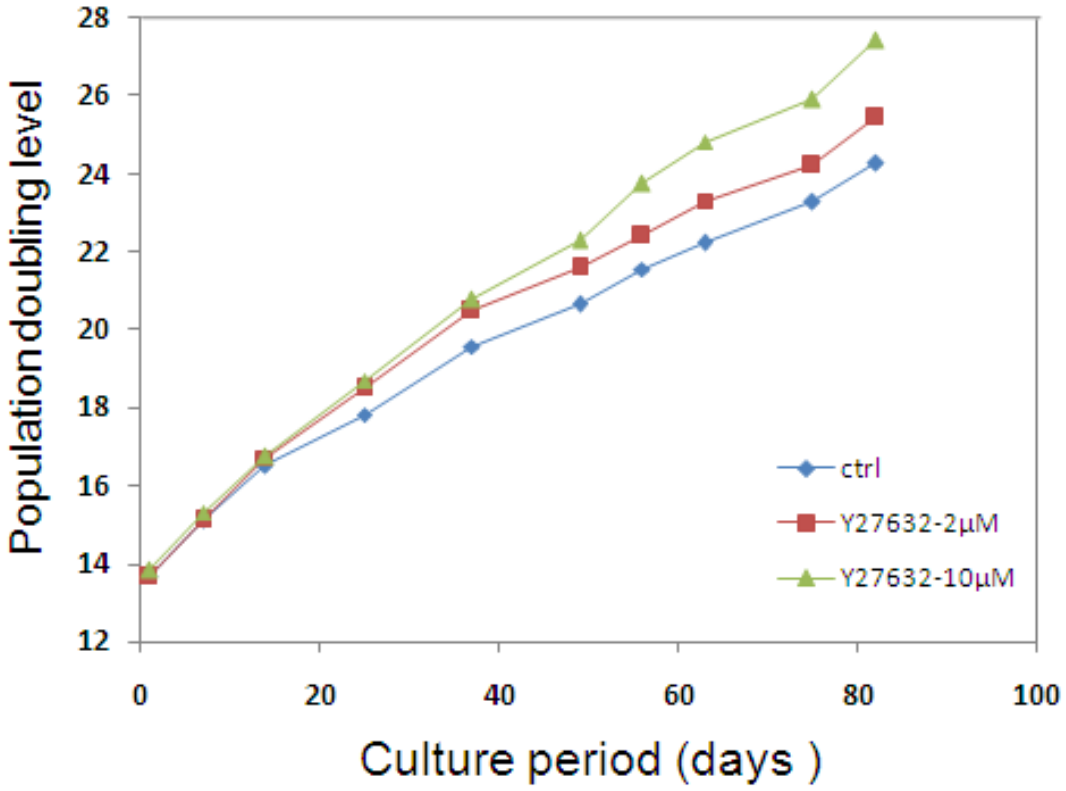

Fig.2.13 Long-term growth of MSC with modified actin cytoskeleton. Compared to the control cells, treating the MSCs with Y-27632 during a culture period of 100 days clearly increased the division number.

	Cell count	β-gal	Percentage (%)
Ctrl	282	240	85.1
Y-2μM	351	213	60.7
Y-10μM	742	211	28.4

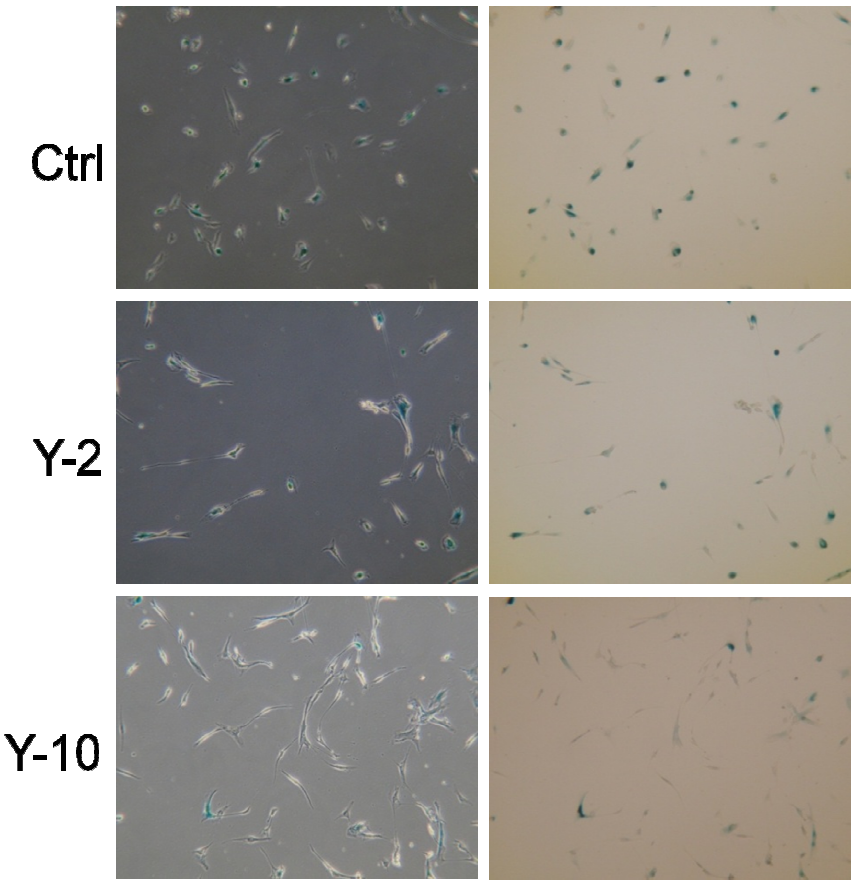

Fig.2.14 β-galactosidase staining assay of MSCs. Aged cells which express high amount of the enzyme stain blue. Percentage of senescent cells was lower in the Y27632-treated cell.

2.4. Discussion

In this study, I experimentally demonstrated two major points relevant to surface stiffness of substrate-adhering rat MSCs. One is that cell stiffness and cell thickness showed an inverse correlation at a single-cell level. The second is that the perinuclear actin cap organization regulates the cell stiffness, thickness, and possibly proliferation activity of rat MSCs. A schematic diagram of the findings are shown in Fig.2.15. Originally, MSCs adhere flat on a given substrate, and their actin stress fibers and perinuclear actin cap are well developed. A developed actin cap flattens out the nucleus and increases surface stiffness. On the other hand, cells with depolymerized stress fibers lose their actin cap, with a resulting decrease in surface stiffness, and the nucleus boosts the cell height according to the plasticity of nuclear lamin A [55]. Thus, although surface stiffness and cell thickness are essentially different physical properties of cells, the perinuclear actin cap coordinates these properties in MSCs. However, these cell properties were not affected by development of the actin cap organization after treatment with either calyculin A or wiskostatin. In particular, calyculin A is an activator for actomyosin formation, and it increases surface stiffness in Drosophila embryonic S2R+ cells by accelerating cortical actin formation [51]. Cortical actin determines isotropic cortical tension of non-adherent or mitotic cell [63], and the surface stiffness of some cells is mainly determined by this cortical actin formation [51]. Thus, it is believed that anisotropic surface tension that arises from the perinuclear actin cap is higher than the isotropic cortical tension in MSCs, which would explain why behavior of the stiffness of rat MSCs differed from the above cell. In addition, further-developed stress fibers and actin cap of MSCs may induce partial buckling of the actin

cytoskeleton [64] or fluidization of cell [65]; the physical properties are unaffected by augmentation of the actin cap formation. Interestingly, the stress fiber-attenuated MSCs tended to show a high proliferation activity. This result corresponds with the previous study relating cell thickness with proliferation activity in human MSCs [35, 36]. These results additionally show that the states of the actin cap and actin stress fibers in MSCs are potent regulators of the proliferation activity of each cell. It is well known that mechanical properties of cell environments control cell life [66, 67]. It was also demonstrated that proliferation capacity of MSCs can be improved over time by regulating their actin cytoskeleton. Normal MCSs enter senescence and lose their valuable potentials gradually during in vitro culture period. It is known that beta-GAL activity increases in late passage MSC, but report no differences between MSC from young and aged donors [68]. The experimental data from β-galactosidase assay reveals that actin cytoskeleton is closely correlated with cellular senescence of MSCs. Commitment of differentiation lineage of MSCs is specified by matrix elasticity which is sensed by actomyosin contraction [69]. Furthermore, the surface stiffness of MSCs changes depending on the substrate elasticity. The surface stiffness of MSCs also changes during cell differentiation [70]. The present study reveals that the surface stiffness of MSCs is regulated by actin stress fibers, including the perinuclear actin cap, and is related with proliferative activity. Thus, the mechanical properties of MSCs are potent indicators for their cell behavior and physiological functions. The evaluation of cell quality and estimation of cell activities of MSCs are essential cytotechnology for applications in regenerative medicine and tissue engineering. I predict

that in the future non-destructive and high-speed methods of measuring mechanical properties of MSCs will become an essential part of the cytotechnology.

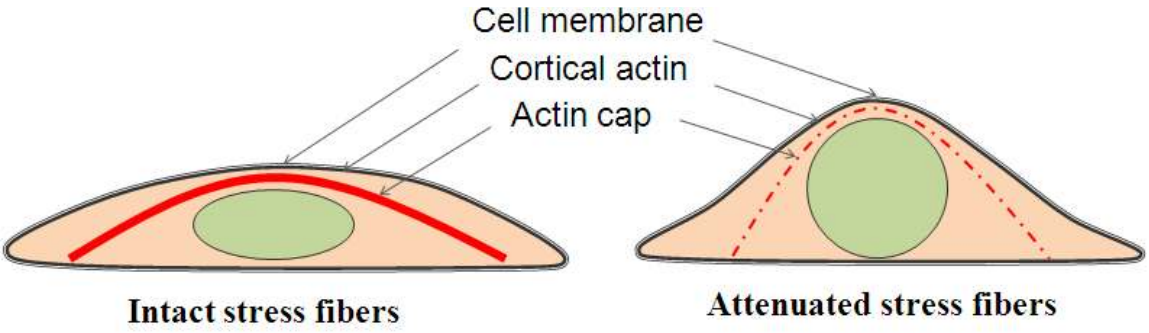

Surface stiffness	High	low
Thickness	Low	High
Tension source	Actin cap	Cortical actin
Proliferative activity	Normal	Increased
Replicative Senescence	Normal	Postponed

Fig.2.15 Overview of the physical properties of MSCs. In normal MSCs, developed perinuclear actin caps generate high surface tension and press tightly against the nucleus, giving the cells a rigid surface stiffness and flat thickness. In contrast, in stress fibers-attenuated MSCs, the surface tension was decreased and the cell surface was boosted by the nucleus, resulting in the cells with elastic surfaces and a high thickness. Furthermore, elastic and tall cells tended to have high proliferative activity.

2.5 Summary

Mesenchymal stem cells (MSCs) have been extensively investigated for their applications in regenerative medicine. Successful use of MSCs in cell-based therapies will rely on the ability to effectively identify their properties and functions with a relatively non-destructive methodology. In this study, I measured the surface stiffness and thickness of rat MSCs with atomic force microscope and clarified their relation at a single-cell level. The role of the perinuclear actin cap in regulating the thickness, stiffness, and proliferative activity of these cells was also determined by using several actin cytoskeleton-modifying reagents. This study has helped elucidate a possible link between the physical properties and the physiological function of the MSCs, and the corresponding regulatory role of the actin cytoskeleton.

Chapter 3

Elastic features of adherent and suspended cells

3.1 Introduction

Alterations of biological activities and transformations of cell states often entail mechanical behavior change of the composed cells. In particular, alteration in cell stiffness/elasticity has emerged as a marker for cellular phenotypic events and diseases [71 -73]. During optic-cup morphogenesis, change in the level of stiffness of the retinal epithelium is important for formation of neural retina tissue [74]. The stiffness of red blood cells increases by infection with Plasmodium falciparum [75]. Malignant cancer cells are less stiff than normal cells [76-78]. Mechanical properties are largely attributable to structure of actin cytoskeleton [52, 79], and thus these stiffness alterations probably show the remodeling process of actin cytoskeleton in these cellular events and disease states [80].

The remodeling regulation of actin cytoskeleton has important role in the cancer cell life. Actin depolymerization and disrupted stress fibers, marked by a shift in F-actin to G-actin, occurs in early stages of malignant transformation [81, 82]. Besides, abnormal distribution of F-actin favoring cell migration occurs in the later stage of cancer corresponding to tumor cell invasiveness and metastasis [83]. Thus, sensitive and high speed estimation methods for the remodeling of actin cytoskeleton in cancer cells act as a powerful tool for early detection of cancer. Then the stiffness and other mechanical properties are potent detectable targets of the cancer cytotechnology.

There are some methods to detect elasticity and other mechanical properties, including micropipette aspiration, magnetic twisting cytometry, optical traps, cell poking, scanning acoustic microscopy and atomic force microscopy [11, 40, 8, 42, 84, 7,]. These technologies reveal cell stiffness and mechanical properties in adhered or suspended state of cells with diverse scale. The micropipette aspiration and optical traps aim to suspended cells, and on the other hand, the magnetic twisting cytometry and AFM generally aim to substrate adhered cells. In particular, AFM has been incrementally used to directly measure the cancer cell stiffness in many studies [85-87].

AFM can be used to image live cells and probe their mechanical properties in physiological conditions in a nondestructive manner and at a high spatial resolution [44, 79]. It analyzes these stiffness of a living cell by the probe indentation method, an AFM cantilever serves as a microindenter to probe the cell directly [45]. Thus, AFM analysis can sensitively disclose the difference of structure of actin cytoskeleton between adherent normal and cancer cells as the difference of cell surface stiffness [88-91]. For the present, these stiffness cytotechnologies for cancer cells are only adapted to adherent cells because the difference of structure of actin cytoskeleton between cancer and normal cell is well known only in adherent state. However, most useful cytotechnology for detection of cancer cells, such as circulated tumor cell in blood and biopsy of cancer, should be applicable to suspended cell states. To that end, it is required to demonstrate the cell stiffness and the structure of actin cytoskeleton of suspended cancer cells in comparison with normal cells.

The stiffness of suspended leukocytes and trypsinized cells can be measured with AFM by using a biocompatible anchor for membrane (BAM) substrate [48, 92]. BAM

molecule contains an oleyl group, a poly ethylene glycol (PEG) domain and an NHS-reactive ester group, and the surface presented oleyl group of BAM substrate anchors the suspended cells (Fig.3.1) [93]. The morphology of the substrate adherent and spread cells is different in each cell, and orientation and distribution of their actin cytoskeleton is anisotropy and heterogeneous. On the other hand, BAM anchored suspended cells show homogeneous round shape and isotropic actin cytoskeleton vicinity of their plasma membrane [92]. These cortical actin structures of rounded cells have no apparent discrimination in different cell types [92]. Therefore, there is a possibility that the structure and features of actin cytoskeleton of suspended cancer cells are not difference from those of suspended normal cells. Though the cortical actin structure of trypsinized and mitotic round cells seemed to develop similarly, the surface stiffness of the trypsinized round cells showed greater stiffness than that of mitotic round cells [92]. Thus, the stiffness/elasticity measurements may detect invisible information about the maturation or strength of the actin cytoskeleton network in vicinity of cell surface.

In this study, I examined the structures and regulatory mechanisms of actin cytoskeleton and surface stiffness of cancer and normal cells between adherent and suspended states. Furthermore, to demonstrate the difference of features of actin cytoskeleton between cancer and normal cells, I compared those with human embryonic kidney HEK293 cells, which bearing immature actin cytoskeleton. Normal cells had developed actin stress fibers, but cancer cells and HEK293 cells did not have developed fiber structures of actin cytoskeleton. The BAM anchored suspended all cells showed similar cortical actin structures without recourse to cell types. Only cancer cells, however,

had many microvillus structures consists of F-actin on their surface in both adherent and suspended states. Although the difference of stiffness between cancer and normal cells decreased by detaching the cells from substrate, the difference of stiffness response for actin cytoskeleton modifying reagent of cancer and normal cells kept in even suspended states. Thus, the regulatory mechanism for actin cytoskeleton of cancer and normal cells are probably different in not only adherent states but also suspended states. In addition, these results demonstrate that it is able to discriminate the features and structures of actin cytoskeleton between cancer and normal cells in suspended states using stiffness measuring method.

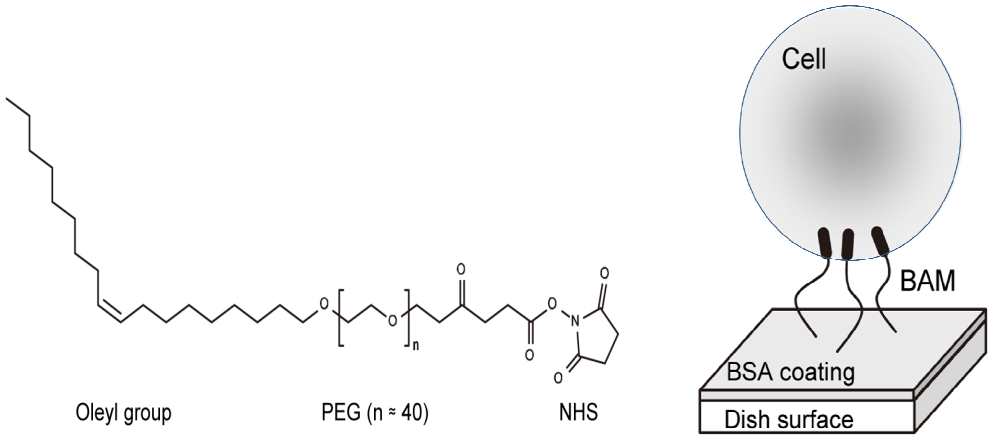

Fig.3.1 Structure of a BAM molecule (left) and schematic of BAM coating to which a suspended cell is anchored (right).

3.2 Experimental procedure

3.2.1 Materials

The pyramidal probe (SN-AF01S-NT; spring constant: 0.02 N/m) was purchased from Seiko Instruments Inc. (Tokyo, Japan). Human diploid fetal lung fibroblasts, TIG-1 cells, established at the Tokyo Metropolitan Institute of Gerontology [94], human embryonic kidney cells, HEK293 cells, human cervix cancer cells, HeLa cells, and human fibrosarcoma cells, HT1080 cells were obtained from Health Science Research Resources Bank (Osaka, Japan). Fisher 344 male rats were purchased from Japan SLC (Shizuoka, Japan). Eagle's minimal essential medium (MEM), Dulbecco's modified Eagle's medium (DMEM), and antibiotics were purchased from Sigma-Aldrich (St. Louis, MO). Fetal bovine serum (FBS) was purchased from JRH Biosciences (Lenexa, KS). Biocompatible Anchor for Membrane (BAM; SUNBRIGHT OE-020CS) was purchased from NOF Corporation (Tokyo, Japan). F-actin labeling kit was purchased from AAT Bioquest, Inc (Sunnyvale, CA). Glass based culture dishes were purchased from Asahi Glass Co., Ltd (Tokyo, Japan). Other reagents were obtained from Sigma-Aldrich, Wako Pure Chemical Industries Ltd. (Osaka, Japan), or Life Technologies Ltd. (Tokyo, Japan).

3.2.2 Preparation of BAM-coated dishes

The BAM coated dishes were prepared as follows. The polystyrene and glass based tissue culture dishes were coated with 5% bovine serum albumin (BSA) in PBS for 1 hour. After washing with Milli-Q water, the surfaces were treated with 1 mM BAM in PBS for

30 minutes. Then, the BAM coated dishes were washed and dried. The without BAM coated dishes means regular cell culture dishes.

3.2.3 Preparation and culture of MSCs

Rat MSCs were isolated and primarily cultured as described previously [54]. In brief, bone marrow cells were obtained from the femoral shafts of 7-week-old male Fisher 344 rats. The cells were obtained from at least 2 rats and mixed. The culture medium was MEM containing 15% FBS and antibiotics (100 units/mL penicillin G, 100 μg/mL streptomycin sulfate, and 0.25 μg/mL amphotericin B). The medium was renewed twice a week, and cells at passages 2–6 were used in this study. The animal experiment was approved by the ethics committee of National Institute of Advanced Industrial Science and Technology (AIST), Japan.

3.2.4 Cell cultures and drug treatment

TIG-1, HeLa, HT1080, and HEK293 cells were maintained in DMEM containing 10% FBS and antibiotics. The culture medium was replaced twice a week or triweekly. For the adherent and suspended states examination, cells were treated with Y-27632 (20 μM) and Calyculin A (0.1 nM) and incubated 12 h. For the suspended state, cells were removed from the culture dish by treatment with 0.25% trypsin-0.02% EDTA in PBS and plated on the BAM-coated dish for 30 minutes in normal culture medium then washed with PBS to remove the unattached cells and incubated 12 h in the drug-included medium. The cells attached on the culture dishes and BAM-coated surfaces with or without the drug were

manipulated by AFM (Fig.3.2). Actin-depolymerization of the cells was induced by treatment with 5 μM cytochalasin D for 2 h.

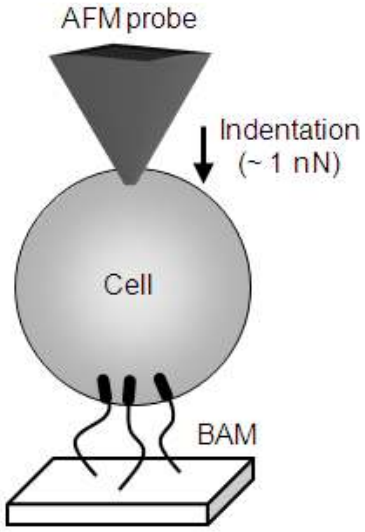

Fig.3.2 Indentation of BAM-anchored round cells by AFM

3.2.5 Evaluation of actin cytoskeleton

To visualize different actin cytoskeleton microstructures, the cultured cells on glass base dishes with or without BAM coating (for suspended and adherent states) were fixed with 4% paraformaldehyde, permeabilized with 0.5% Triton X-100, and then stained with the F-actin labeling kit for actin filaments. Specimens were observed by confocal laser scanning microscope equipped with × 60 oil immersion lens (NA = 1.42) in 0.5 μm serial sections. Superimposition of the serial images processed with ImageJ software (NIH, Bethesda, MD).

3.2.6 AFM measurements

Adherent and suspended cells in the medium were examined by AFM at room temperature. Combination of optical microscope (IX-71, Olympus) and atomic force microscope allows positioning the probe onto a particular region of a cell. Here, the atomic force microscope probe was indented into the top of the cell nucleus up to 1 nN at 5 μm/s. The Young's modulus of the cell was calculated in accordance with the Hertz model [30]. The force-distance curve at the region up to about 500 nm of cell surface indentation was fitted by JPK data processing software (JPK instruments AG) as:

$$F = \frac{E}{1-\nu^2}\frac{\tan\alpha}{\sqrt{2}}\delta^2$$

where, F = force, δ = depth of probe indentation, ν = Poisson's ratio (0.5), α = face angle of the pyramidal probe (20º), and E = Young's modulus. All experiments were performed in more than 20 cells, and each cell was examined at more than 25 points on the top of the cell. The median value was adopted for the Young's modulus of each cell [79].

3.2.7 Statistic analysis

The alteration similarity of Young's modulus of cells was clustering analyzed with College Analysis software created by Prof. Masayasu Fukui (Fukuyama Heisei University, Hiroshima, Japan). I used the alterations of logarithmic average value of the Young's modulus in the analysis. The responsiveness of the Young's modulus for Y-27632 or calyculin A in adhered or suspended states were used as variables in each cell. The distance of each element was calculated with standardized Euclidean distance method and the clustering construction was used as Ward method.

3.3 Results

3.3.1 Actin cytoskeleton organization of adherent and suspended cancer and normal cells

In this study, I used two types of normal stromal cells, rat MSCs and human fibroblasts TIG-1, two types of cancer cell lines, HeLa and HT1080 cells, and single kidney cell line HEK293 cells. The adhered normal MSCs and TIG-1 cells showed flat and elongated morphology (Fig.3.3). HeLa, HT1080 and HEK293 cells adhered on the culture substrate but they did not show large and highly elongated morphologies like normal cells (Fig.3.3). After cell detachment from the culture substrate by trypsinization, these suspended cells anchoring on BAM substrate showed almost round shapes without recourse to cell types (Fig.3.3). By detachment cells from normal culture substrate, their morphological asymmetry was apparently canceled.

To characterize the structure of actin cytoskeleton of adhered these cell types and the reorganization from adhered to suspended states, F-actin of these cells in adherent and suspended states were stained by fluorescein labeled phalloidin and observed by CLSM. In the adherent MSCs and TIG-1 cells showed highly developed actin stress fibers across the cell body (Fig.3.4). Particularly they clearly bore filamentous perinuclear actin cap at their apical surface (Fig.3.5). The actin cap is an F-actin structure that forms a cap or dome above the apical surface of the nucleus [53], and it regulates the surface stiffness and thickness of adherent rat MSCs [79]. By contrast, the adhered HeLa, HT1080 and HEK293 cells showed weak stress fibers and scattering spot-like F-actin structures at the base and ruffling lamellipodia at the edge (Fig.3.4). In the focusing on their apical surface, they did not have any developed actin cap structures and have some dense protrusions, and particularly on Hela and HT1080 cells, they had many microvillus structures on their surface (Fig.3.5). Therefore, F-actin structures are obviously different from adhered normal stromal cells and cancer and HEK293 cells; apical surface actin cap structures were developed in normal stromal cells but absent in cancer and HEK293 cells, and furthermore asymmetry of F-actin structures were high in normal cells but scarcely determinable in cancer and HEK cells.

On the other hand, the F-actin structures of these cells changed the whole situation on the BAM surface (Fig.3.6). Without recourse to cell types, they showed apparently same F-actin structures; that is, suspended cells including normal stromal, cancer and HEK293 cells had clear cortical actin structures vicinity of their plasma membrane (Fig.3.6). Although some spotted actin structures were observed inside cells, nothing filamentous

structures were observed. The F-actin of cells on BAM surface showed almost symmetric structures. Fluorescence images also showed that granule-like actin structures replaced the stress fibers in HeLa, HT1080 and HEK293 cells.

To summarize, in the process of cell detachment from the normal substrate, F-actin structures of adhered normal stromal cells were dynamically reorganized from asymmetric stress fibers to symmetric cortical actin (Figs.3.6). In the case of cancer cells, the basal undeveloped F-actin and lamellipodia reorganized to the cortical actin (Figs.3.6). Although the actin structures of adherent normal stromal and cancer cells were obviously different, it was difficult to determine the difference of actin structures of these cells in suspended states.

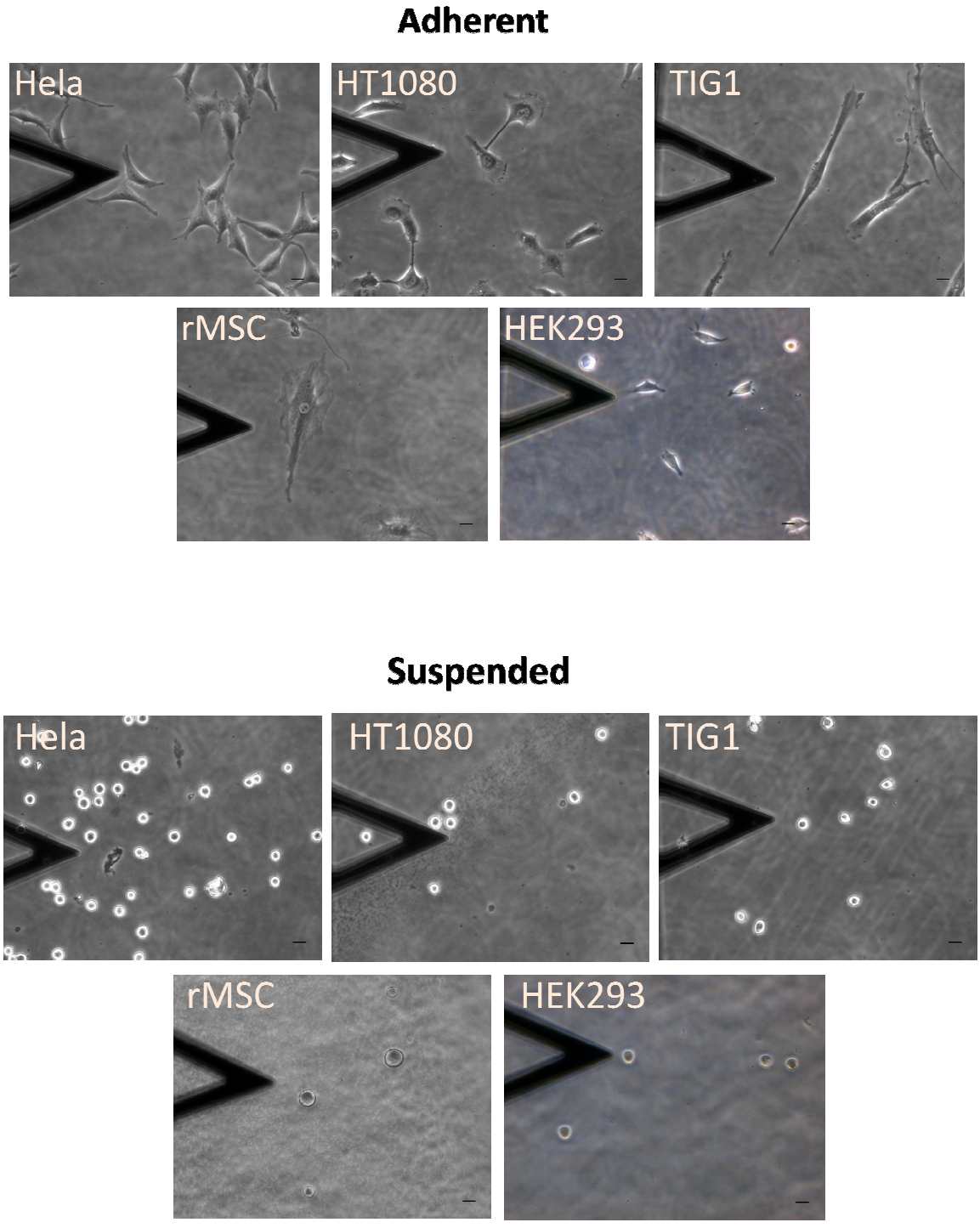

Fig.3.3 Phase contrast images of the examined adherent and suspended cells. Bar is 20μm.

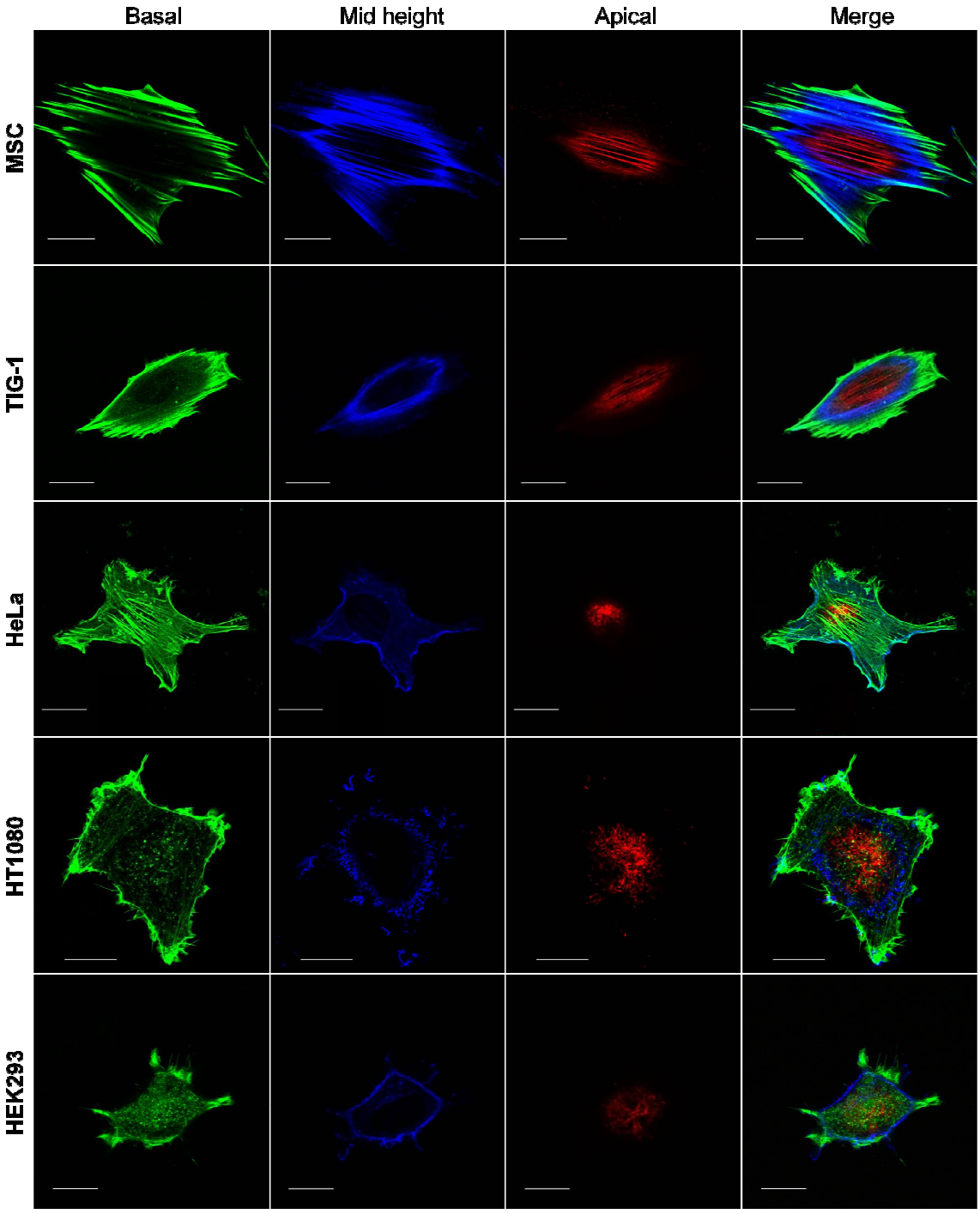

Fig.3.4 Whole actin microstructures of all examined cells from bottom to top. Bar is 20μm.

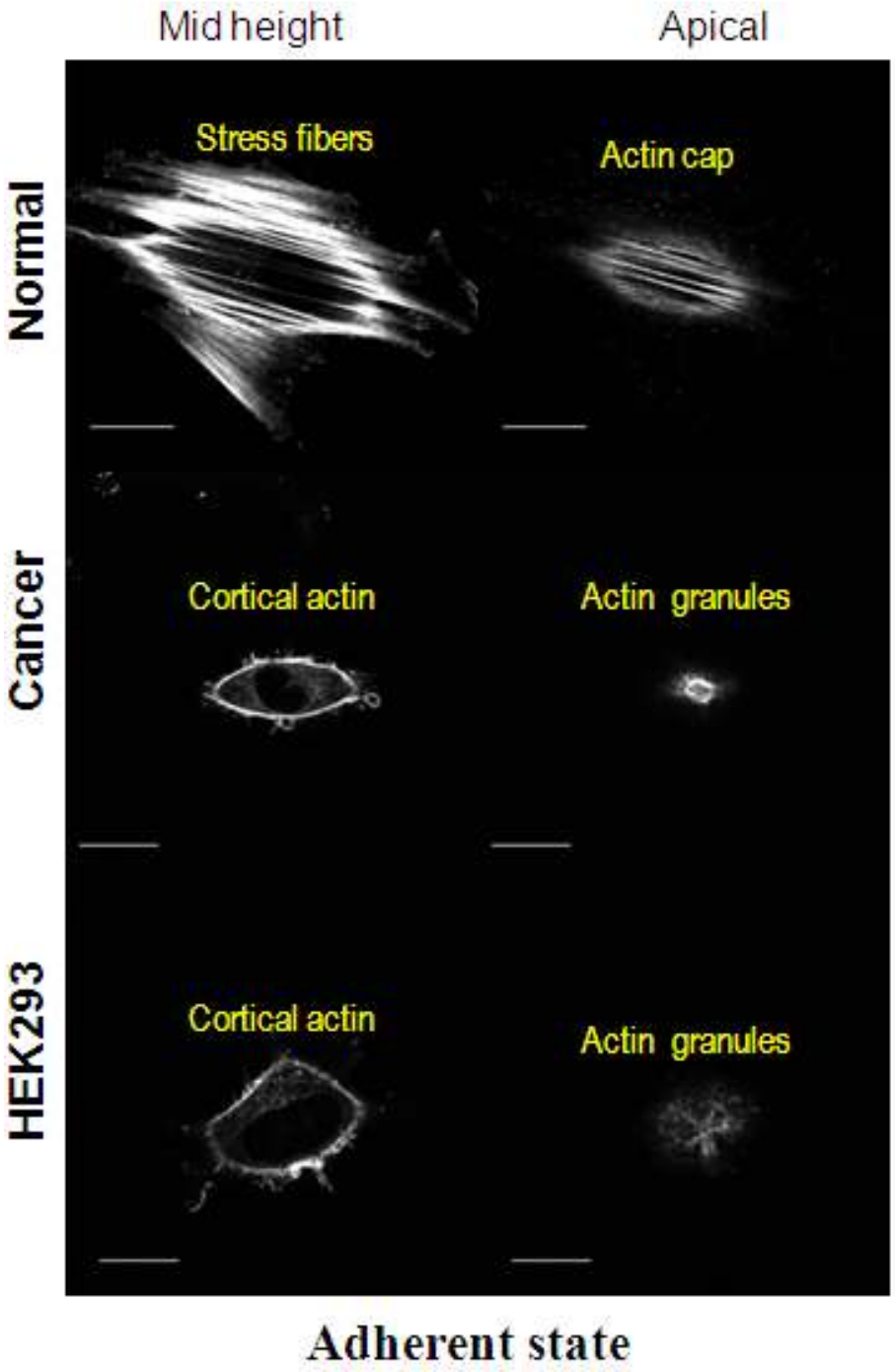

Fig.3.5 Surface actin microstructures of the adherent cell types. Bar is 20μm.

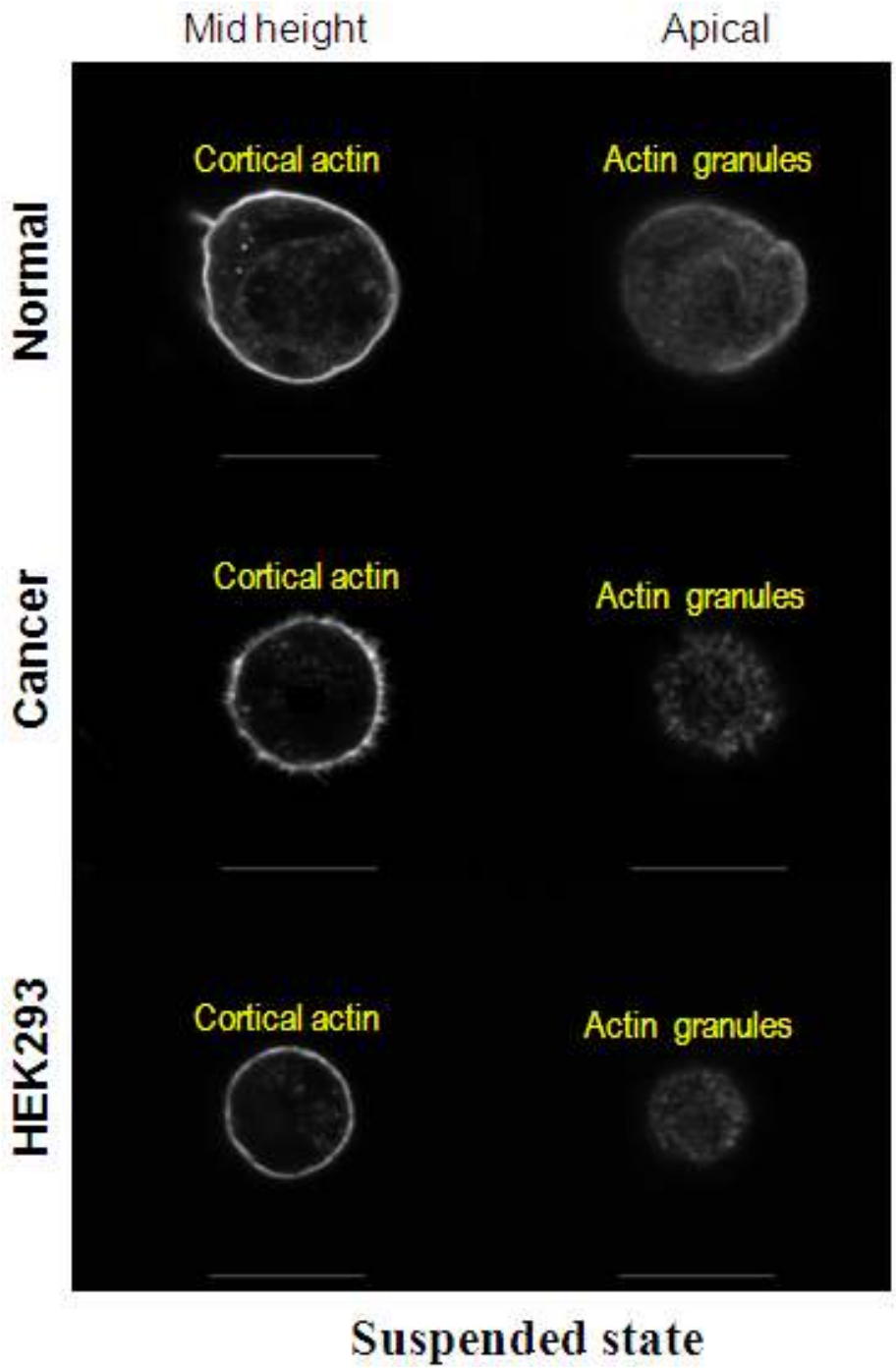

Fig.3.6 Surface actin microstructures of the suspended cells types. Bar is 20μm.

3.3.2 Biomechanical properties of adherent and suspended cancer and normal cells

I then determined the biomechanical properties of these cells in adhered and suspended states by AFM nanoindentation method. To reduce the affect of various cell morphologies, I placed the AFM probe at the points above the nucleus of adhered cells. The Young's modulus distributed broadly without recourse of cell types and cell states (Fig.3.7). From the previous studies, the distribution of Young's modulus of cell corresponds to a log-normal pattern [79, 92]. Thus, I showed the logarithmic average of the Young's modulus in each conditions (Fig.3.7).

The Young's moduli of adhered normal stromal cells were clearly higher than that of cancer cells (Fig.3.7). The Young's modulus of HEK293 cells showed lowest distribution. By detachment from substrate and alteration in cell morphology, the Young's modulus of normal stromal cells slightly decreased but that of cancer cells relatively unchanged (Fig.3.7). On the other hand, the Young's modulus of HEK293 cells obviously increased by detachment of cells from the normal culture dish (Fig.3.7). The difference of the value of Young's modulus in each cell type decreased by release these cells from adhesion state.

The Young's modulus of the suspended state in this study was measured after 12 h from the cell detachment. It is reported that the rigidity of trypsinized suspended MSCs measured by optical stretching increases with time progress [97]. Then, I examined the transitions of the Young's modulus of suspended normal TIG-1 and cancer HeLa cells. The Young's modulus of TIG-1 cells clearly decreased after 1 h of cell detachment (Fig.3.8). On the BAM surface, the Young's modulus of the anchored round TIG-1 cells gradually

increased in a time-dependent manner (Fig.3.8). Though, the Young's moduli of the TIG-1 cells on the BAM surface at 24 h were relatively lower than that in the adhesion states (Fig.3.8). On the other hand, the Young's modulus of suspended HeLa cells anchored on BAM surface were relatively constant, and those on BAM surface were almost same in adhesion state (Fig.3.8).

These Young's modulus values of adherent and suspended cells excepting adhered HEK293 cells were higher than those of cytochalasin D treated actin depolymerized cells (Fig.3.9), and thus these obtained mechanical properties reflect the mechanical characteristics of actin filaments around the cell surface. As regarding to adhered HEK293 cells, it would seem that their actin filaments vicinity of apical surface hardly supported their body mechanically. However, by cancel their adhesion, actin filaments shifted to support their surface mechanically.

Taken together, the mechanical properties of both adhered and suspended cells reflect the mechanical characteristics of actin filament structures in the vicinity of cell surface. The mechanical properties of adhered normal stromal cells were obviously higher than that of cancer cells. In the process of cell detachment from the normal culture substrate, mechanical properties of normal stromal cells decreased (Figs.3.7). In the case of cancer cells, the mechanical properties were almost unchanged in the process of cell detachment from the culture substrate (Figs.3.7). Even in the suspended state, the mechanical properties of normal stromal cells were still higher than that of cancer cells (Fig.3.7).

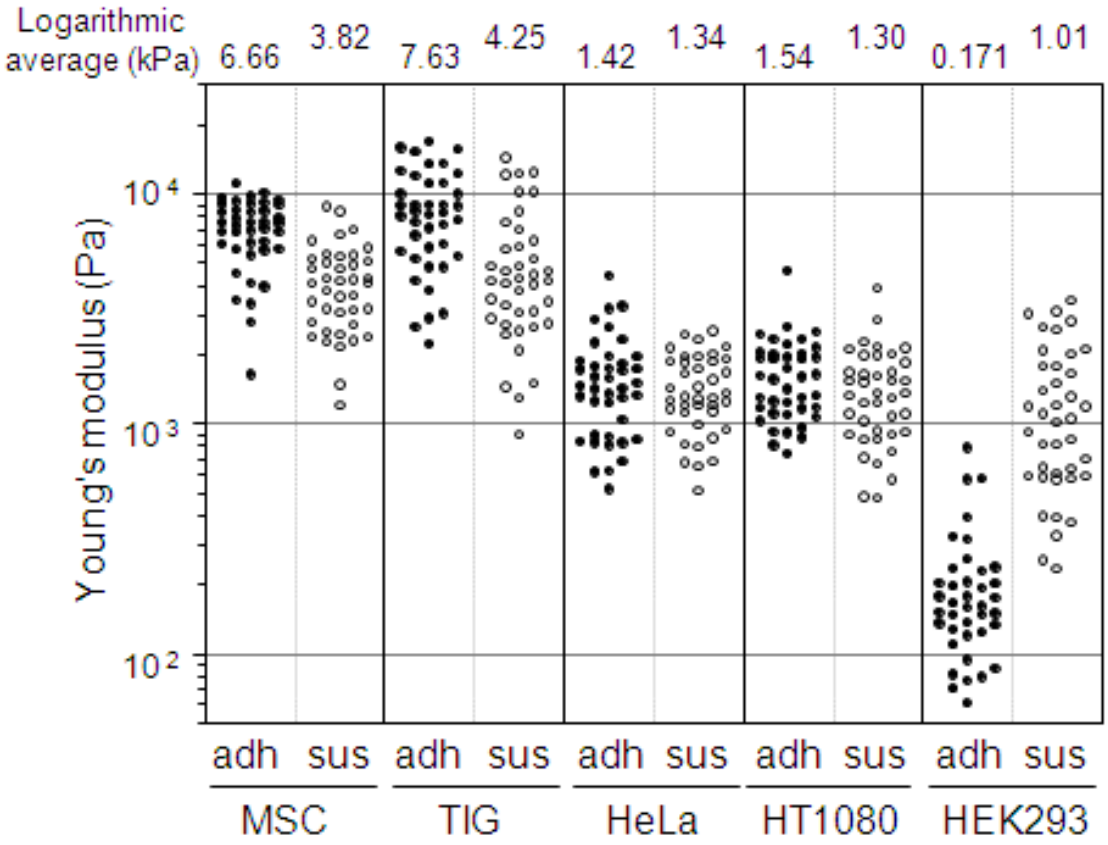

Fig.3.7 Young's modulus of the untreated adherent and suspended cells. Elastic values of normal cells highly dropped after detachment. Cancer cells showed almost no change in their mechanical phenotype upon trypsinization and cell rounding. Strikingly, HEK293 cells showed a significant elastic increase in suspended state compared to adherent state.

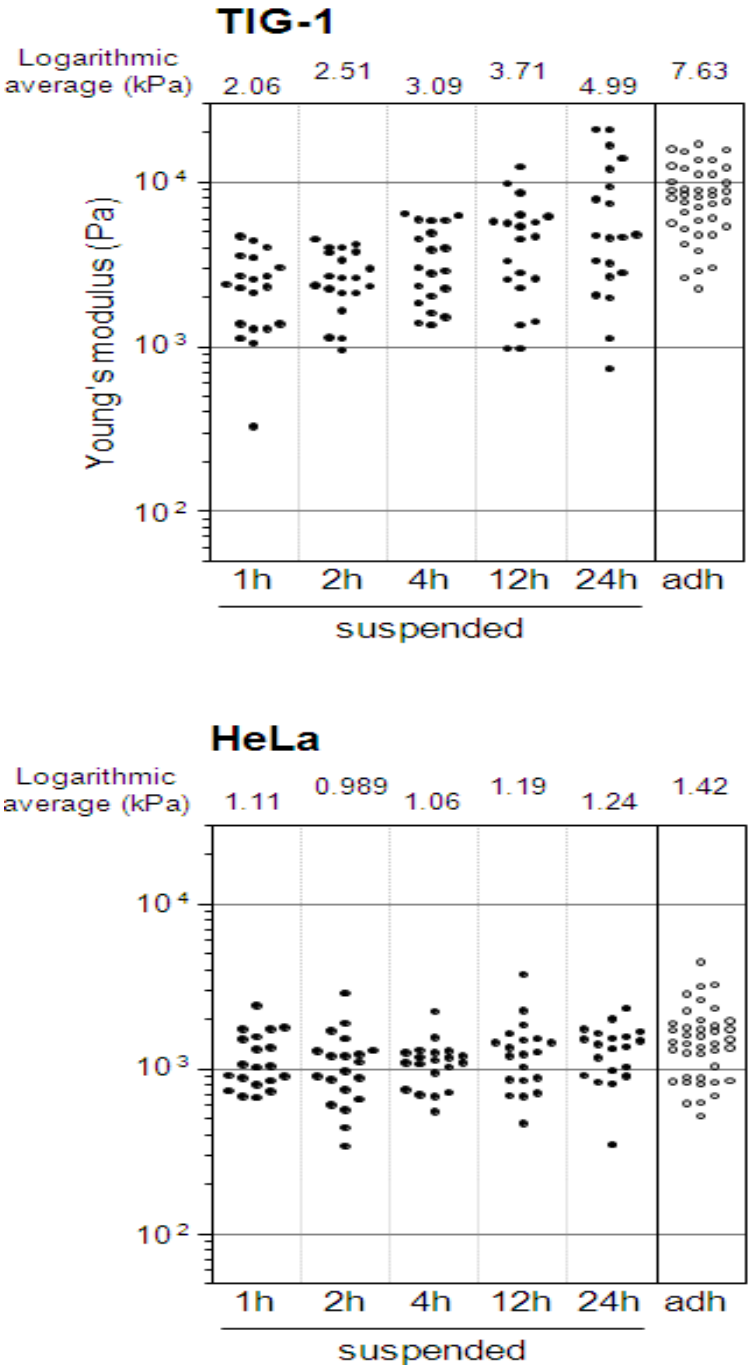

Fig.3.8 Time course elastic changes of TIG-1 (normal) and Hela (cancer). Young's moduli of suspended TIG-1 cells increased in a time-dependent manner but those of suspended HeLa cells remained almost unchanged over time.

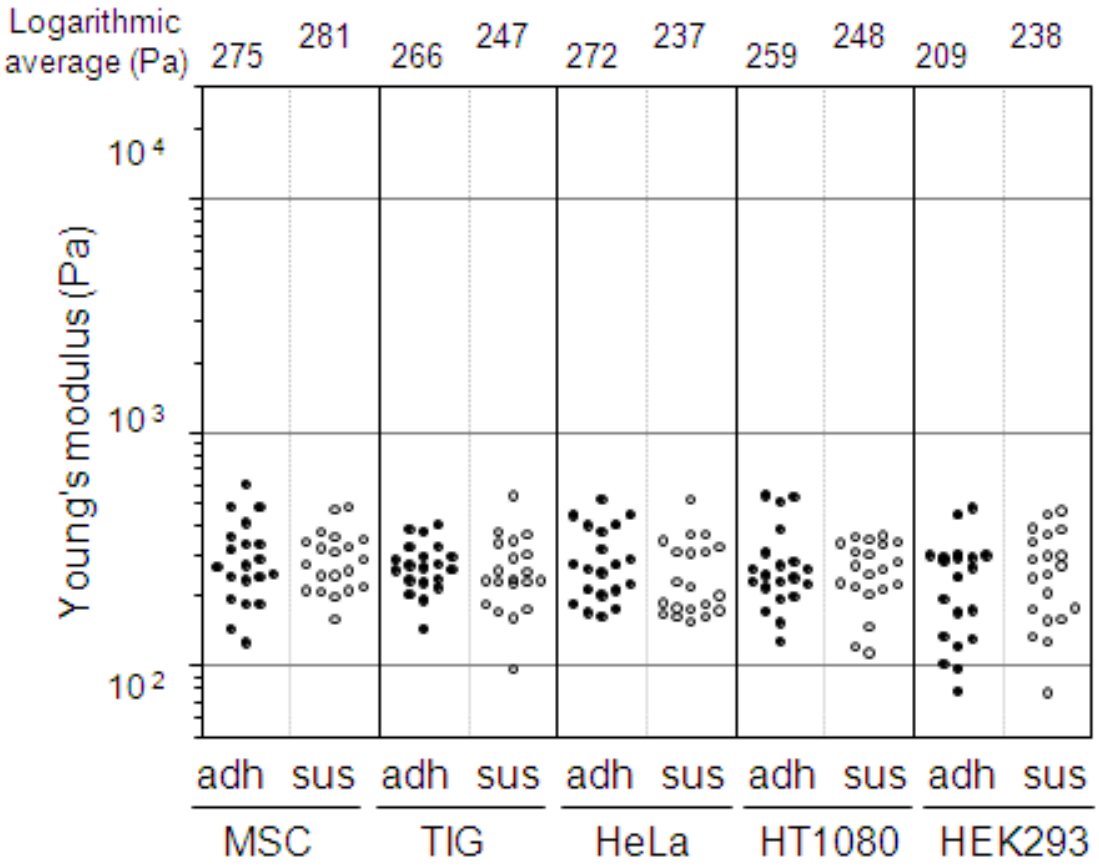

Fig.3.9 Sharp elastic decline of F-actin depolymerized adherent and suspended cells. Disruption of actin filaments by cytochalasin D treatment caused a considerable decrease in elastic values of all cells regardless of their type and adhesion state, which confirms the critical role of actin cytoskeleton in regulation of mechanical properties.

3.3.3 Mechanical responsiveness of cancer and normal cells

It can be inferred that the defined difference of mechanical properties between adhered normal stromal and cancer cells reflect on the completely difference of F-actin structures at the apical surface of those cell types. On the other hand, because suspended cells including normal stromal and cancer cells had almost similar cortical actin structures vicinity of their plasma membrane, it is unclear what does the difference of mechanical properties between suspended normal stromal and cancer cells based on. To clarify the difference of the contribution of various F-actin structures to the mechanical properties of cell surface, I examined the responsiveness of mechanical properties of cells for actin cytoskeleton modifying reagents, Y-27632 and calyculin A. Y-27632 is a ROCK inhibitor and prevents and attenuates stress fiber formation [58, 95]. On the other hand, calyculin A is a myosin light chain phosphatase inhibitor and activates actomyosin formation and enhances actin polymerization [60, 98].

Addition of Y-27632 to the cultured cells reduced their Young's modulus in all the cell types and adhesion and suspended states (Fig.3.10). Particularly the Young's modulus of normal stromal cells significantly decreased both in adhered and suspended states. On the other hand, the reduction rates of the Young's modulus by treatment of Y-27632 in cancer cells were lower and almost same in adhered and suspended states (Fig.3.10). The Y-27632 treated mechanical properties of suspended normal stromal cells became almost same as suspended cancer cells (Fig.3.10). For HEK293 cells, although the adhered mechanical properties were slightly decreased by treatment with Y-27632, mechanical properties in suspended state largely decreased (Fig.3.10). Thus, the responsiveness of

mechanical properties for Y-27632 varied between normal stromal, cancer and HEK293 cells.

Treating the normal stromal cells with calyculin A, the Young's modulus were almost unchanged in adhered and suspended states (Fig.3.10). On the other hand, for cancer cells, the Young's modulus were slightly increased both in adhered and suspended states by treatment with calyculin A (Fig.3.10). For HEK293 cells, the Young's modulus of adhered cells increased but that of suspended state was unchanged (Fig.3.10). Therefore, the responsiveness of mechanical properties for calyculin A slightly varied between normal stromal and cancer cells.

The tendency of responsiveness of mechanical properties for actin cytoskeleton modifying reagents varied between normal stromal and cancer cells but was similar in adhered and suspended states of each cell type (Fig.3.10). Thus, it will be assumed that the regulatory structures of actin filaments for mechanical properties fundamentally varied in normal stromal and cancer cells without recourse of cell adhesion states.

Finally I statistical analyzed the alteration similarity of Young's modulus of cells. The responsiveness of Young's modulus for Y-27632 or caluculin A in adhered or suspended state were used as variables in each cell. Fig.3.11 shows the dendrogram of the results of the clustering analysis. Normal stromal cells and cancer cells belonged in other clusters (Fig.3.11). The responsiveness behavior of HEK293 cells for actin cytoskeleton modifying reagent relatively closed to the cluster of cancer cells (Fig.3.11). The responsiveness characters of normal stromal, cancer and HEK293 cells for Y-27632 and calyculin A in adhered and suspended states were indicated in radar chart (Fig.3.12).

Normal stromal cells were strongly affected by Y-27632 in adhered and suspended states compared with cancer cells (Fig.3.12). On the other hand, cancer cells were strongly affected by calyculin A compared with normal stromal cells (Fig.3.12). The responsiveness for actin modifying reagents were almost unchanged between in adhered and suspended cells both in normal stromal and cancer cells (Fig.3.12). For HEK293 cells, they indicated unique responsiveness for these reagents between in adhered and suspended states. In adhered states, the responsiveness of HEK293 cells was similar to cancer cells (Fig.3.12). However, in suspended states, the responsiveness was close to normal stromal cells (Fig.3.12). Probably, regulatory actin filaments structures of HEK293 cells for mechanical properties would be varied in adhered and suspended states. The regulatory structures of actin filaments for mechanical properties fundamentally varied in normal stromal and cancer cells without recourse of cell adhesion states, and thus the mechanical properties would become the characteristic marker of cancer cells even in the suspended states.

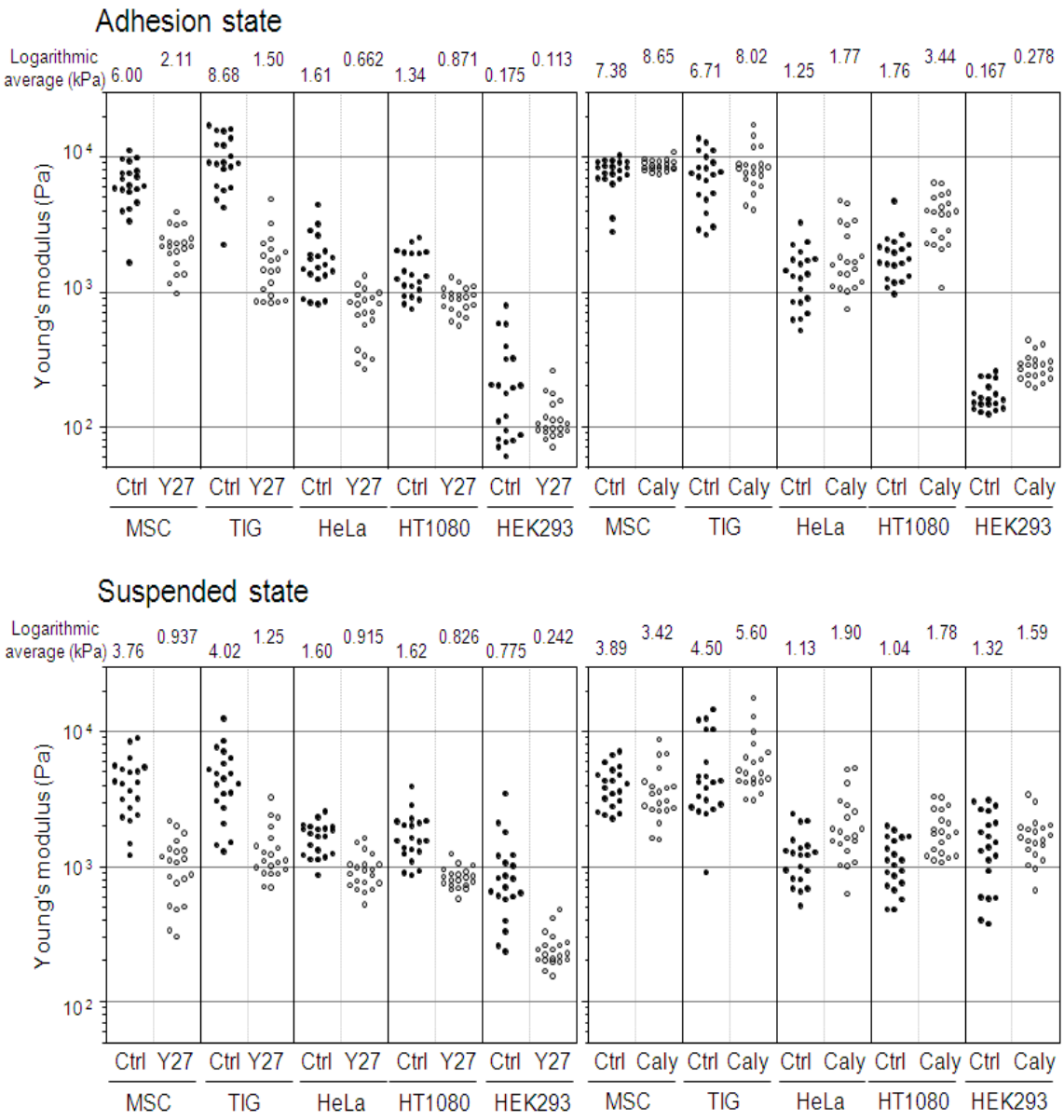

Fig.3.10 Elastic behavior of the adherent and suspended cells after treatment with Y-27632 and Calyculin A. Downregulation of actin filaments by Y-27632 reduced the elasticity of all adherent and suspended cells yet the mechanical response of the cells were different. Upregulation of actin filaments by Calyculin A had little impact on the Young's moduli of the cells in both adhesion states but their responsiveness was varied.

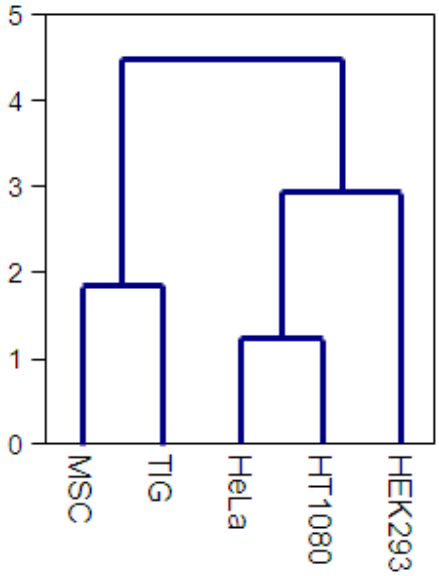

Fig.3.11 Dendogram of elastic response of the adherent and suspended cells after treatment with actin modifying agents. Normal, cancer and HEK293 cells belong to separate clusters.

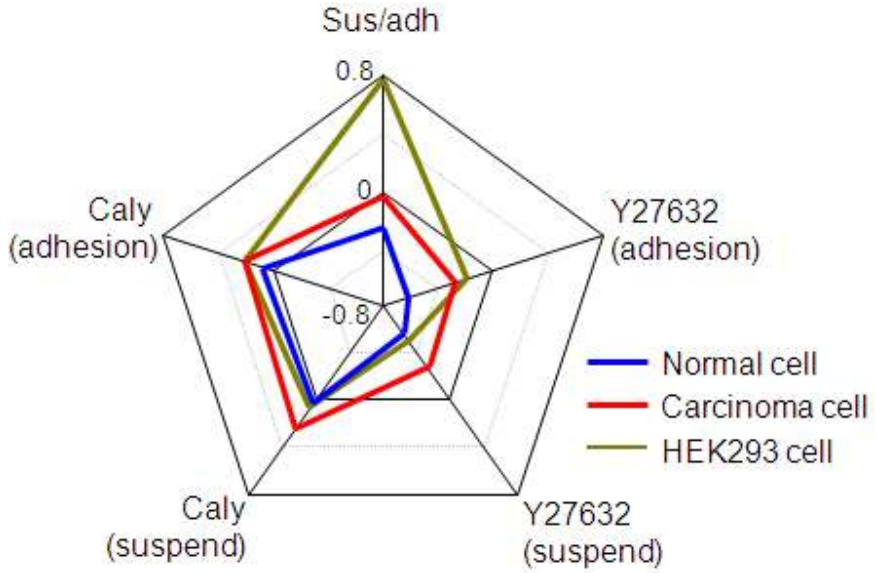

Fig.3.12 Radar chart display of relative elastic response and ratio of the adherent and suspended cells after treatment with Y-27632 and Calyculin A. Mechanical response of normal, cancer and HEK293 cells varied in adhesion states.

3.4 Discussion

This study presents an overview of surface mechanics and actin cytoskeleton architecture of normal stromal and cancer cells in adherent and suspended state. The adhered normal stromal cells form a highly organized actin cap structures and shows great stiffness on their apical surface (Figs.3.5 & 3.7). To the contrary, adhered cancer and HEK293 cells without actin cap structures show lower stiffness in comparison with the normal cells (Figs.3.5 & 3.7). By detachment from substrate and reorganization of F-actin structures to cortical actin vicinity of plasma membrane, the surface stiffness of the normal stromal cells decreased but was still higher than that of the cancer cells (Figs.3.6 & 3.7). Furthermore, the responsive features of surface stiffness for actin modifying reagents, Y-27632 and calyculin A, in the normal stromal and cancer cells were kept in adhered and suspended states (Fig.3.10). Therefore, the regulatory mechanism for actin cytoskeleton in the vicinity of plasma membrane of cancer and normal cells are probably different in not only adherent states but also suspended states.

Actin cap is an actin structure that forms a cap above the apical surface of the nucleus, tightly regulates the nuclear shape of adherent fibroblasts [53]. The stiffness and thickness of adhered MSCs, which are correlated inversely, are coordinated by the actin cap organization, actin cap well organized cells show high stiffness [79]. Furthermore, the proliferative activities of MSCs are related with the cell thickness, thick cell populations show highly proliferative activity [35, 36], and possibly regulated by the actin cap organization [79]. On the other hand, the cancer cells do not form actin cap on the apical surface but form some dense protrusions (Fig.3.4). The proliferative activity of cancer cells

could be greater than that of normal cells. The perinuclear F-actin structures like actin cap maybe involved in proliferative activity of these cells, but it is unclear whether it is directly or indirectly. On the other hand, it is reported that the range of inverse correlation between stiffness and thickness of adhered cells belong distinct groups in normal and cancer cells [100]. It is required that fundamental understanding for regulation of cell proliferation by F-actin structures.

Although the CLSM observable F-actin structures were obviously different from adhered normal stromal and cancer cells, those of suspended states on BAM surface showed apparently similar structures (Figs.3.6). However, the stiffness of these suspended cells were different and normal cells showed higher stiffness than cancer cells (Fig.3.7). Disconformities of surface stiffness and CLSM imaging of F-actin structures was also observed at the round shaped cells in mitosis and trypsinized-detahced state; the detached round cells show higher stiffness than that of mitotic round cells. Probably, the AFM measurement for surface stiffness can reveal the different physical properties of cell cortex of mitotic and trypsinized cells. Thus, difference of the surface stiffness between suspended normal and cancer cells would indicate the different features of the cortical actin in these cells. In fact, the responsiveness of surface stiffness for actin cytoskeleton modifying reagents, Y-27632 and calyculin A, was different in suspended normal and cancer cells (Fig.3.10). The responsiveness of suspended cells was almost same as that of adhered states although the F-actin structures of adhered and suspended normal cells were completely disparate (Figs.3.10 & 3.12). Thus, the regulatory factors for actin cytoskeleton of normal

cells are different from that of cancer cells, and it maybe undisturbed cell morphological alterations.

In the case of HEK293 cells different from other cell types, their stiffness increased by cell detachment from adherent substrate and reorganization of their F-actin structures (Fig.3.7). It is unclear why did only HEK293 cells show these unique stiffness alterations. But Yamane et al. reported that detachment of HEK293T cells, which is HEK293 cells stably expresses SV40 large T antigen gene, from the substrate by trypsinization and inhibition of reattachment induces phosphorylation of Ezrin/Radixin/Moesin (ERM) proteins [101]. ERM proteins crosslink the plasma membrane to the underlying actin cortex [99, 102], and they highly regulate surface stiffness and cell rounding at the onset of mitosis [51]. Therefore, the augmentation of phosphorylated ERM proteins by detachment of HEK293 cells from substrate induces organization of cortical actin and then probably increases their surface stiffness. How about cancer cells? The CLSM imaging of F-actin showed similar structures in adherent HEK293 and cancer cells (Figs.3.5 & 3.6). Why is the stiffness of cancer cells unchanged after cell detachment? ERM proteins are observed in various cytoskeleton-based structures including microvilli, and ERM are considered essential for the formation or maintenance of microvilli, [103]. Cancer cells bore many microvillus structures on their surface [116], and their ERM proteins may be already phosphorylated in adhered state. For the reason, the surface stiffness of cancer cells in adhered and suspended states would be almost same (Fig.3.7). However, it is still unclear why did the stiffness of HEK293 cells show different responsiveness for actin modifying reagents in adhered and suspended states. The responsiveness in adhered state is close to

that of cancer cells but in suspended state is close to that of normal cells. To understand the puzzle of actin cytoskeletal regulation in various cells, it is hoped to elucidate the modulation role of actin binding or regulation proteins including ERM proteins for structures and mechanical features of actin cytoskeleton.

The need for biomarkers for cancer detection and analysis is critical due to the complexity of the disease. Therefore, realization of the detection for cancer cells in suspended state will be a one of the most important progress in cytotechnology area. In this study, I presented the capability of the discrimination of cancer cells from normal cells using cell surface stiffness in suspended state. I also indicated that the difference of regulatory mechanism of F-actin structures vicinity of plasma membrane between cancer and normal cells. It is difficult to directly detect of the differences of actin regulation pattern in cancer and normal cells. Though biomechanical features depend on the structures of actin network appear as a deformation or membrane fluidics. The principle of the detection methods of cell biomechanics is fundamentally different from the most available cytotechnology, i.e. flow cytometry. Moreover, the measuring of cell biomechanics are unique technology providing the valuable information of structures and features of actin cytoskeleton of intracellular space. I hope that in the future high-speed and high-precise methods of measuring biomechanical properties of suspended cells using flow channels of existing the flow cytometry are an essential part of the cancer cytotechnology. The summary of the findings of this section are shown in Fig.3.14.

A

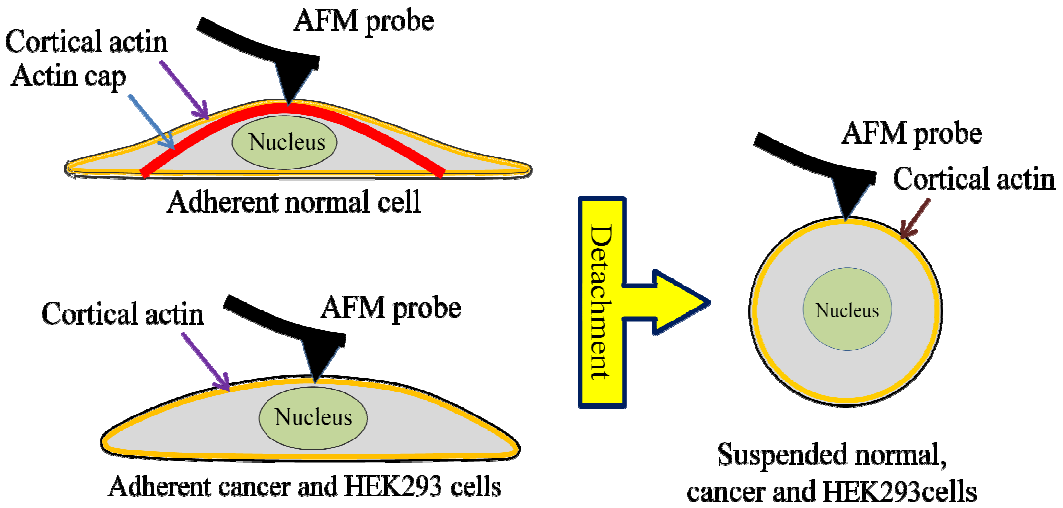

B

Cell Category	State Stiffness
Normal	Adherent > Suspended
Cancer	Adherent ≈ Suspended
HEK293	Adherent < Suspended

Fig.3.14 Summary of elastic and structural findings in this section. (A) Normal cells exhibit a highly contractile actin cap on their surface while in cancer and HEK293 cells actin cap is absent and cortical actin could be the source of tension. By detachment, actin cytoskeleton of all the cell types remodeled and cortical actin appeared as the main elastic actin structure in the suspended cells. (B) Adherent normal cells are stiffer than the suspended ones. Cancer cells show relatively similar elastic phenotype in both adherent and suspended states; however adherent HEK293 cells are softer than their suspended counterparts.

3.5 Summary

The mechanical features of individual cells are unique indicators of their states and constantly change in accordance with cellular events and diseases. Particularly, cancer progression is characterized by the disruption and/or reorganization of actin filaments causing mechanical changes. Thus, precise mechanical characterization of cells is expected to become an effective cytotechnological approach for early detection of cancer. In this study, I investigated the actin microstructures and surface mechanical behavior of cancer and normal cells in the adherent and suspended states using atomic force microscope and confocal laser scanning microscope. Adherent normal stromal cells had developed actin cap structures on their apical surface, generating high surface stiffness, whereas cancer cells did not have developed filamentous actin structures, and their surface stiffness was low. Although the filamentous actin structures of normal stromal cells reorganized to the cortical region when the cells were detached from the adherent substrate, resulting in a decrease in surface stiffness, the stiffness of suspended normal cells remained higher than that of cancer cells. Additionally, these suspended-state actin structures were similar, regardless of the cell type. Furthermore, the mechanical responses of the cancer and normal stromal cells to perturbation of the actin cytoskeleton were different. Thus, the mechanisms regulating the actin cytoskeleton in cancer and normal cells are probably different not only in the adherent state but also in the suspended state. These results demonstrate the possibility of discriminating the features and structures of the actin cytoskeleton in cancer and normal cells in the suspended and adherent states using stiffness measurement methods.

Chapter 4

Elastic character of round mitotic and trypsinized cells

4.1 Introduction

The mechanical features of cells are unique indicators of their states and constantly change in accordance with cellular events. During optic-cup morphogenesis, alterations in the level of stiffness of the retinal epithelium are important for the self-formation of neural retina tissue [74]. Malignant cancer cells exhibit less stiffness than normal cells [39]. Furthermore, the mechanical features of mesenchymal stem cells are attributed to their diverse characteristics and states [79, 96, 47]. These mechanical changes in cells are widely mediated by actin cytoskeleton. Thus, by analyzing the mechanical properties of cells, it is possible to know and evaluate the characteristics of the complicated actin networks on the surface of cells. For example, studies analyzing the physical response of actin filaments networks [64], detecting the cell contraction force depending on cell substrate [104], and examining the penetration efficiency of fine nanoneedle through cell surface membrane [48] have shown that the actin cytoskeleton can be potentially characterized by analyzing the mechanical properties of cells.

Actin cytoskeleton also controls the dynamic shape of cells during various morphological events. Thus analyzing the mechanical changes with the events helps elucidate the dynamical roles of actin cytoskeleton. During cell division, changes in the organization and dynamics of actin cytoskeleton cause retraction of the cell mar-gin, cell

rounding, and formation of the cleavage furrow [105, 106, 51]. The stiffness of the cleavage furrow region of cells in cytokinesis drastically increases as compared to that of the top region of cells in metaphase [107]. The cleavage furrow contains an actomyosin contractile ring, which controls the changes in stiffness of the region. Apart from this, cortical stiffness of metaphase rounded cells was greater than that of interphase adherent cells of Drosophila embryonic S2R+ cells [51]. Cortical rigidity and cell rounding at the onset of mitosis are highly regulated by the ERM family of actin-binding proteins [51]. ERM proteins crosslink the plasma membrane to the underlying actin-rich cortex by phosphorylated activation [102]. Thus, activation of the ERM proteins is a key factor in cell rounding and formation of the rigid actin cortex during mitosis [108]. Passive cell rounding, which is marked by a morphological change, can be induced by trypsin treatment. The surface morphology of trypsinized cell exhibits blebs, spherical protuberances, and microvillous projections [109,110]. These surface morphological changes are similar to that during cell mitosis [111]. Yamane et al. reported that detachment of HEK293 cells from the substrate by trypsinization and inhibition of reattachment induces phosphorylation of ERM proteins [101]. Thus, suspending the trypsinized round cells might induce the formation of a rigid actin cortex, similar to that observed during mitosis. Furthermore, suspended forms of adherent cells are found not only in artificial trypsinized condition but also in natural blood, e.g., metastatic cancerous cells and stem/progenitor cells [112, 113, 114]. Thus, the mechanical characterization of the actin cortex of the round-shaped cells helps elucidate the regulatory mechanisms underlying the dynamic morphological changes by the actin cytoskeleton.

The stiffness of leukocytes and trypsinized cells has been measured by using atomic force microscope and a biocompatible anchor for membrane (BAM) substrate for anchoring the suspended cells [48, 92]. In this study, I determined the cortical stiffness of the trypsinized round cells anchored by BAM substrate and compared it with that of mitotic round cells. To identify and examine the mitotic cells, Fucci (Fluorescent Ubiquitination-based Cell Cycle Indicator) system was employed. This system contains 2 fusion proteins, namely, the monomeric Kusabira Orange fused to human Cdt1 (mKO2-hCdt1) and the monomeric Azami Green fused to human geminin (mAG-hGeminin) for visualizing the cell cycle phase [115]. Fucci system shows the cell cycle by phase-dependent color variation in fluorescence (Fig.4.1). Cells at the G1/G0 phase display red fluorescent nuclei, whereas those at the S/G2 phase show green fluorescent nuclei. Mitotic cells with diminished nuclear membrane show green fluorescence of the entire cell, allowing the measurement of cortical stiffness of round cells by AFM. The mitotic and trypsinized round cells both showed actin-rich cortical regions on the cell surface. Although the cortical actin regions observed using confocal laser scanning microscope were almost the same irrespective of the cell state, the cortical rigidity of trypsinized round cells showed greater stiffness as than that of mitotic round cells. Thus, the cortical rigidity of round cells varies according to the cell state, and analyzing the cell cortex rigidity is useful for characterizing the actin network on the cell surface.

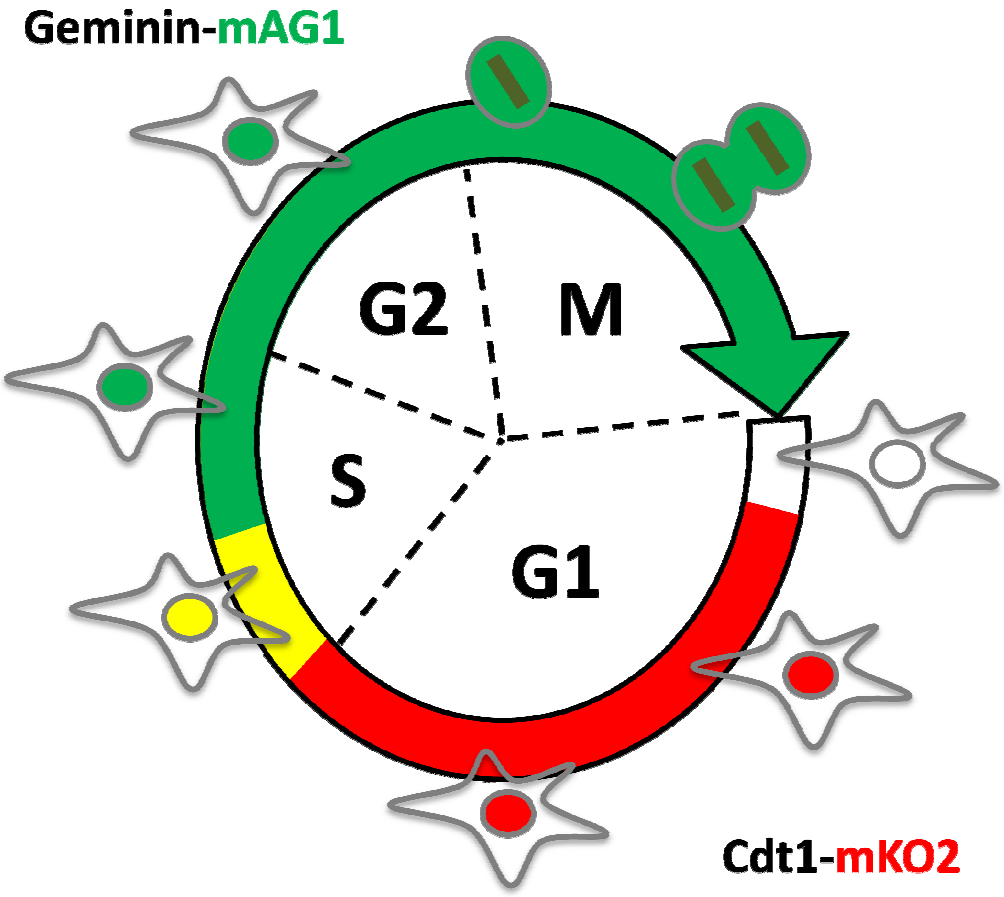

Fig.4.1 Cell cycle progression in FUCCI system. Red- and green-emitting fluorescent proteins are used to develop dual color indicator for individual cell cycle phases.

4.2 Experimental procedure

4.2.1 Materials

A quadratic pyramidal AFM probe (SN-AF01-S-NT; spring constant: 0.02 N/m) was purchased from SII NanoTechnology Inc. (Chiba, Japan). Hela.S-Fucci (RCB2812) and NMuMG-Fucci (RCB2813) cells [115] were obtained from RIKEN BioResource Center (Saitama, Japan) by permission of Dr. Atsushi Miyawaki (Riken, Japan). Cell culture medium was purchased from Sigma-Aldrich (St. Louis, MO). Fetal bovine serum (FBS) was purchased from JRH Biosciences (Lenexa, KS). Antibiotics were purchased from Life Technologies Japan Ltd. (Tokyo, Japan). BAM (SUNBRIGHT OE-020CS) was purchased from NOF CORPORATION (Tokyo, Japan). Other reagents were obtained from Sigma-Aldrich, Wako Pure Chemical Industries Ltd. (Osaka, Japan), or Life Technologies Japan Ltd. (Tokyo, Japan).

4.2.2 Preparation of BAM-coated dishes

BAM contains a membrane anchoring oleyl group, a hydrophilic poly ethylene glycol (PEG) domain, and an NHS-reactive ester group [93]. The BAM-coated dishes were prepared as follows. Briefly, polystyrene tissue culture dishes were coated with 5% BSA in PBS for 1 h. After washing with PBS, the surfaces were treated with 1 mM BAM in PBS for 30 min. Then, the BAM-coated dishes were washed and dried.

4.2.3 Cell cultures

Hela.S-Fucci and NMuMG-Fucci cells were maintained in DMEM containing 10% FBS and antibiotics (100 units/mL penicillin G and 100 μg/mL streptomycin sulfate). The culture medium was replaced three times a week. Cells were detached from the culture dish by treatment with 0.25% trypsin–0.02% EDTA in PBS and then plated on the BAM-coated dish for 3 h in culture medium. The cells attached to the BAM surface were manipulated by AFM (Fig.4.2). Actin-depolymerization of the cells was induced by treatment with 2 μM cytochalasin D for 2 h.

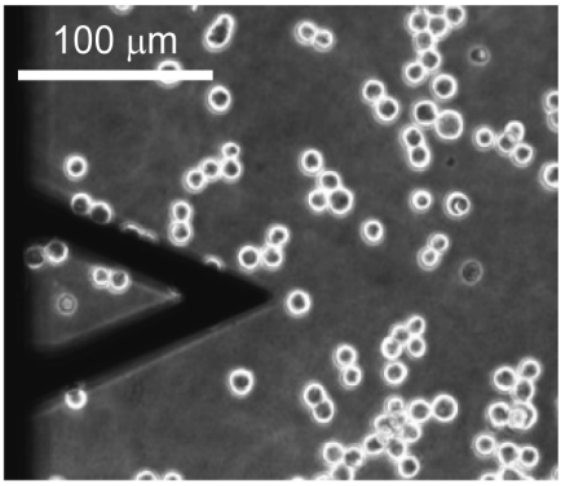

Fig.4.2 Phase-contrast micrograph of Hela.S-Fucci cells on the BAM substrate. The trypsinized detached cells were anchored to the substrate, which allowed them to maintain their round shape. The object on the left is the AFM cantilever.

4.2.4 AFM measurements

Hela.S-Fucci and NMuMG-Fucci cells adhered to the tissue culture dishes or attached to the BAM-coated dishes in the medium were examined by AFM at room temperature. The atomic force microscope was combined with fluorescence microscope (IX71; Olympus, Tokyo, Japan) so that cell cycle phases could be determined by observing the Fucci fluorescence (Fig.4.1). The probe indented the top of the cells up to 1 nN at 5 μm/s. The Young's modulus of the cell calculated in accordance with the Hertz model (Hertz, 1881). Unless otherwise indicated, the force–distance curve at the region up to approximately 300 nm of the cell surface indentation was fitted by JPK data processing software (JPK instruments AG) as follows:

$$F = \frac{E}{1-\nu^2}\frac{\tan\alpha}{\sqrt{2}}\delta^2$$

where F = force, δ = depth of indentation, α = half angle to face of pyramidal probe (20◦), ν = Poisson's ratio (0.5), and E = Young's modulus (Fig.4.3). All experiments performed using more than 20 cells, and each cell was examined at 25 points on the top of the cell. The median value adopted for the Young's modulus of each cell [79].

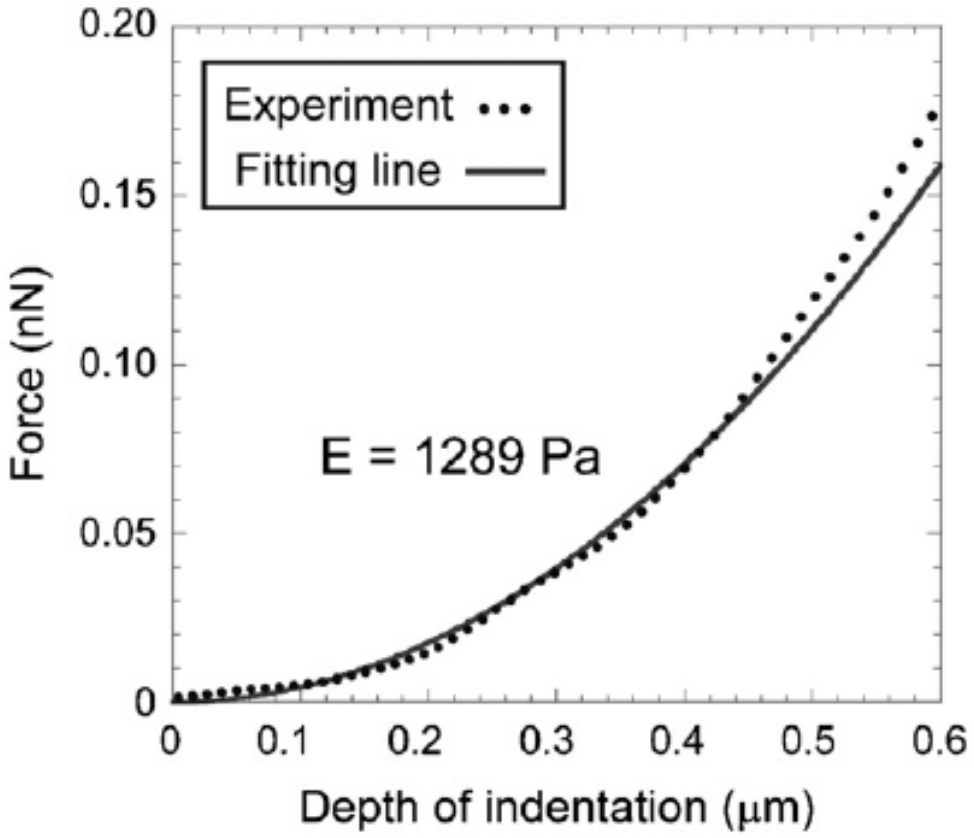

Fig.4.3 Typical force–distance curve obtained from the AFM indentation experiments with adherent interphase Hela.S-Fucci cells. The black points show experimental force curve lines, and the gray line shows the Hertz model fitting line. The force–distance curve at the region approximately 300 nm of cell surface indentation was fitted to the Hertz model.

4.2.5 F-actin imaging

The cells were fixed with 4% paraformaldehyde, permeabilized with 0.5% Triton X-100, and then stained with rhodamine-phalloidin for actin filaments. Specimens were observed by CLSM equipped with 60× oil immersion lens (NA = 1.42) in 0.5 μm serial sections. Superimposition of the serial images processed with ImageJ software.

4.3 Results

4.3.1 Cortical actin imaging of Hela.S-Fucci and NMuMG-Fucci Cells

One of the typical morphological characteristics of adherent mitotic cells is its spherical shape, yet it is difficult to discriminate mitotic round cells from other cells in various phases, including dead round-shaped cells. Therefore, this study used the Fucci system [115] to determine the mitotic phase of adherent cells. Most of these cells showed clear green/red fluorescent nuclei; however, some round cells showed green fluorescence in the entire cell body (Fig.4.4). Thus, I identified that cells with round shape and green fluoresce in whole cell body are in mitotic phase (Fig.4.4). Trypsinized detached cells were fixed on the BAM substrate (Fig.4.2). The detached cells spontaneously attached to the BAM substrate and maintained a round shape (Fig.4.2). They anchored tightly to the BAM, which enabled AFM manipulation of the live round cells. The mitotic and trypsinized round cells show activation of the ERM proteins [51, 101]. To compare the cortical actin structure, F-actin of the mitotic and trypsinized round cells was stained. The adherent Hela.S-Fucci cells did not show any actin stress fibers but had many short microvillus

protrusions on their surface (Fig.4.5). The mitotic Hela.S-Fucci cells showed many long microvilli structures on their cell surface and F-actin-rich regions in the cortex (Fig.4.5). The trypsinized round Hela.S-Fucci cells showed short microvilli structures on their surface and clear cortical actin filaments (Fig.4.5). In NMuMG-Fucci cells, interphase adherent cells showed many actin filaments structures, basal stress fibers, and dense protrusions on their surface (Fig.4.5). The mitotic NMuMG-Fucci cells had long retraction fibers, some short microvilli structures, and cortical actin structure (Fig.4.5). The trypsinized NMuMG-Fucci cells showed developed cortical actin and many small blebb-like structures on their surface (Fig.4.5). Emergence of many long microvilli protrusions and long retraction fibers in mitotic Hela.S-Fucci and NMuMG-Fucci cells is in agreement with the mitotic cell image by electron microscopy [111]. Moreover, surface structure of trypsinized round cells was similar to the reports about surface morphological changes by trypsinization [109]. The F-actin structures in mitotic and trypsinized round cells tended to be similar, with both cells showing a clear cortical actin on the cell surface.

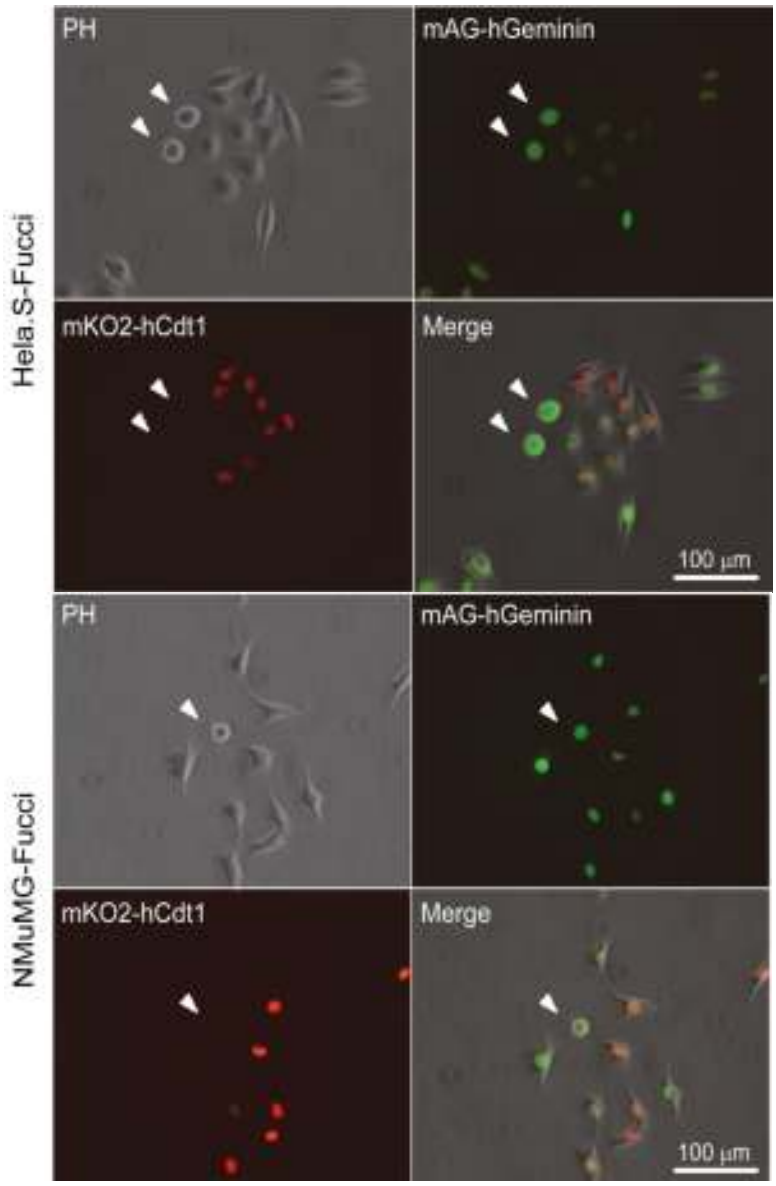

Fig.4.4 Fluorescence images of Fucci system. The Hela.S-Fucci and NMuMG-Fucci cells were cultured in normal culture dishes. The phase-contrast image (PH), green fluorescence image (mAG-hGeminin), red fluorescence image (mKO2-hCdt1), and merged image (Merge) are displayed. Green fluorescent nuclei and red fluorescent nuclei are shown in the spreading cells. Mitotic cells are round and emit green fluorescence (arrowheads).

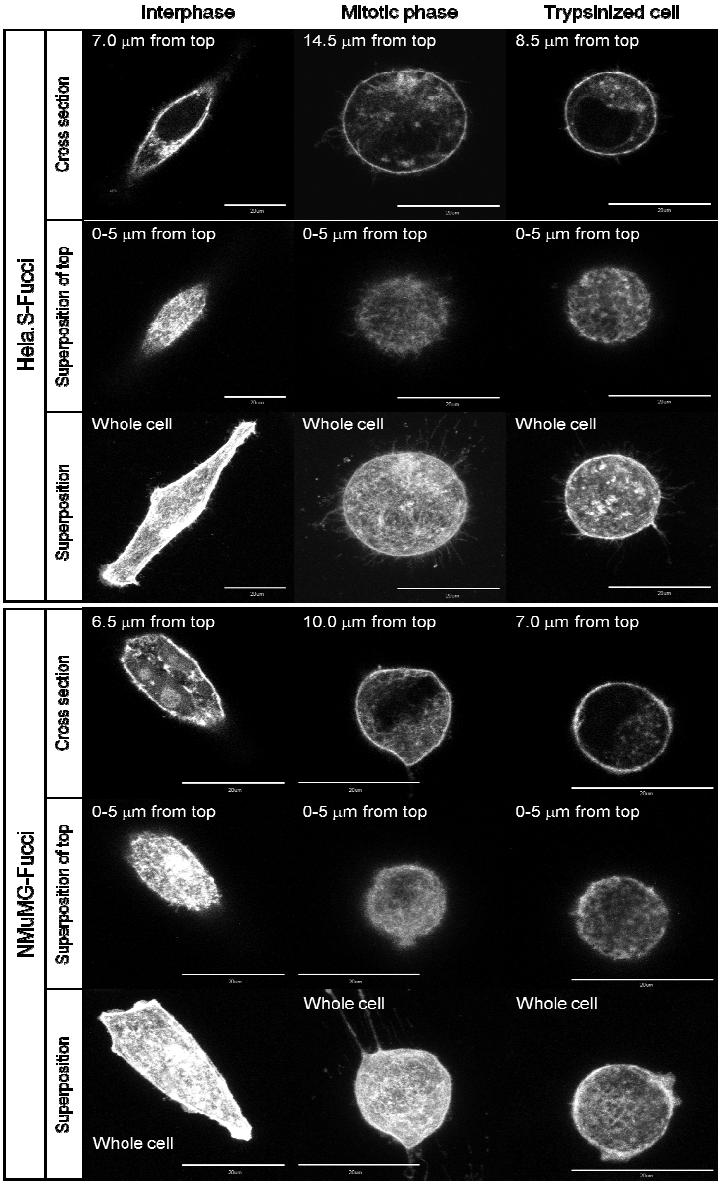

Fig.4.5 CLSM images of F-actin structures in Hela.S-Fucci and NMuMG-Fucci cells during interphase, mitosis, and trypsinized states. All the indicated cells originally expressed mAG-hGeminin (S/G2/M phase), and F-actin was labeled with rhodamine-phalloidin. The mitotic cell is larger than that of trypsinized round cell. Middle part images clearly indicate the cortical actin structure of the cells. Bar = 20 μm.

4.3.2 Young's modulus of mitotic and trypsinized round cells

This study evaluated the mechanical properties of the cortical region of cells. At interphase, the Young's modulus of adhered NMuMG-Fucci cells was higher than that of Hela.S-Fucci cells (Fig.4.6). The average value of the logarithmic Young's modulus of these cells was 7.7 kPa (NMuMG-Fucci cells) and 1.5 kPa (Hela.S-Fucci cells). During mitosis, the average values of the logarithmic Young's modulus of these cells decreased to 0.40 kPa (NMuMG-Fucci cells) and 0.60 kPa (Hela.S-Fucci cells) (Fig.4.6). In contrast, the average values of the logarithmic Young's modulus of these cells after trypsinization and attachment to the BAM surface were 1.8 kPa (NMuMG-Fucci cells) and 1.9 kPa (Hela.S-Fucci cells) (Fig.4.6). These round cells at either condition showed almost the same degree of stiffness in NMuMG-Fucci and Hela.S-Fucci cells. How-ever, the cortical rigidity of trypsinized round cells was apparently greater than that of mitotic round cells. These Young's modulus values were higher than those of cytochalasin D-treated actin-depolymerized cells (Fig.4.6). Therefore, these obtained mechanical properties during each condition reflect the mechanical characteristics of actin networks around the cell surface. Although most studies have fitted the force–distance curve to the Hertz model at small indentation region from cell surface (around 300 nm here), the nanoindentation measurement by AFM can even detect the surface brush structure of cells [117]. The mitotic cells showed relatively long microvilli protrusions on their surface compared to trypsinized round cells (Fig.4.5), which might have affected these results. To check this possibility, I calculated the apparent Young's modulus of each cell using the region at the indentation region of maximum 600–1000 pN of force–distance curve. The results

indicated that the trypsinized cells were indeed stiffer than mitotic cells (Fig.4.7). Thus, the experiments showed the stiffness of the cell cortex but not the surface protrusions, and most importantly, the rigidity of cortical actin in the round-shaped cells changed during different cell conditions.

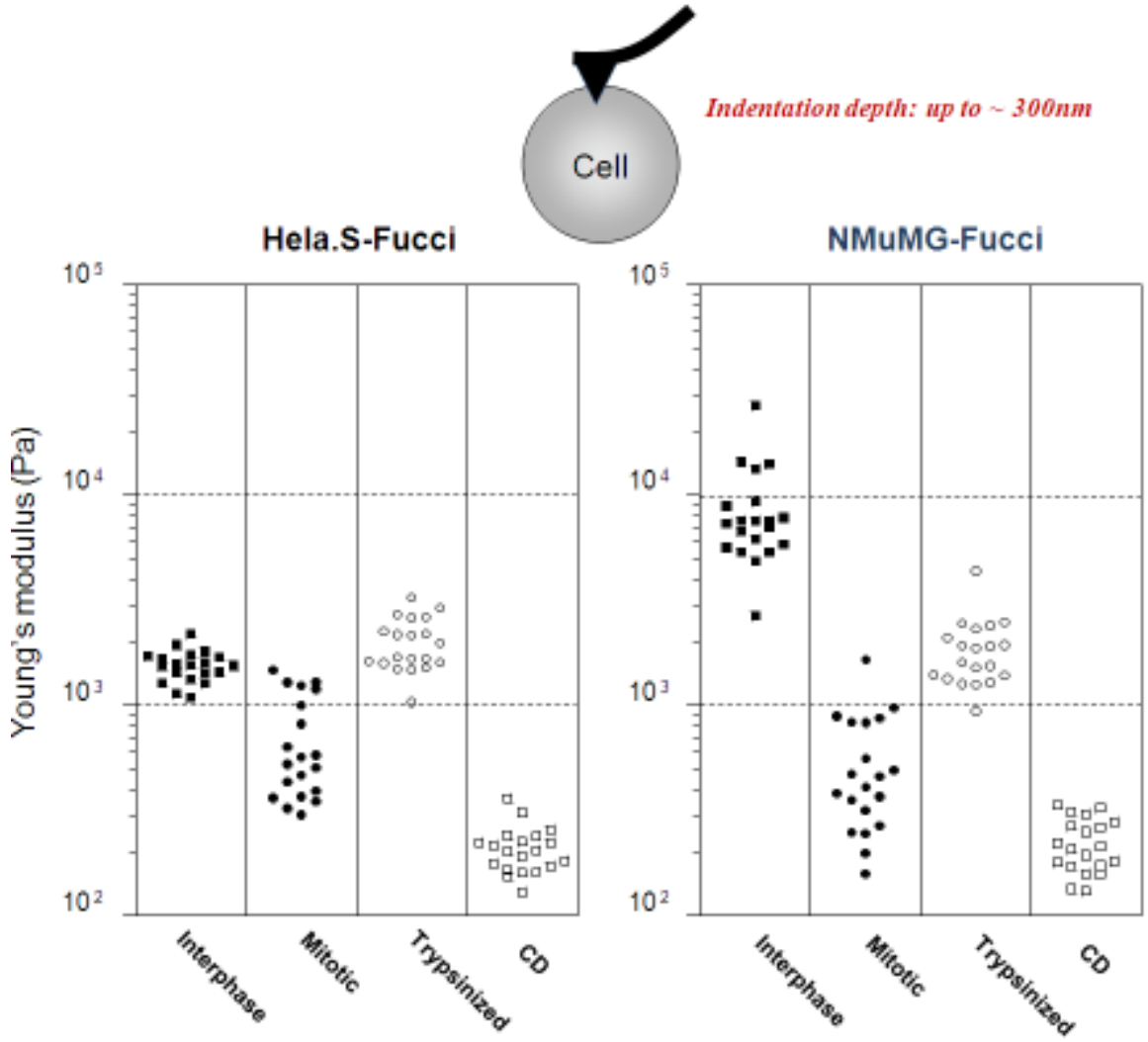

Fig.4.6 Young's modulus of Hela.S-Fucci and NMuMG-Fucci cells under various conditions. Young's moduli of the cell surface during interphase, mitotic phase, trypsinized round state, and cytochalasin D treatment (CD) are shown. The scale of Young's modulus is logarithm. Each condition shows the Young's modulus of 20 independent cells and each cell was measured 25 times on the cell top.

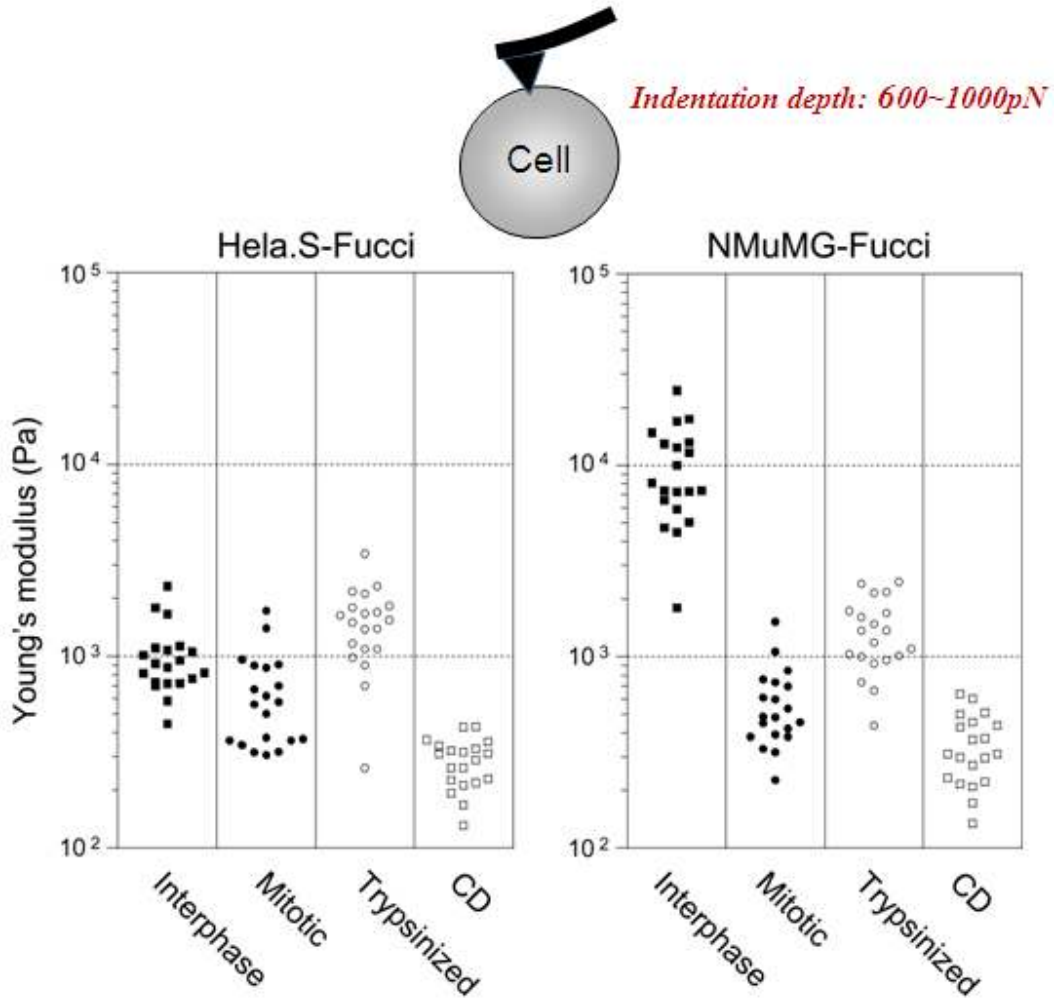

Fig.4.7 Young's modulus of Hela.S-Fucci and NMuMG-Fucci cells recalculated using the region at the indentation region of maximum 600 to 1000 pN of the experimentally obtained Force-distance curve. The Young's moduli of the cell surface during interphase, mitotic phase, trypsinized round state, and cytochalasin D treatment (CD) are shown. The scale of Young's modulus is logarithmic. Each condition shows the Young's modulus of 20 independent cells and each cell was measured 25 times on the cell top. The pattern for elastic difference of the trypsinized and mitotic cells did not change.

4.4 Discussion

This study showed that the cortical rigidities of round-shaped cells in mitosis and in trypsinized-detached state are different. In the latter state, the cell cortex was stiffer than that of mitotic round cells (Fig.4.4). The difference in the mechanical properties of the cell cortex is inconsistent with the results obtained by CLSM imaging of F-actin (Fig.4.5). The mechanical properties of the actin cytoskeleton showed a possible qualitative actin construction of the cell surface, which is different from their morphological structures. Thus, the elucidation of these qualitative features of actin cytoskeleton around the cell surface will help determine the regulatory mechanism underlying cell dynamics and morphology. The process of cell rounding in mitotic Drosophila S2R+ cells is mainly controlled by ERM and moesin proteins [51]. At the onset of mitosis of S2R+ cells, activated moesin helps in the conversion of protrusive lamellipodial actin structures, which are predominantly present during interphase, into a uniform cortex in which the actin filaments lie parallel to the plane of the plasma membrane; this uniform cortex is the characteristic feature of mitotic cells. In particular, ERM proteins, rather than myosin II, play a major role in cell rounding and cortical rigidity. Some studies have reported that stiffness of the cell cortex increases as they enter mitosis [51, 107]. However, in this study, the cortical rigidity of Hela.S-Fucci and NMuMG-Fucci cells in mitosis was lower than that of adherent interphase cells (Fig.4.6). In case of NMuMG-Fucci cells, many actin fibers and dense surface protrusions in adherent interphase cells diminished in mitotic phase (Fig.4.5), and thus the stiffness decline is small wonder. On the other hand, Hela.S-Fucci cells had many F-actin microvilli protrusions on their cell surface both in interphase and

mitotic phase. Yet, it is unclear why the surface stiffness decreased in mitotic phase. In contrast, cortical rigidity of trypsinized round cells was greater than that of mitotic cells (Fig.4.4). Especially trypsinized Hela.S-Fucci cells were slightly stiffer than that of interphase cells (Fig.6). CLSM analysis of F-actin structures showed that both mitotic and trypsinized round cells similarly induced the formation of actin cortex (Fig.4.5). Thus, although the development and solidity of the cortical actin may appear the same in both mitotic and trypsinized cells, they generate different mechanical phenotype during mitosis and detachment.

There are several known differences between physical proper-ties of mitotic and trypsinized cells. Stewart et al. reported that rounding pressure, generated by an osmotic pressure, of mitotic cells (including prometaphase and metaphase) is more than 3-fold higher than that of trypsinized cells [118]. In addition, the surface area and volume of cells decrease as they round and enter metaphase due to depletion of surface membrane reservoir through preventing the secretion and recycling the membrane traffic [119, 120]. This finding indicates that cells probably control their internal osmotic pressure by changing their volume and surface area. On the other hand, the cell surface of trypsinized cells is the same as untreated cells [119]. Therefore unlike mitotic cells, the endosomal recycling and surface membrane reservoir, which is associated with membrane tension [121], would be normal in trypsinized cells.

Since the surface tension is balanced with osmotic pressure, surface membrane reservoir, cell radius, and actomyosin cortex, I assumed that trypsinized cell, with normal membrane reservoir, cell radius, and weak rounding osmotic pressure, highly maintains its

shape via actomyosin cortex which is an important factor for surface tension in trypsinized round cell. Moreover, Maloney et al. reported that the surface bleb formation of trypsinized floating cell decreases with time and that the rigidity of trypsinized cell increases within 60 min [97]. The AFM measurements for trypsinized cells were conducted after 3 h incubation on BAM surface during which the cells' actomyosin cortex could have become fully developed. On the other hand, the mitotic round cells with high osmotic pressure, relatively small cell radius, and low surface membrane reservoir, may require to minimize the maintaining round force. Moreover, the combined period of prometaphase and metaphase during mitosis is around 60 min in many cases. This period may be relatively short for the cell to fully develop actomyosin cortex structure. The widely varied Young's modulus in mitotic cells probably indicates the affect of the alterations of osmotic pressure and actin cortex (Fig.4.6). In sum, the strength of the actomyosin cortex would be higher in trypsinized round cells compared to mitotic (prometaphase and metaphase) cells.

Other assumptions for the difference between Young's modulus of round trypsinized cell and mitotic cell are conceived as follows. One is the difference of cell shape. The morphology of trypsinized detached cell is almost spherical; however, the height to width ratio in metaphase cell is 0.86 which indicates an oval shape [118]. The bottom-to-side region of the oval mitotic cell contains many retraction fibers which anchor to actin cortex [122]. Thus, the cortical actin density or strength of the top region of oval-shaped mitotic cell may be small compared to both the bottom-to-side region of the oval shape and to the trypsin treated cell with complete spherical shape. The other is that trypsinized round cell can maintain some F-actin structures on the cell surface. The

mechanism of redistribution of actin filaments structures to a relatively uniform cortex in trypsinized round cells remains unclear. For this reason, trypsinized round Hela.S-Fucci cells with cortical actin and some surface F-actin structures might show more stiffness than interphase cells (Fig.4.6). However, further investigation of the regulatory mechanism underlying cell rounding by ERM proteins is required.

Meanwhile, no defined differences were observed in phalloidin labeled F-actin cortices of round mitotic and trypsinized cells (Fig.4.3). The CLSM imaging of F-actin makes a significant contribution to determination of their localization but it can hardly provide information about the maturation or strength of F-actin structures. The AFM nanoindentation method, however, tackles this issue and measures the mentioned parameters.

In this study, I used Fucci system expressing cells. The Fucci system is a fluorescent indicator for the cell cycle [115]. Thus, it is possible to compare the surface stiffness of cells at the G0/G1 phase with that of cells at the S/G2 phase. I randomly measured the surface stiffness of interphase cells, but I could not find cluster of each cell phase (Fig.4.6). Hence, to examine the delicate difference between cell surface stiffness and cell cycle stages, especially G1, S, and G2 phases, high-precision tools and discriminatory methods for S- and G2-phase cells are needed.

In summary, cortical rigidity of round cells varies according to the cell state, and the analysis of the mechanical properties of the cell cortex by AFM proves to be a useful method for evaluating the complex actin cytoskeleton network of cell surface. In the future, to clarify and evaluate the actomyosin cortex of trypsinized cells, I will examine the effects

of the osmotic pressure and shape on the cortical rigidity of trypsinized cells. Furthermore, I plan to investigate the mechanical role of actomyosin cortex in various cell types and states using some actin-perturbing agents and then evaluate the homology and discrepancy between fluorescence imaging and AFM measurements. I also intend to examine the mechanics and organization of actin cytoskeleton of spontaneously detached metastatic cancerous cells by using the adopted method for suspended cell measuring.

4.5 Summary

This chapter describes the results of the analysis of cortical rigidity in two round cell states: mitotic round cells and detached round cells after trypsinization using atomic force microscopy. These two states are primary cell events with dynamic morphological alterations in vitro. The trypsinized detached cells were fixed on the substrate of membrane anchoring oleyl surface. Fluorescent images taken by confocal laser scanning microscopy revealed diverse cell surface protrusions and cortical actin development in the round cells under different conditions. Although the cortical actin of these cells seemed to develop similarly, cortical rigidity of the trypsinized round cells showed greater stiffness than that of mitotic round cells. The elasticity measurements by AFM may detect invisible information about the maturation or strength of F-actin structures and such measurements may indicate that the strength of the actomyosin cortex would be higher in trypsinized round cells compared to mitotic cells. The mechanical properties can help provide better insights into the characteristics of the actin cytoskeleton network in vicinity of cell surface during dynamic morphological alterations.

Conclusion and perspective

An alternative approach with particular relevance to biomechanics showed that cells could be regarded as biomechanical living machines. They sense and respond to applied forces by dynamically changing their biological activities and states as a consequence of alterations in their function, intracellular structure and mechanical behavior.

The observations demonstrate a possibility that actin cytoskeleton architecture and elasticity reflect the physiology and fate of MSCs. Depolymerization of actin filaments of the cell surface reduce the apparent Young's modulus of these cells but increase their thickness suggesting an inverse relation between the two. The actin assembly and actomyosin contractility modulates the MSCs stiffness and thickness. It was also found that proliferative activity and replecative senescence of MSCs could be improved and controlled through regulation of actin cytoskeleton.

It was shown by examining the actin cytoskeleton organization and mechanical properties of several kinds of cell that actin microstructures and elastic features could be used for effective cell characterization. Distinct mechanical responsiveness of the cells indicates different regulatory mechanism for the actin cytoskeleton among cell types. As appears to be the case here, elastic character of adherent and suspended cells is a function their actin cytoskeleton which remodels according to adhesion state of the cells. Apical actin structures including contractile actin stress fibers seem to be responsible for surface mechanics of each cell type. In particular, actin cap and cortical actin are probably the major structural players of elasticity in all cell types and states. The mechanical properties of the cells were proved to be very local yet they could be used to discriminate the normal

and cancer cells. Regardless of adhesion state or cell type, actin cytoskeleton was confirmed to be the main regulator of biomechanical properties.

Cortical stiffness and actin cytoskeleton of the naturally round mitotic cells and artificially-induced round detached cells were investigated. The experimental data may define a clear distinction between elastic behaviors of mitotic and detached cells. Elastic pattern for mitotic and detached states of both normal and cancer cells was alike. The rigidity of cell cortex was shown to be regulated by cortical actin but not by long and short actin protrusions of the cell surface. Elastic difference of apparently identical round cells exhibits the advantage of physical properties for predication of physiological states.

Ample evidence was provided here in support of AFM potentials in cell-based researches especially in combination with other techniques. Living cells were studied under different physiological conditions by AFM which inflicts relatively low damage to the examined cells. Broad distribution of elastic values of the cells shows high sensitivity of this nanotechnology gadget in detection of underlying actin networks which have diverse spatial and structural organizations. AFM also determined the mechanical properties of a number cell types providing with high resolution. It could further estimate the contribution of cell surface brush to cortex stiffness at a pico-Newton scale. AFM showed a prominent capability in discrimination of morphologically identical cells based on their elastic phenotype. Making use of BAM coating for immobilization of suspended cells created a novel opportunity for measuring and analyzing the biomechanical features of adherent and suspended cells which in turn expands the conventional application of AFM in science and technology.

Consistent with earlier studies, it was shown that cells possess specific mechanical signatures of their own with cancer cells remarkably squishier than normal ones. Such a finding emphasizes the importance of mechanical properties in proper diagnosis of diseases. It is assumed that reorganization of actin cytoskeleton has led to cell morphology changes from highly elongated normal cells to polygonal cancer cells. In particular, loss of apical stress fibers in cancer cells could be held accountable for their considerable softness.

Pharmacological induction of cytoskeletal and mechanical alterations ended up increasing cell proliferation and senescence. In addition, flat and round-shaped cells displayed different elastic response to the applied loading force of AFM cantilever. These observations suggest that cells likely transduce physicochemical stimuli into a multitude of mechanical, chemical, structural and morphological responses probably through specific changes in gene expression and protein synthesis to adjust numerous vital functions.

The presented results in this study establish a rigorous framework for a prospective approach (Fig. 5.1). Briefly, cells from either body fluids, tissue sections of patients or from laboratory cell cultures could be analyzed with AFM nanoindentation technique to extract their biomechanical profile in adherent and suspended states. The mechanical properties will be then correlated with other biological features such as cell potentials, physiology, state, fate and structure from which the corresponding information could be inferred. Synergistic effect of biomechanical data fusion with biochemical and morphological properties obtained from conventional methods of spectroscopy, biochemistry and imaging could certainly lead to a wide range of applications particularly in the fields of biomedicine and biotechnology.

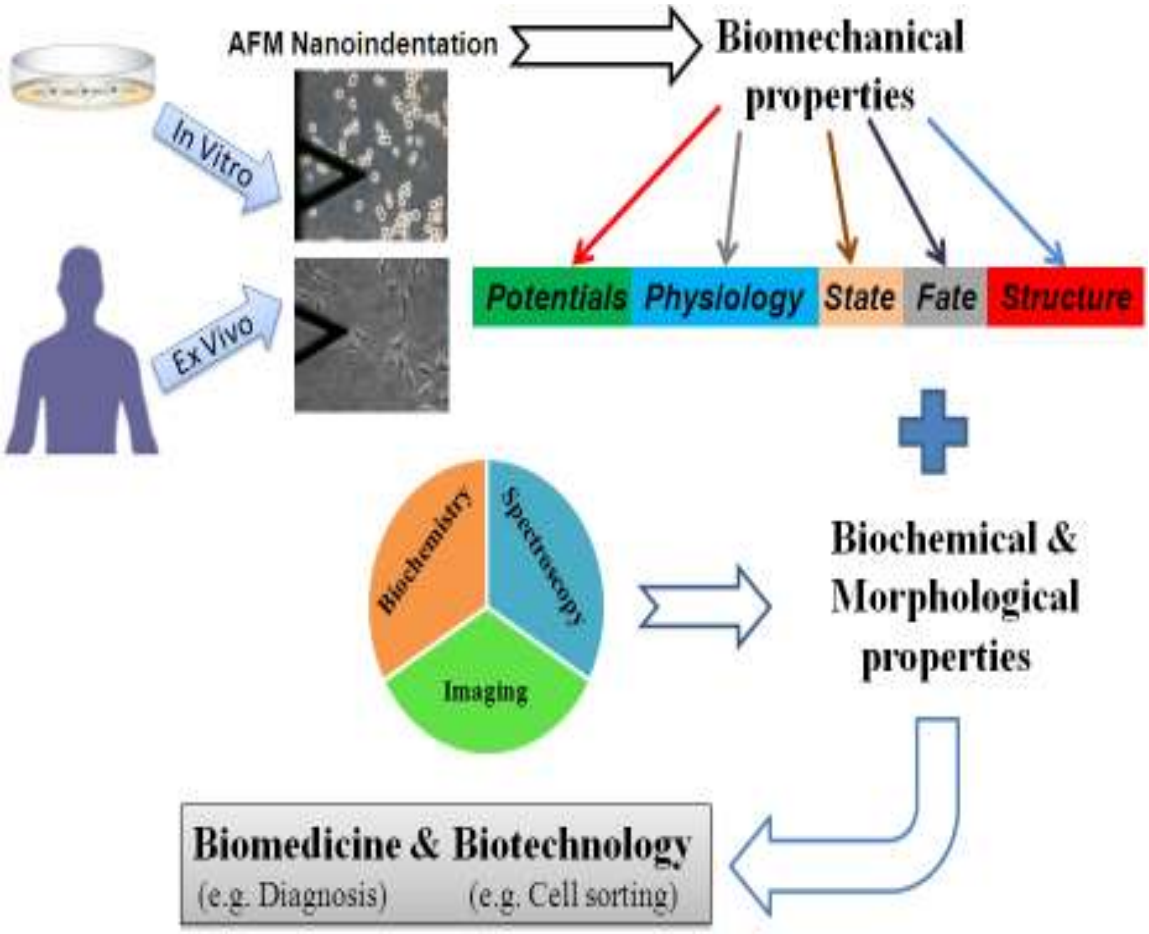

Fig. 5.1 schematic representation of prospective approach

Collectively, this thesis provides a biomechanical overview for better understanding of the mechanical and actin cytoskeletal features of diverse cell types in the adhesion states. It also clarifies the putative functional involvement of actin cytoskeleton in regulation of cell physiology. It further introduces a new method for extending the application of AFM technique for cell-based studies in various fields. The presented findings may have significant implications for relevant research projects and render new insights into regulatory mechanisms which are critical to many pathological conditions and physiological processes. Nevertheless, the exact structural rearrangements and molecular events leading to distinct elastic properties of adherent and suspended cells are still unknown and remain a distant goal for foreseeable future.

Bibliography

[1] Weiss P. A. (1961). The Molecular Control of Cellular Activity. *McGraw-Hill* 1–72.

[2] Pelling A.E. and Horton M.A. (2008). An historical perspective on cell mechanics. *Pflugers Arch - Eur J Physiol.* 456:3–12.

[3] Frixione E. (2000). Recurring Views on the Structure and Function of the Cytoskeleton: A 300-Year Epic. *Cell Motil Cytoskeleton.* 46:73–94.

[4] Fletcher D. A. and Mullins R. D. (2010). Cell mechanics and the cytoskeleton. *Nature*. 463: 485–492.

[5] Zhu C, Bao G, Wang N (2000). CELLMECHANICS: Mechanical Response, Cell Adhesion, and Molecular Deformation. *Annu Rev Biomed Eng.* 2:189-226.

[6] McConnaughey W. B. and Petersen N. O. (1980). Cell poker: An apparatus for stressstrain measurements on living cells. *Rev. Sci. Instrum.* 51: 575-580.

[7] Lüers H, Hillmann K, Litniewski J, Bereiter-Hahn J. (1991). Acoustic microscopy of cultured cells. Distribution of forces and cytoskeletal elements. *Cell Biophys.* 18: 279– 293.

[8] Van Vliet K.J., Bao G., Suresh S. (2003). The biomechanics toolbox: experimental approaches for living cells and biomolecules. *Acta Materialia.* 51: 5881–5905.

[9] Crick F.H.C., Hughes A.F.W. (1965). The physical properties of the cytoplasm. A study by the means of the magnetic particle method. *Exp Cell Res.* 1: 37–80.

[10] Helmke B.P. (2002). Shear stress-induced deformation of the endothelial cytoskeleton. *J Faseb.* 16: 519-A519.

[11] Hochmuth R.M. (2002). Micropipette aspiration of living cells. *J Biomech.* 33: 15–22.

[12] Daehwan S., Kyriacos A. (1999). Cytoindentation for obtaining cell biomechanical properties. *J Orthop Res.* 17: 880–890.

[13] Brown, T.D. (2000). Techniques for mechanical stimulation of cells in vitro: a review. *J Biomech.* 33: 3-14.

[14] Thoumine O., Ott A., Cardoso O., Meister J.J. (1999). Microplates: a new tool for manipulation and mechanical perturbation of individual cells. J. Biochem Biophys *Methods.* 39: 47-62.

[15] Rodan G.A., Mensi T., Harvey, A. (1975). A quantitative method for application of compressive forces to bone in tissue culture. *Calcif Tissue Res.* 18: 125-131.

[16] Tan J.L., Tie J., Pirone D.M., Gray D.S., Bhadriraju K., and Chen C.S. (2003). Cells lying on a bed of microneedles: An approach to isolate mechanical force. *PNAS.* 100: 1484-1489.

[17] Galbraith C.G. and Sheetz M.P. (1997). A micromachined device provides a new bend on fibroblast traction forces. *PNAS.* 94: 9114–9118.

[18] Bao G. and Suresh S. (2003). Cell and molecular mechanics of biological materials. *Nat. Materials*. 2: 715 – 725.

[19] Gerber C. and Lang, H.P (2006). How the doors to the nanoworld were opened. *Nat. Nanotechnol.* 1: 3−5.

[20] Muller D.J. and Dufrene Y.F. (2008) . Atomic force microscopy as a multifunctional molecular toolbox in nanobiotechnology. *Nat. Nanotechnol.* 3: 261 – 269.

[21] Ulcinas A, Snitka V. (2001). Intermittent contact AFM using the higher modes of weak cantilever, *Ultramicroscopy.* 86: 217- 222.

[22] Weisenhorn A.L., Hansma P.K., Albrecht T.R., and Quate C.F. (1989). Forces in atomic force microscopy in air and water. *Appl. Phys. Lett.* 54: 2651-2653.

[23] Käs J.A. (2010). Scanning Force Microscopy I: Imaging and Cellular Elasticity. *Biophysics Lab Course WS.*

[24] Radmacher M., Fritz M., Hansma H.G., and Hansma P.K. (1994). Direct observation of enzyme activity with the atomic force microscopy. *Science*. 265: 1577-1579.

[25] Dorobantu L.S., Bhattacharjee S., Foght J.M., and Gray M.R. (2008). Atomic force microscopy measurement of heterogeneity in bacterial surface hydrophobicity. *Langmuir.* 24: 4944- 4951.

[26] Sotres J., Lostao A., Ebner A., Gomez-Moreno C., Gruber H.J., Hinterdorfer, P., and Baro A.M. (2008). Unbinding molecular recognition force maps of localized single

receptor molecules by atomic force microscopy. *Chemphyschem.* 9: 590-599.

[27] Rief M., Gautel M., Oesterhelt F., Fernandez J.M., and Gaub H.E. (1997). Reversible unfolding of individual titin immunoglobulin domains by AFM. *Science*. 276: 1109-1112.

[28] Stolz M., Raiteri R., Daniels A.U., VanLandingham M.R., Baschong W., and Aebi U. (2004). Dynamic elastic modulus of porcine articular cartilage determined at two different levels of tissue organization by indentation-type atomic force microscopy. *Biophys. J.* 86: 3269-3283.

[29] w.w.w.JPK.com, JPK-DOC0070

[30] Hertz H. (1881). On the elastic contact of elastic solids. *Journal of Reine Anew Math.* 92: 156-171.

[31] Mahaffy R.E., Park S., Gerde E., Käs J., Shih C.K. (2004). Quantitative analysis of the viscoelastic properties of thin regions of fibroblasts using atomic force microscopy. *Biophys J.* 86: 1777-1793.

[32] Rosenbluth M.J., Wilbur A., Lam y., and Fletcher D.A. (2006). Force Microscopy of Nonadherent Cells: A Comparison of Leukemia Cell Deformability. *Biophys J.* 90: 2994−3003.

[33] Barry F.P., Murphy J.M. (2004). Mesenchymal stem cells: clinical applications and biological characterization. *Int. J. Biochem. Cell. Biol.* 36: 568−584.

[34] Liu Z.J., Zhuge Y., Velazquez O.C. (2009). Trafficking and differentiation of mesenchymal stem cells. *J. Cell. Biochem.* 106: 984−991.

[35] Katsube Y., Hirose M., Nakamura C., Ohgushi H. (2008). Correlation between proliferative activity and cellular thickness of human mesenchymal stem cells. *Biochem. Biophys. Res. Commun.* 368: 256−260.

[36] Tokumitsu A., Wakitani S., Takagi M. (2009). Noninvasive estimation of cell cycle phase and proliferation rate of human mesenchymal stem cells by phase shifting laser microscopy. *Cytotechnology*. 59: 161−167.

[37] Settleman J. (2004). Tension precedes commitment even for a stem cell. *Mol. Cell.* 14: 148−150.

[38] McBeath R., Pirone D.M., Nelson C.M., Bhadriraju K., Chen C.S. (2004). Cell shape, cytoskeletal tension, and RhoA regulate stem cell lineage commitment. *Dev. Cell.* 6: 483−495.

[39] Cross S.E., Jin Y.S., Rao J., Gimzewski J.K. (2007). Nanomechanical analysis of cells from cancer patients. *Nat. Nanotechnol.* 2: 780−783.

[40] Dai J., Sheetz M.P. (1995). Mechanical properties of neuronal growth cone membrane studied by tether formation with laser optical tweezers. *Biophys. J.* 68: 988−996.

[41] Lamontagne C.A., Cuerrier C.M., Grandbois M. (2008). AFM as a tool to probe and manipulate cellular processes. *Pflugers Arch - Eur J Physiol*. 456: 61–70.

[42] Huang H., Kamm R.D., Lee R.T. (2004). Cell mechanics and mechanotransduction: pathways, probes, and physiology. *Am. J. Physiol. Cell Physiol.* 287: 1−11.

[43] Kihara T., Nakamura C., Suzuki M., Han S.W., Fukazawa K., Ishihara K., Miyake J. (2009). Development of a method to evaluate caspase-3 activity in a single cell using a nanoneedle and a fluorescent probe. *Biosens. Bioelectron.* 25: 22−27.

[44] Costa K.D. (2006). Imaging and probing cell mechanical properties with the atomic force microscope. *Methods Mol. Biol.* 319: 331−361.

[45] Collinsworth A.M., Zhang S., Kraus W.E., Truskey G.A. (2002). Apparent elastic modulus and hysteresis of skeletal muscle cells throughout differentiation. *Am. J. Physiol. Cell Physiol.* 283: 1219−1227.

[46] Trickey W.R., Vail T.P., Guilak F. (2004). The role of the cytoskeleton in the viscoelastic properties of human articular chondrocytes. *J. Orthop. Res.* 22: 131−139.

[47] Titushkin I., Cho M. (2006). Distinct membrane mechanical properties of human mesenchymal stem cell determined using laser optical tweezers. *Biophys. J.* 90: 2582−2591.

[48] Kagiwada H., Nakamura C., Kihara T., Kamiishi H., Kawano K., Nakamura N., Miyake J. (2010). The mechanical properties of a cell, as determined by its actin cytoskeleton, are important for nanoneedle insertion into a living cell. *Cytoskeleton* 67: 496−503.

[49] Lu L., Oswald S.J., Ngu H., Yin F.C. (2008). Mechanical properties of actin stress fibers in living cells. *Biophys. J.* 95: 6060−6071.

[50] Maddox A.S., Burridge K. (2003). RhoA is required for cortical retraction and rigidity during mitotic cell rounding. *J. Cell Biol.* 160: 255-265.

[51] Kunda P., Pelling A.E., Liu T., Baum B. (2008). Moesin controls cortical rigidity, cell rounding, and spindle morphogenesis during mitosis. *Curr. Biol.* 18: 91−101.

[52] Sugitate T., Kihara T., Liu X.Y., Miyake J. (2009). Mechanical role of the nucleus in a cell in terms of elastic modulus. *Curr. Appl. Phys.* 9: e291−e293.

[53] Khatau S.B., Hale C.M., Stewart-Hutchinson P.J., Patel M.S., Stewart C.L., Searson P.C., Hodzic D., Wirtz D. (2009). A perinuclear actin cap regulates nuclear shape. *Proc. Natl. Acad. Sci. USA* 106: 19017−19022.

[54] Kihara T., Hirose M., Oshima A., Ohgushi H. (2006). Exogenous type I collagen facilitates osteogenic differentiation and acts as a substrate for mineralization of rat marrow mesenchymal stem cells in vitro. *Biochem. Biophys. Res. Commun.*341: 1029−1035.

[55] Rotsch C., Jacobson K., Radmacher M. (1999). Dimensional and mechanical dynamics of active and stable edges in motile fibroblasts investigated by using atomic force microscopy. *Proc. Natl. Acad. Sci. USA* 96: 921−926.

[56] Huang H., Sylvan J., Jonas M., Barresi R., So P.T., Campbell K.P., Lee R.T. (2005). Cell stiffness and receptors: evidence for cytoskeletal subnetworks. *Am. J. Physiol. Cell Physiol.* 288: 72−80.

[57] Chardin P., Boquet P., Madaule P., Popoff M.R., Rubin E.J., Gill D.M. (1989). The mammalian G protein rhoC is ADP-ribosylated by Clostridium botulinum exoenzyme C3 and affects actin microfilaments in Vero cells. *EMBO J.* 8: 1087−1092.

[58] Uehata M., Ishizaki T., Satoh H., Ono T., Kawahara T., Morishita T., Tamakawa H., Yamagami K., Inui J., Maekawa M., Narumiya S. (1997). Calcium sensitization of smooth muscle mediated by a Rho-associated protein kinase in hypertension. *Nature*. 389: 990−994.

[59] Straight A.F., Cheung A., Limouze J., Chen I., Westwood N.J., Sellers J.R., Mitchison T.J. (2003). Dissecting temporal and spatial control of cytokinesis with a myosin II Inhibitor. *Science*. 299: 1743−1747.

[60] Ishihara H., Ozaki H., Sato K., Hori M., Karaki H., Watabe S., Kato Y., Fusetani N., Hashimoto K., Uemura D. (1989). Calcium-independent activation of contractile apparatus in smooth muscle by calyculin-A. *J. Pharmacol. Exp. Ther.* 250: 388−396.

[61] Peterson J.R., Bickford L.C., Morgan D., Kim A.S., Ouerfelli O., Kirschner M.W., Rosen M.K. (2004). Chemical inhibition of N-WASP by stabilization of a native autoinhibited conformation. *Nat. Struct. Mol. Biol.* 11: 747−755.

[62] Sethe S., Scutt A., Stolzing A. (2006). Aging of mesenchymal stem cells. *Ageing Res Rev.* 5:91–116.

[63] Fouchard J., Mitrossilis D., Asnacios A. (2011). Acto-myosin based response to stiffness and rigidity sensing. *Cell Adh. Migr.* 5:16−19.

[64] Chaudhuri O., Parekh S.H., D.A. (2007). Fletcher, Reversible stress softening of actin networks. *Nature.* 445:295−298.

[65] Trepat X., Deng L., An S.S., Navajas D., Tschumperlin D.J., Gerthoffer W.T., Butler J.P., Fredberg J.J. (2007). Universal physical responses to stretch in the living cell. *Nature.* 447: 592−595.

[66] Discher D.E., Janmey P., Wang Y.L. (2005). Tissue cells feel and respond to the stiffness of their substrate. *Science*. 310: 1139−1143.

[67] Ingber D.E. (2006). Cellular mechanotransduction: putting all the pieces together again. *FASEB J.* 20: 811−827.

[68] Stenderup K., Justesen J., Eriksen E.F., Rattan S.I., Kassem M., (2001). Number and proliferative capacity of osteogenic stem cells are maintained during aging and in patients with osteoporosis. *J. Bone Miner. Res.* 16: 1120–1129.

[69] Engler A.J., Sen S., Sweeney H.L., Discher D.E. (2006). Matrix elasticity directs stem cell lineage specification. *Cell*. 126: 677−689.

[70] Darling E.M., Topel M., Zauscher S., Vail T.P., Guilak F. (2008). Viscoelastic properties of human mesenchymally-derived stem cells and primary osteoblasts, chondrocytes, and adipocytes. *J. Biomech.* 41: 454−464.

[71] Bercoff J., Chaffai S., Tanter M., Sandrin L., Catheline S., Fink M., Gennisson J.L., Meunier M. (2003). In vivo breast tumor detection using transient elastography. *Ultrasound Med Biol.* 29: 1387-96.

[72] McKnight A.L., Kugel J.L., Rossman P.J., Manduca A., Hartmann L.C., Ehman R.L. (2002). MR elastography of breast cancer: preliminary results. *AJR Am. J. Roentgenol.* 178: 1411–1417.

[73] Kelly G. M., Kilpatrick J., Vanes M.H., Weafer P.P., Prendergast P.J., Jarvis S. P. (2011). Bone cell elasticity and morphology changes during the cell cycle. *J Biomech.* 44: 1484–1490.

[74] Eiraku M., Takata N., Ishibashi H., Kawada M., Sakakura E. (2011). Self organiz-ing optic-cup morphogenesis in three-dimensional culture. *Nature*. 472: 51–56.

[75] Nash G.B., O'Brien E., Gordon-Smith E.C., Dormandy J.A. (1989). Abnormalities in the mechanical properties of red blood cells caused by Plasmodium falciparum. *Blood*. 74: 855–861.

[76] Suresh S., Spatz J., Mills J.P., Micoulet A., Dao M., Lim C.T., Beil M., Seufferlein T. (2005). Connections between single-cell biomechanics and human disease states: gastrointestinal cancer and malaria. *Acta Biomaterialia.* 1: 15–30.

[77] Guck J., Schinkinger S., Lincoln B., Wottawah F., Ebert S., Romeyke M., Lenz D., Erickson H.M., Ananthakrishnan R., Mitchell D., Käs J., Ulvick S., Bilby C. (2005). Optical deformability as an inherent cell marker for testing malignant transformation and metastatic competence. *Biophys J.* 88: 3689–3698.

[78] Swaminathan V., Mythreye K., O'Brien E.T., Berchuck A., Blobe G.C., Superfine R. (2011). Mechanical stiffness grades metastatic potential in patient tumor cells and in cancer cell lines. *Cancer Res.* 71: 5075-80.

[79] Kihara T., Haghparast S.M.A., Shimizu Y., Yuba S., Miyake J. (2011). Physical properties of mesenchymal stem cells are coordinated by the perinuclear actin cap. *Biochem Biophys Res Commun.* 409: 1–6.

[80] Lu Q.Y., Jin Y.S., Pantuck A., Zhang Z.F., Heber D., Belldegrun A., Brooks M., Figlin R., Rao J. (2005). Green tea extract modulates actin remodeling via rho activity in an in vitro multistep carcinogenic model Clin. *Cancer Res.* 11: 1675-1683.

[81] Rao J.Y., Hurst R.E., Bales W.D., Jones P.L., Bass R.A., Archer L.T., Bell P.B., Hemstreet G.P. (1990). Cellular F-actin levels as a marker for cellular transformation: relationship to cell division and differentiation. *Cancer Res.* 50:2215-2220.

[82] Hemstreet G.P., Rao J.Y., Hurst R.E., Bonner R.B., Jones P.L.,Vaidya A.M., Fradet Y., Moon R.C., Kelof G.J. (1992). Intermediate endpoint biomarkers for chemoprevention. *J Cell Biochem Suppl.* 16I:93-110.

[83] Rao J.Y., Hemstreet G.P., Hurst R.E., Bonner R.B., Jones P.L., Min K.W., Fradet Y. (1993). Alterations in phenotypic biochemical markers in bladder epithelium during tumorigenesis. *Proc. Natl Acad. Sci.* 90: 8287–8291.

[84] Petersen N.O., McConnaughey W.B., and Elson E.L. (1982). Dependence of locally measured cellular deformability on position on the cell, temperature and cytochalasin B. *Proc Natl Acad Sci U S A*. 79: 5327–5331.

[85] Lin C.C. , Yin T.I., Lin Y.D., Lin T.I., Chen Y.T., Lin J.F., Wu H.L., Chang H.C. (2010).Study on mechanical properties of thrombomodulin-transfected cancer cells by atomic force microscopy. *JMBE*. 30: 313-320.

[86] Faria E.C., Ma N., Gazi E., Gardner P., Brown M., Clarke N.W. and Snook R.D. (2008). Measurement of elastic properties of prostate cancer cells. *The Analyst.* 133: 1498-1500.

[87] Li Q.S., Lee G.Y.H., Ong C.N., Lim C.T. (2008). AFM indentation study of breast cancer cells. *Biochem Biophys Res Commun.* 374: 609–613.

[88] Kirmizis D., Logothetidis S. (2010). Atomic force microscopy probing in the measurement of cell mechanics. *Int J Nanomedicine.* 5: 137-45.

[89] Cross S.E., Jin Y-S, Lu Q-Y, Rao J.Y., and Gimzewski J.K. (2011). Green tea extract selectively targets nanomechanics of live metastatic cancer cells. *Nanotechnology.* 22: 215101.

[90] Lekka M., Gil D., Pogoda K.a, ska-Litewka J. D., Jach R., Gostek J., Klymenko O., Prauzner-Bechcicki S., Stachura Z., Wiltowska-Zuber J., Okon K., Laidler P. (2012). Cancer cell detection in tissue sections using AFM. *Arch Biochem Biophys.* 518: 151−156.

[91] Bastatas L., Martinez-Marin D. , Matthews J., Hashem J., Lee Y. J., Sennoune S., Filleur S., Martinez-Zaguilan R., Park S. (2012). AFM nano-mechanics and calcium dynamics of prostate cancer cells with distinct metastatic potential. *Biochimica et Biophysica Acta.* 1820: 1111−1120.

[92] Shimizu Y., Haghparast S. M. A., Kihara T., Miyake J. (2012). Cortical rigidity of round cells in mitotic phase and suspended state. *Micron.* 43: 1246−1251.

[93] Kato K., Umezawa K., Funeriu D.P., Miyake M., Miyake J. (2003). Immobilized culture of nonadherent cells on an oleyl poly(ethylene glycol) ethermodified surface. *Biotechniques.* 35: 1014–1018, 1020–1011.

[94] Ohashi M., Aizawa S., Ooka H., Ohsawa T., Kaji K., Kondo H., Kobayashi T., Noumura T., Matsuo M., Mitsui Y., Murota S., Yamamoto K., Ito H., Shimada H., Utakoji T. (1980). A new human diploid cell strain, TIG-1, for the research on cellular aging. *Exp Gerontol.* 15: 121-133.

[95] Takehara T., Teramura T., Onodera Y., Kakegawa R., Fukunaga N., Takenoshita M., Sagawa N., Fukuda K, Hosoi Y. (2008). Rho-associated kinase inhibitor Y-27632 promotes survival of cynomolgus monkey embryonic stem cells. *Mol Hum Reprod.*

14: 627-34.

[96] Pan W., Petersen E., Cai N., Ma G., Run L.J., Feng Z., Liao K., Leong K. (2005). Viscoelastic properties of human mesenchymal stem cells. *Conf Proc IEEE Eng Med Biol Soc.* 5: 4854-7.

[97] Maloney J.M., Nikova D., Lautenschlager F., Clarke E., Langer R., (2010). Mesenchymal stem cell mechanics from the attached to the suspended state. *Biophys J.* 99: 2479–2487.

[98] Gu L., Zhang H., Chen Q., Chen J. (2003). Calyculin A-induced actin phosphorylation and depolymerization in renal epithelial cells. *Cell Motil Cytoskeleton.* 54: 286-95.

[99] Tsukita S., Yonemura S., Tsukita S. (1997). ERM proteins: head-to-tail regulation of actin-plasma membrane interaction. *Trends Biochem Sci.* 22: 53-8.

[100] Prabhune M., Belge G., Dotzauer A., Bullerdiek J., Radmacher M. (2012). Comparison of mechanical properties of normal and malignant thyroid cells. *Micron.* 43: 1267–1272.

[101] Yamane J., Ohnishi H., Sasaki H., Narimatsu H., Ohgushi H., Tachibana K., (2011). Formation of microvilli and phosphorylation of ERM family proteins by CD43, a potent inhibitor for cell adhesion: cell detachment is a potential cue for ERM phosphorylation and organization of cell morphology. *Cell Adh. Migr.* 5: 119–132.

[102] Bretscher A., Edwards K., Fehon R.G. (2002). ERM proteins and merlin: integrators at the cell cortex. *Nat. Rev. Mol. Cell Biol.* 3: 586–599.

[103] Chhabra E.S., Higgs H.N. (2007). The many faces of actin: matching assembly factors with cellular structures. *Nat Cell Biol.* 9:1110-1121.

[104] Mitrossilis D., Fouchard J., Guiroy A., Desprat N., Rodriguez N., Fabry B., Asnacios A. (2009). Single-cell response to stiffness exhibits muscle-like behavior. *Proc. Natl. Acad. Sci. U.S.A.* 106: 18243–18248.

[105] Cramer L.P., Mitchison T.J. (1997). Investigation of the mechanism of retraction of the cell margin and rearward flow of nodules during mitotic cell rounding. *Mol. Biol. Cell.* 8: 109–119.

[106] Hickson G.R., Echard A., O'Farrell P.H. (2006). Rho-kinase controls cell shape changes during cytokinesis. *Curr. Biol.* 16: 359–370.

[107] Matzke R., Jacobson K. Radmacher M. (2001). Direct, high-resolution measurement of furrow stiffening during division of adherent cells. *Nat. Cell Biol.* 3: 607–610.

[108] Thery M., Bornens M. (2008). Get round and stiff for mitosis. Hfsp J. 2: 65–71.

[109] Harrison C.J., Allen T.D. (1979). Cell surface morphology after trypsinisation depends on initial cell shape. *Differentiation.* 15: 61–66.

[110] Kinn S.R., Allen T.D. (1981). Conversion of blebs to microvilli: cell surface reorganisation after trypsin. *Differentiation.* 20: 168–173.

[111] Porter K., Prescott D., Frye J. (1973). Changes in surface morphology of Chinese hamster ovary cells during the cell cycle. *J. Cell Biol.* 57: 815–836.

[112] Hristov M., Weber C. (2004). Endothelial progenitor cells: characterization, pathophysiology, and possible clinical relevance. *J. Cell. Mol. Med.* 8: 498– 508.

[113] Pantel K., Brakenhoff R.H., Brandt B. (2008). Detection, clinical relevance and specific biological properties of disseminating tumour cells. *Nat. Rev. Cancer.* 8: 329–340.

[114] Stappenbeck T.S., Miyoshi H. (2009). The role of stromal stem cells in tissue regeneration and wound repair. *Science.* 324: 1666–1669.

[115] Sakaue-Sawano A., Kurokawa H., Morimura T., Hanyu A., Hama H., Osawa H., Kashiwagi S., Fukami K., Miyata T., Miyoshi H., Imamura T., Ogawa M., Masai H., Miyawaki A., (2008). Visualizing spatiotemporal dynamics of multicellular cell-cycle progression. *Cell.* 132: 487–498.

[116] Kolata G.B., (1975). Microvilli: a major difference between normal and cancer cells? *Science.* 188: 819–820.

[117] Iyer S., Gaikwad R.M., Subba-Rao V., Woodworth C.D., Sokolov I. (2009). Atomic force microscopy detects differences in the surface brush of normal and cancerous cells. *Nat. Nanotechnol.* 4: 389–393.

[118] Stewart M.P., Helenius J., Toyoda Y., Ramanathan S.P., Muller D.J., Hyman A.A. (2011). Hydrostatic pressure and the actomyosin cortex drive mitotic cell rounding. *Nature.* 469: 226–230.

[119] Boucrot E., Kirchhausen T. (2007). Endosomal recycling controls plasma membrane area during mitosis. *Proc. Natl. Acad. Sci. U.S.A*. 104: 7939–7944.

[120] Boucrot E., Kirchhausen T. (2008). Mammalian cells change volume during mitosis. *PLoS One*. 3: e1477.

[121] Raucher D., Sheetz M.P. (1999). Membrane expansion increases endocytosis rate during mitosis. *J. Cell Biol.* 144: 497–506.

[122] Thery M., Racine V., Pepin A., Piel M., Chen Y., Sibarita J.B., Bornens M. (2005). The extracellular matrix guides the orientation of the cell division axis. *Nat. Cell Biol.* 7: 947–953.

Publication list

I) Takanori Kihara, **Seyed Mohammad Ali Haghparast** , Yuji Shimizu, Shunsuke Yuba, Jun Miyake (2011). Physical properties of mesenchymal stem cells are coordinated by the perinuclear actin cap. *Biochem Biophys Res Commun.* 409: 1–6.

II) Yuji Shimizu, **Seyed Mohammad Ali Haghparast**, Takanori Kihara, Jun Miyake (2012). Cortical rigidity of round cells in mitotic phase and suspended state. *Micron*. 43: 1246−1251.

III) **Seyed Mohammad Ali Haghparast**, Takanori Kihara, Yuji Shimizu, Shunsuke Yuba, Jun Miyake (2012). Biomechanical properties of suspended normal and cancer cells are defined by different regulatory mechanisms for actin cytoskeleton. Submitted